論文 / 著書情報
Article / Book Information

題目(和文)	
Title(English)	Transport Studies in Molten Salts:Mass Transport and Conduction of Heat in Molten Salts
著者(和文)	小田原修
Author(English)	OSAMU ODAWARA
出典(和文)	学位:工学博士, 学位授与機関:東京工業大学, 報告番号:甲第1100号, 授与年月日:1979年3月26日, 学位の種別:課程博士, 審査員:河村 和孝
Citation(English)	Degree:Doctor of Engineering, Conferring organization: , Report number:甲第1100号, Conferred date:1979/3/26, Degree Type:Course doctor, Examiner:
学位種別(和文)	博士論文
Type(English)	Doctoral Thesis

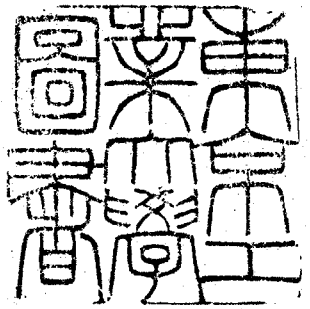

TRANSPORT STUDIES IN MOLTEN SALTS:

MASS TRANSPORT AND CONDUCTION OF HEAT IN MOLTEN SALTS

A DOCTORAL DISSERTATION

SUBMITTED TO THE FACULTY OF THE GRADUATE

SCHOOL OF TOKYO INSTITUTE OF TECHNOLOGY.

BY

OSAMU ODAWARA

IN PARTIAL FULFILLMENT OF THE REQUIREMENTS

FOR THE DEGREE OF DOCTOR OF ENGINEERING

DECEMBER, 1978

TABLE OF CONTENTS

ABSTRACT

This thesis deals with the investigations of mass transport and thermal conduction in molten salts.

In order to clarify the mass transport phenomena in molten salts, cationic mobilities in the molten (Li-Tl)NO_3 and (Rb-Tl)NO_3 systems, high-dilution diffusion coefficients of K^+, Rb^+, Cs^+, and Tl^+ in the molten (li-K)NO_3 system, and tracer diffusion coefficients of Rb^+ and Cs^+ in the binary molten alkali nitrate systems are determined by means of a counter-current electromigration technique, wave-front-shearing interferometry, and a paper strip method, respectively.

The obtained characteristics are qualitatively interpreted with the simple assumption that the size of moving ions compared with that of the free space formed by the corresponding system and the interaction between the moving ion and the surrounding ions mainly govern the mass transport process in molten salts.

In order to determine the thermal conductivity in molten salts, the thermal diffusivities of $NaNO_3$ and HTS are measured by means of wave-front-shearing interferometry. The thermal conduction in molten salts are discussed by relating the thermal conductivity with the sound velocity and the mean vibrational frequency in the molten salts. We confirmed that the approach with adopting the Debye frequency of molten salts would give an excellent approximation of the thermal conductivity of molten salts.

A wave-front-shearing interferometer constructed as a part of the present work offers reliable data for diffusion coefficients and thermal conductivities of molten salts up to 500°C.

INTRODUCTION

The interest in ionic melts at high temperature has rapidly increased from the point both of fundamental aspects and of technical applications.

Some molten salts are applied as heat treatment baths, electrolyte fuel cells, the solvent or the catalyst for the preparation of organo-metallic compounds, and the fuel carrier and the coolant for nuclear reactors such as Molten Salt Breeder Reactor (MSBR)[1,2]; they have good heat transfer properties and high electric conductivity compared with organic liquids, and relative inertness and low vapour pressure compared with liquid metals. Molten salt mixtures are also being utilized in the nuclear industry where plutonium and other products of nuclear fission are recovered chemically by means of molten salts in the "Molten Salt Transport Process".

The scientific research activity for molten salts has been accelerated by the fact that some of them constitute one of the simplest classes of liquid electrolyte, and a relatively large number of investigations have been expended to make the mechanism of transport phenomena in molten salts clear. Several models on transport process in molten salts have been proposed with the assumption that the transport properties would be determined by an approach from the "solid" state, the "gaseous" state, or the "intermediate" contribution between both states; for example, the absolute reaction rate theory[3] and the paired ion diffusion theory[4,5] are based on a quasi-

lattice model, and the hole theory[6] is based on a gas like approach, while the significant structure theory[7] and the free volume theory[8] are based on an intermediate contribution between the solid state and the gaseous state. As typical liquid models, the cooperative rearrangement theory[9] and the microjump model[10] have been proposed. However, most theories are not able to interpret all the properties properly well; a model might be successful in describing some property of molten salts but not another.

Although it is obvious that an important part of the experimental data for molten salts concerns the thermal conductivity or the diffusion coefficient, the existing information on their properties is very limited because of the experimental difficulties encountered in dealing with a strongly corrosive liquid at high temperature. Although viscosities and electric conductivities have been measured in a number of pure molten salts and mixtures, only a few data for the ionic mobility and the diffusion coefficient are known, and much less for the thermal conductivity.

The major purpose of this work is to study the transport properties of molten salts, in particular, the mass transport and the conduction of heat. Experimentally, we have determined the internal cation mobilities in the molten (Li-Tl)NO_3 and (Rb-Tl)NO_3 systems by means of a countercurrent electromigration technique(Klemm's method)(CHAPTER 1), the diffusion coefficients of various monovalent cations in binary molten alkali nitrate systems by means of wave-front-shearing interferometry and a paper strip method (CHAPTERs 2 and 3, respectively), and the thermal conductivity of HTS (Heat Transfer Salt) with wave-front-shearing interferometry (CHAPTER 4). Very little work has been done in the latter field.

In PART I, the results of cationic mobility and diffusion coefficent obtained in the present work are qualitatively interpreted with the simple assumption that the size of the free space compared with that of migrating ions and the pair potential between cation and anion would be the main factors which rule a mass transport process in molten salts such as diffusion and electromigration.

The investigation on the conduction of heat in molten salts are reported in PART II, which consists of two chapters; the measurement of the thermal diffusivity of HTS by the use of a wave-front-shearing interferometer, which was constructed in the present work, is described in CHAPTER 4, and in CHAPTER 5 some approaches to the mechanism of thermal conduction in molten salts are tried out by relating the thermal conductivity with the sound velocity in molten salts measured at our laboratory.

References

[1] K. Furukawa et al., J. At. Energy Soc. Japan, 16, 249 (1974)

[2] K. Furukawa et al., " 溶融塩増殖炉 (Molten Salt Breeder Reactor)", At. Energy Soc. Japan (1977)

[3] H. Eyring, J. Chem. Phys., 4, 283 (1936)

[4] A.Z. Borucka, J.O'M. Bockris, and J.A. Kitchner, J. Chem. Phys., 24, 1282 (1956)

[5] A.Z. Borucka, J.O'M. Bockris, and J.A. Kitchner, Proc. Roy. Soc., A241, 554 (1957)

[6] R. Furth, Proc. Cambridge Phil. Soc., 37, 252, 281 (1941)

[7] H. Eyring and T. Ree, Proc. Nat. Acad. Sci., 47, 526 (1961)

[8] M.H. Cohen and D. Turnbull, J. Chem. Phys., 31, 1164 (1959)

[9] G. Adams and J.H. Gibbs, J. Chem. Phys., 43, 139 (1965)

[10] R.A. Swalin, Acta Met., 7, 736 (1959)

PART I

MASS TRANSPORT IN MOLTEN SALTS.

CHAPTER 1

Internal Cation Mobilities in the Molten (Li-Tl)NO_3 and (Rb-Tl)NO_3 Systems.

The relative differences in internal cation mobilities are measured for the molten systems $LiNO_3$-$TlNO_3$ and $RbNO_3$-$TlNO_3$ over a wide range of temperature and concentration by means of countercurrent electromigration technique (Klemm's method), and the internal mobilities are calculated from the existing data on the electric conductivity for these systems. For the system $LiNO_3$-$TlNO_3$, a marked dependence of the relative internal mobility differences on temperature is found particularly in the Li^+ rich region, and a considerable concentration dependence is found over the investigated temperature range. This is qualitatively explained in terms of a model which takes into account mainly the differences of the cation-anion pair potentials and of the sizes of the two cations. On the other hand, for the system $RbNO_3$-$TlNO_3$, only a slight temperature dependence is observed and no concentration dependence, if present, is detected within the experimental error.

1 Introduction

Since the rather surprising finding by Chemla and coworkers[1,2] that under certain conditions K^+ is more mobile than Li^+ in the molten mixture LiBr-KBr, the study on the mobilities of binary molten systems with monovalent cations and a common anion has attracted much attention, and for systems of chrolides[3], bromides[4,5], nitrates[6], and sulphates [7,8], mobilities, mobility differences, or transport numbers have been investigated systematically by means of zone electrophoresis, countercurrent electromigration, Hittorf's method, and EMF measurement[9]. The investigation of cation mobilities in binary mixtures offers useful information on what factors affect the electromigration process since the mobilities of two different cations can be studied at the same time under various conditions.

In the present work the dependence of relative differences in the internal cation mobilities on temperature and concentration is studied for the systems $LiNO_3$-$TlNO_3$ and $RbNO_3$-$TlNO_3$, the differences of the cation radii being large in the former and very small in the latter. The countercurrent electromigration method (Klemm's method) is adopted here, with which even very small relative mobility differences of two cations can be accurately measured, although the information on the external mobilities cannot be obtained. By using the salts only in a small-volume separation tube, the countercurrent method is readily applicable to such expensive salts as $RbNO_3$ and $TlNO_3$.

2 Experimental

The arrangement of the electromigration cell was similar to that previously employed for isotope effect measurements by Okada et al.[10], which is illustrated in Fig. 1. A separation tube of Vycor (int. diam. : 4 mm) packed with quartz powder of 80-100 mesh was inserted into a small vessel containing a molten mixture of $LiNO_3$-$TlNO_3$ or $RbNO_3$-$TlNO_3$. The chemicals were of analytical reagent grade and fully dried before use without further purification. When the salts permeated the diaphragm by capillary action, the separation tube was transferred to a large vessel containing a eutectic mixture of $NaNO_3$-KNO_3 or $LiNO_3$-KNO_3 which was to serve as a cathode compartment, and immediately electrolysis was started. After several hours' electromigration, the separation tube was taken out of the large vessel, cooled and cut into several fractions for chemical analysis. An aliquot of each fraction was subjected to the determination of the cations by flame spectrophotometry. On the other hand, the total amount of cations in each fraction was checked by eluting another aliquot through a column of H^+-type ion exchanger and titrating the eluted solution with a standard NaOH solution. Detailed results for a typical experiment in the molten (Rb-Tl)NO_3 system are shown in Table 1.

The lowest limit for the electromigration temperature was chosen in the light of the phase diagrams of the system[11,12].

Radioactive tracer ^{204}Tl ($T_{1/2}$ = 4.1 y) was purchased from New England Nuclear Corp. in U. S. A. The radioactivity was measured with a GM counter.

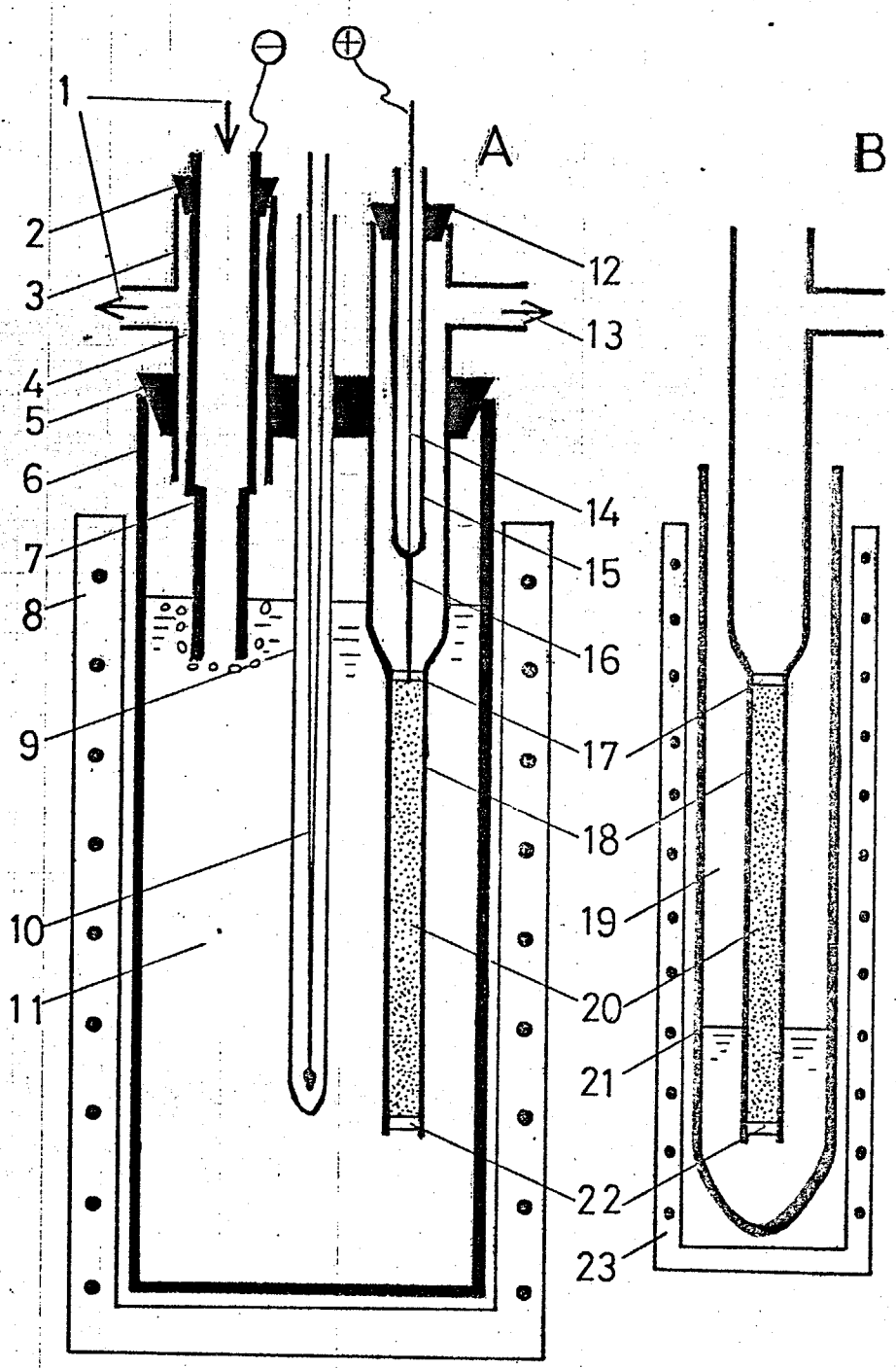

Fig.1 Electromigration cell. A) Electromigration cell. B) Vessel for filling molten $TlNO_3$-$RbNO_3$(or $TlNO_3$-$LiNO_3$) into the separation tube.

1,13. Mixture of NO_2 and O_2; 2,5,12. Silicone stopper; 3,15. Pyrex glass tube; 4. Stainless steel tube; 6. Quartz vessel (Int.diam.: 5.5 cm, Hight: 30cm); 7. Aluminum tube (Int.diam.: 9mm); 8,23. Electric furnace; 9. Pyrex glass sheath for the thermocouple; 10. Thermocouple; 11. Molten KNO_3-$NaNO_3$(or KNO_3-$LiNO_3$); 14. Stainless steel wire; 16. Platinum wire; 17. Quartz wool; 18. Separation tube (Vycor glass); 19. Molten $TlNO_3$-$RbNO_3$(or $TlNO_3$-$LiNO_3$); 20. Diaphragm (Quartz powder); 21. Pyrex glass vessel; 22. Quartz frit (Thickness: ca.5mm)

Table 1. Detailed results for a typical electromigration experiment in the system $(Rb\text{-}Tl)NO_3$.

Temperature 303 (°C)

Transported charge 739.9 (mgCu)

Fraction No.	Length (mm)	Tl $x10^4$ (mol)	Rb $x10^4$ (mol)	Tl + Rb $x10^4$ (mol)	Tl ratio (%)	Na $x10^4$ (mol)	K $x10^4$ (mol)	Total $x10^4$ (mol)	Total* (mol)
1	15	1.14±0.05	9.95±0.05	11.09	10.3			11.09	10.72±0.13
2	15	3.25±0.05	13.30±0.05	16.55	19.6			16.55	16.54±0.13
3	16	4.20±0.05	11.30±0.05	15.50	27.1			15.50	14.62±0.13
4	15	4.90±0.05	13.05±0.05	17.95	27.3			17.95	17.14±0.13
5	17	5.00±0.05	13.30±0.05	18.30	27.3			18.30	17.47±0.13
6	20	5.95±0.05	15.80±0.05	21.75	27.4	0.03	0.05	21.83	21.24±0.13
7	25	7.45±0.05	18.05±0.05	25.50	29.2	0.30	0.05	25.85	26.40±0.13
8	24	4.85±0.05	9.25±0.05	14.10	34.4	4.80	3.35	22.25	23.56±0.13
9	20	1.74±0.05	3.80±0.05	5.54	31.4	8.30	11.50	25.34	21.11±0.13
10	18	0.42±0.05	1.50±0.05	1.92	21.9	9.50	9.28	20.70	18.59±0.13

Stock Solution Tl ratio = 27.6 (%)

"Total*" was determined by neutralization titration with NaOH.

3 Results

The salts in the large cathode compartment diffused into the separation tube during electromigration. If the duration of electromigration, t, was adjusted, however, so that $t < \ell^2 / \{\pi (\sqrt{D_{s\ eff}} + \sqrt{D_{c\ eff}})^2\}$ [13,14], there existed an extended part around the middle of the separation tube where the initial chemical composition remained unchanged. Here, ℓ is the length of the diaphragm part, and $D_{s\ eff}$ and $D_{c\ eff}$ the effective diffusion coefficients of the investigated salts and of the salts in the cathode compartment into the diaphragm part, respectively. In this case the relative difference in internal mobilities of two cations 1 and 2 can be calculated by[7,14]:

$$\varepsilon_{12} = (b_1 - b_2)/b = (F/Q) \cdot (\sum_i n_{2i}/p_2 - \sum_i n_{1i}/p_1), \quad \ldots\ldots (1)$$

where Q is the transported charge in Coulomb, F the Faraday constant, n_{1i} and n_{2i} the equivalent quantities of cation 1 and 2 in the i-th fraction, respectively, and p_1 and p_2 the initial equivalent fractions of the corresponding cations. The summation is made from the fraction nearest to the anode to the fraction where the initial composition remains unchanged. When cation 2, that is Tl^+ in the present case, is of tracer scale, Eq. (1) is modified as:

$$\varepsilon_{12} = (F/Q) \cdot ((n_2^0/c_2^0) \sum_i c_{2i} - \sum_i n_{1i}), \quad \ldots\ldots (2)$$

where c_{2i} is the radioactivity in cpm of cation 2 in the i-th fraction, and (c_2^0/n_2^0) the specific activity of cation 2 in cpm/eq of the initial sample.

Experimental conditions and the results are tabulated in Tables 2 and 3.

The relative internal mobility differences are plotted against temperature in Figs. 2 and 3.

Table 2 Conditions and the results of electromigration in the system (Li-Tl)NO_3.

Exp. No.	Temp. (°C)	Mole fraction of $TlNO_3$ (%)	Electromign. duration (hr)	Transported charge (C)	$(b_{Li} - b_{Tl})/b$
1	288	0	6.5	2211	0.821 ± 0.009
2	370	0	5.0	1545	0.413 ± 0.003
3	375	0	6.4	2054	0.351 ± 0.011
4	397	0	5.9	1999	0.300 ± 0.009
5	415	0	5.9	2054	0.330 ± 0.002
6	440	0	6.8	2144	0.390 ± 0.002
7	443	0	6.1	1929	0.473 ± 0.006
8	467	0	5.3	1849	0.650 ± 0.003
9	284	3.87 ± 0.01	4.5	1560	0.226 ± 0.020
10	285	3.87 ± 0.01	5.2	1702	0.236 ± 0.017
11	312	3.87 ± 0.01	5.0	1622	0.214 ± 0.019
12	367	3.87 ± 0.01	4.6	1403	0.153 ± 0.018
13	396	3.87 ± 0.01	4.3	1347	0.192 ± 0.023
14	416	3.87 ± 0.01	4.5	1527	0.178 ± 0.020
15	224	25.6 ± 0.1	6.9	2229	0.398 ± 0.003
16	256	25.6 ± 0.1	7.2	2376	0.118 ± 0.002
17	308	25.6 ± 0.1	7.1	2417	0.051 ± 0.002
18	350	25.6 ± 0.1	8.7	3041	0.026 ± 0.001
19	400	25.6 ± 0.1	7.2	2658	0.036 ± 0.002
20	245	50.9 ± 0.1	7.0	2410	0.011 ± 0.001
21	270	50.9 ± 0.1	7.1	2430	- 0.011 ± 0.001
22	310	50.9 ± 0.1	6.8	2299	- 0.032 ± 0.002
23	328	50.9 ± 0.1	7.0	2293	- 0.026 ± 0.002
24	225	68.0 ± 0.2	6.0	1679	- 0.001 ± 0.001
25	274	68.0 ± 0.2	5.2	1654	- 0.003 ± 0.001
26	327	73.8 ± 0.1	6.8	2370	- 0.044 ± 0.001
27	377	73.8 ± 0.1	7.0	2239	- 0.064 ± 0.001
28	380	83.6 ± 0.1	6.8	2290	- 0.084 ± 0.001
29	388	83.6 ± 0.1	6.6	2254	- 0.095 ± 0.002
30	230	88.8 ± 0.4	5.8	1921	- 0.076 ± 0.006
31	275	88.8 ± 0.4	6.5	2236	- 0.071 ± 0.005
32	305	88.8 ± 0.4	6.5	2169	- 0.064 ± 0.006
33	334	88.8 ± 0.4	5.2	1733	- 0.087 ± 0.008
34	340	88.8 ± 0.4	6.5	2130	- 0.082 ± 0.006
35	372	88.8 ± 0.4	5.8	1947	- 0.080 ± 0.007

The temperature was controlled within ±3°C in most of experiments. The sign ± in the column $\Delta b/b$ represents the standard deviation resulting from the errors of chemical analysis and radio-activity counting. That the mole fraction of $TlNO_3$ is 0 means that the radio-active tracer(^{204}Tl) is used.

Table 3 Conditions and the results of electromigration in the system $(Rb\text{-}Tl)NO_3$.

Exp. No.	Temp. (°C)	Mole fraction of $TlNO_3$ (%)	Electromign. duration (hr)	Transported charge (C)	$(b_{Rb} - b_{Tl})/b$
101	325	0	7.1	2353	- 0.054 ± 0.001
102	363	0	7.7	2553	- 0.058 ± 0.001
103	430	0	6.0	1981	- 0.040 ± 0.001
104	269	27.6 ± 0.4	7.0	2209	- 0.082 ± 0.001
105	303	27.6 ± 0.4	7.0	2247	- 0.070 ± 0.001
106	330	27.6 ± 0.4	7.0	2275	- 0.055 ± 0.001
107	347	27.6 ± 0.4	7.0	2376	- 0.055 ± 0.001
108	395	27.6 ± 0.4	7.1	2112	- 0.037 ± 0.001
109	236	50.1 ± 0.1	8.0	1012	- 0.092 ± 0.002
110	272	50.1 ± 0.1	9.5	2960	- 0.075 ± 0.001
111	303	50.1 ± 0.1	10.3	3683	- 0.070 ± 0.001
112	247	74.4 ± 0.2	6.0	1618	- 0.085 ± 0.002
113	294	74.4 ± 0.2	7.0	2430	- 0.070 ± 0.001
114	324	74.4 ± 0.2	7.2	1784	- 0.062 ± 0.002

See the footnote to Table 2.

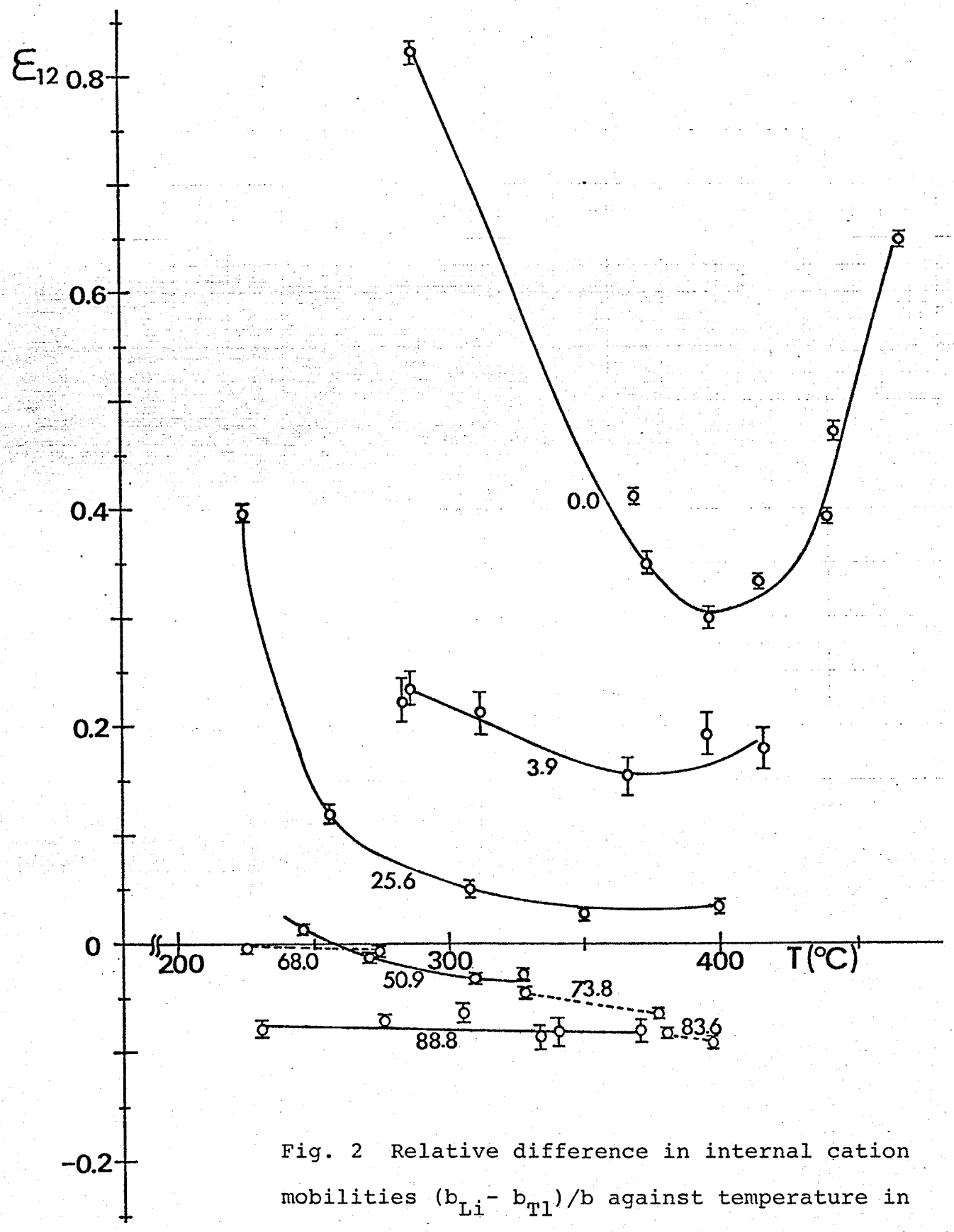

Fig. 2 Relative difference in internal cation mobilities $(b_{Li} - b_{Tl})/b$ against temperature in the system $(Li\text{-}Tl)NO_3$. The numbers in the figure represent the mole fraction of $TlNO_3$ in %.

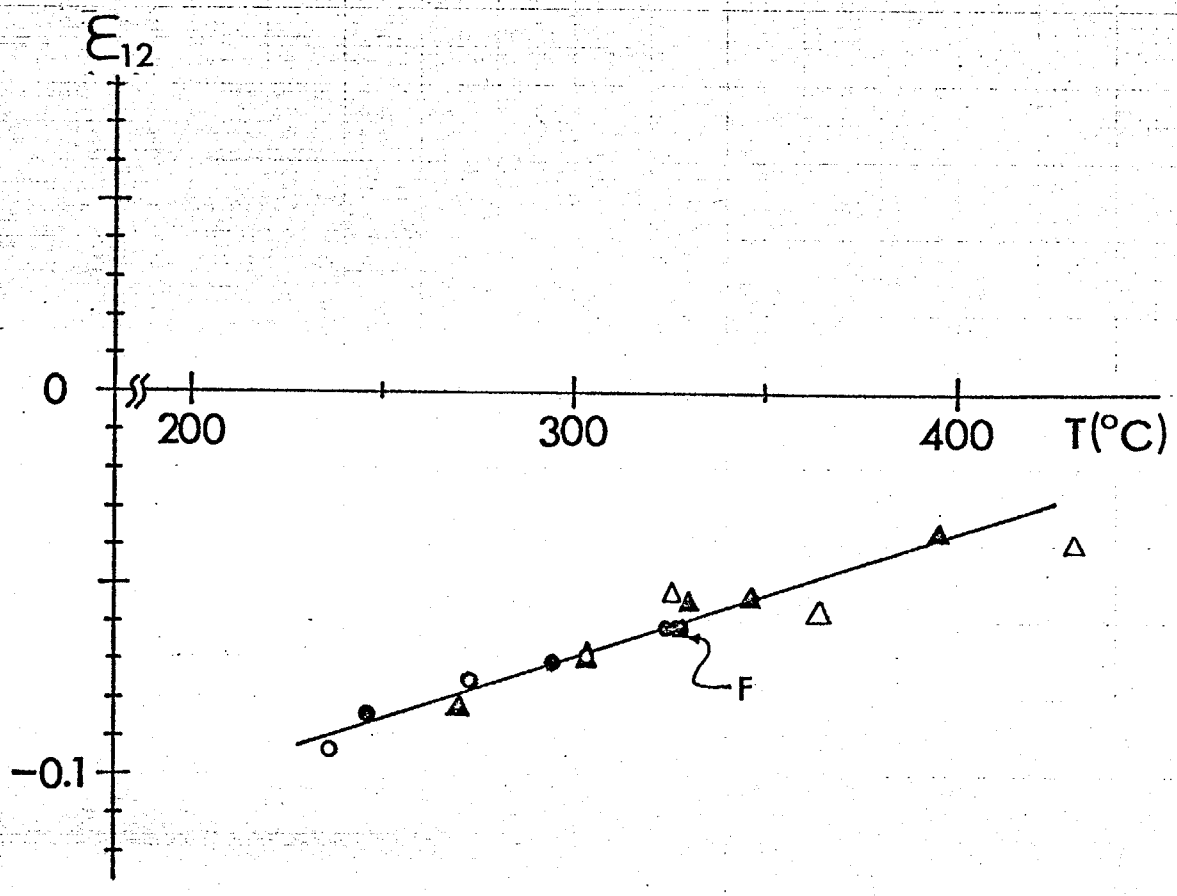

Fig. 3 Relative difference in internal cation mobilities $(b_{Rb} - b_{Tl})/b$ against temperature in the system $(Rb\text{-}Tl)NO_3$.
($TlNO_3$ mole fraction: △ 0%, ▲ 27.6%, ○ 50.1%, ● 74.4%)
The data by Forcheri et al.[23] are also plotted for comparison (F in the figure).

From the present data and the existing data on the electric conductivities for the systems $LiNO_3$-$TlNO_3$[15,16] and $RbNO_3$-$TlNO_3$[15-17], the internal mobilities of these cations are calculated according to Eqs. (3) and (4).

$$b_1 = (\Lambda/F)\,[\,1 + \varepsilon_{12}(\,1 - p_1\,)\,] \qquad \ldots\ldots\ldots (3),$$

$$b_2 = (\Lambda/F)\,[\,1 - \varepsilon_{12}(\,1 - p_2\,)\,] \qquad \ldots\ldots\ldots (4),$$

where Λ is the equivalent conductivity of the mixture.

The isotherms of internal mobilities for the systems $LiNO_3$-$TlNO_3$ and $RbNO_3$-$TlNO_3$ are shown in Figs. 4 and 5, respectively.

4 Discussion

It is known that the trivalent Tl ions are unstable in molten nitrates and, if present, are converted into the monovalent state. The fact that radioactive Tl does not show any irregular behaviour in the system $RbNO_3$-$TlNO_3$ ($RbNO_3$: 100%) as seen from Figs. 3 and 5, excludes the possibility that, because of its extremely low concentration, radioactive Tl behaves irregularly. The quite negligible radioactivity in the washed diaphragm powder after electromigration also denies the possibility that Tl of tracer concentration might be absorbed in the quartz diaphragm. A change of the distribution of salts in a separation tube during solidification was not observed for samples without electromigration in some preliminary experiments for the system $LiNO_3$-$TlNO_3$ (twice for 0 % $TlNO_3$ and twice for 89 % $TlNO_3$).

It is indicated by molecular dynamics simulations of some alkali halides following the mehtod successfully applied to molten salts by Woodcock and Singer[18] that the electric conductivity is correlated with

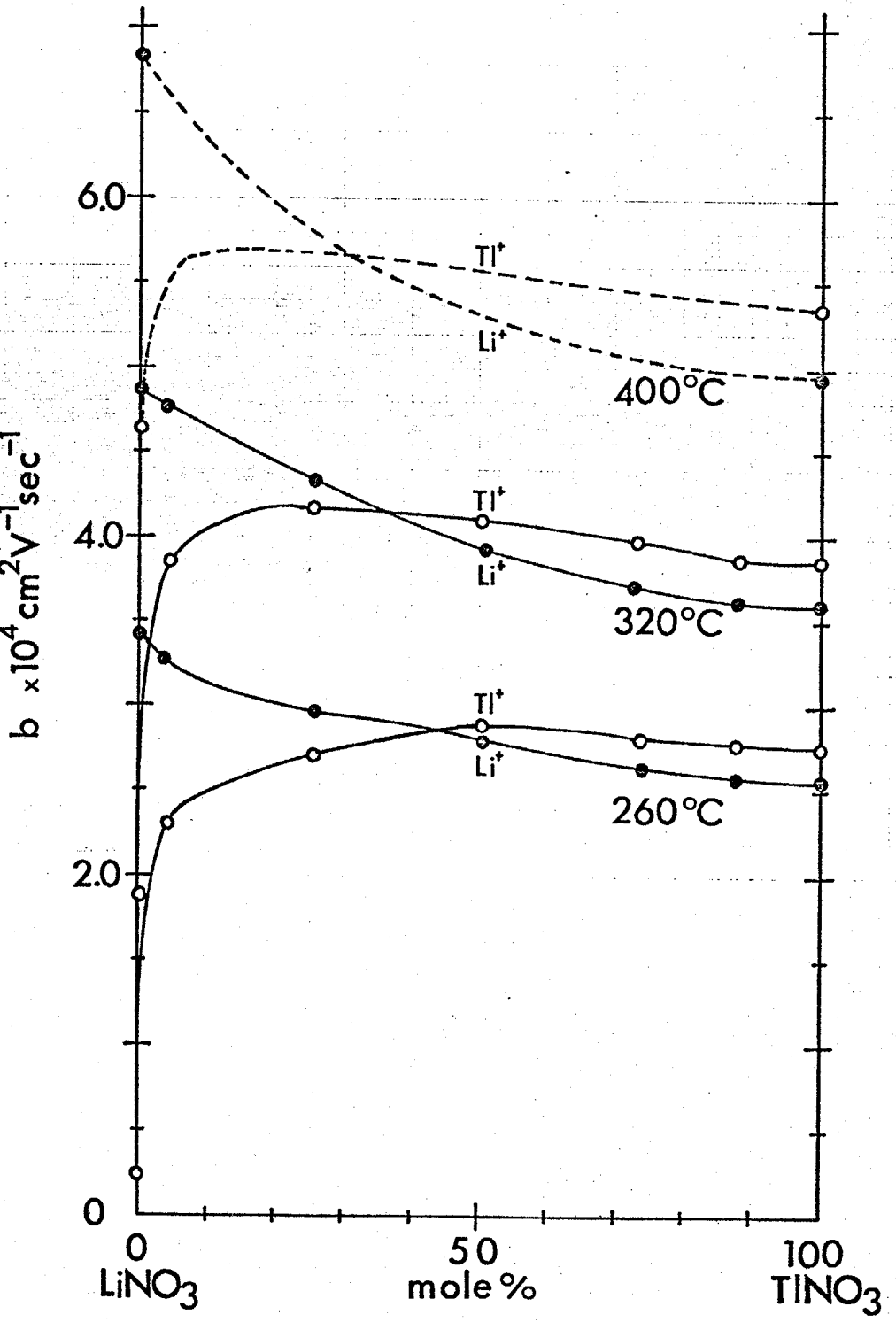

Fig. 4 Isotherms of internal mobilities in the system $(Li\text{-}Tl)NO_3$. The data on the equivalent conductivity of $LiNO_3$ are taken from Ref.[31] and of $TlNO_3$ from Ref.[32]. Most of the values at 400°C are estimated from the extrapolated conductivity data.

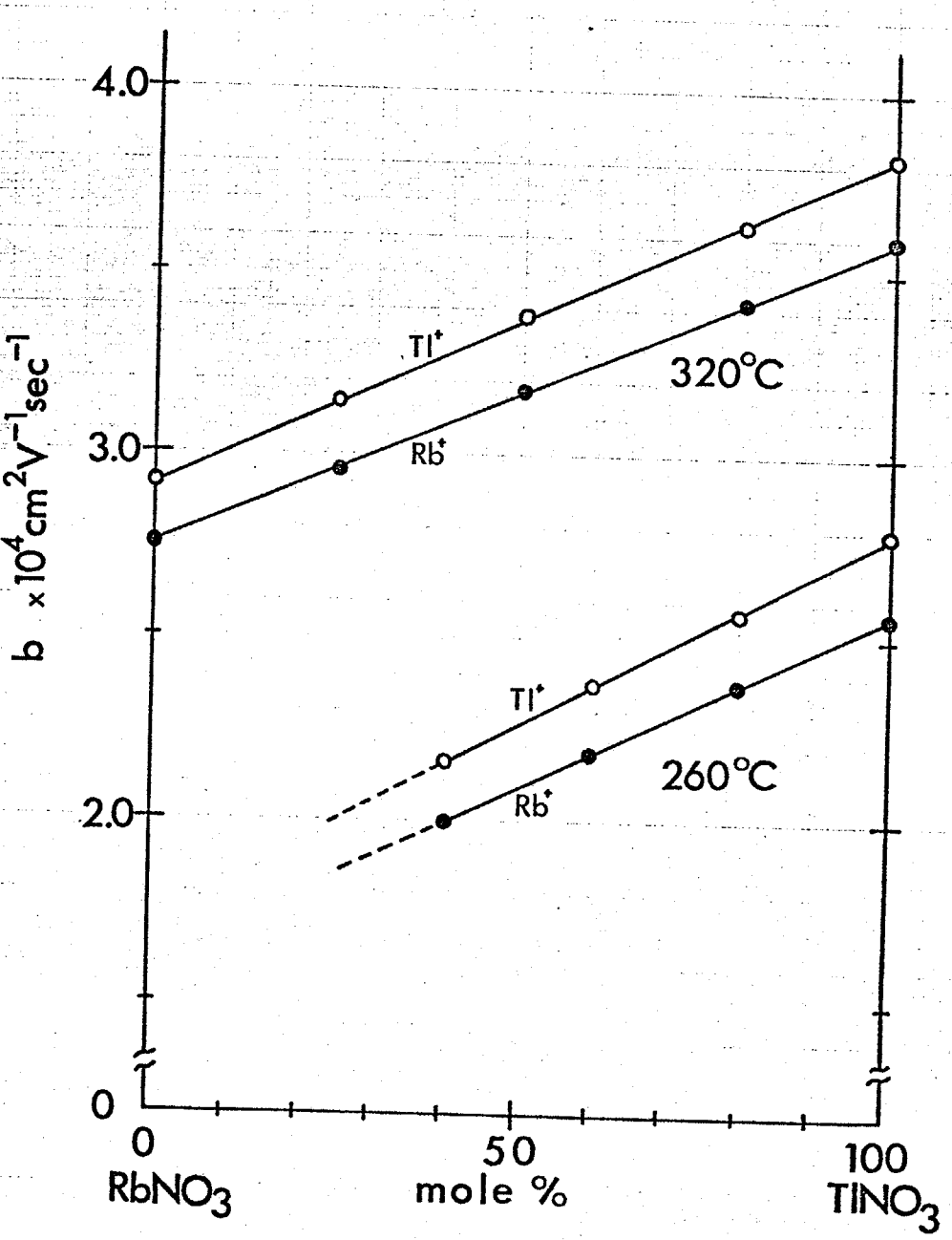

Fig. 5 Isotherms of internal mobilities in the system $(Rb\text{-}Tl)NO_3$. The data on the euivalent conductivity of pure $RbNO_3$ are taken from Ref.[31].

a separating motion of the nearest neighbouring cations and anions[19]. Since the pair potential between the cations and anions is not known for molten nitrates, it is assumed in this discussion to be similar to that in the corresponding solid halides, and the following deductions are drawn in view of the findings obtained with molecular dynamics studies of molten LiCl[20], TlCl[21], and LiCl-RbCl equimolar mixture[21].

The character of the Li^+ motion might be somewhat different at low and high temperatures, while that of the Tl^+ motion might not depend on temperature. At low temperatures, the pair distribution function between Li^+ and NO_3^- would have a sharp maximum around the position where the pair potential has its deep minimum, as speculated from the findings of molecular dynamics simulation of molten LiCl (see Figure 6). This would show that a Li^+ ion moves along the surface of a NO_3^- ion rather than in the Li-NO_3 direction. While moving along the surface of one NO_3^- ion, a Li^+ ion will have a chance to move the surface of a neighbouring NO_3^- ion, since the nearest neighbouring NO_3^- ions are nearly in contact with each other. The peak of the pair distribution function flattens with rising temperature. This would suggest that at high temperatures a Li^+ ion would move vigorously not only along the surface of the nearest NO_3^- ion but also in the Li-NO_3 direction. As for the Tl^+ ions, on the other hand, the valley of the pair potential curve would be shallow around the position where the pair distribution function has its maximum. A Tl^+ ion can readily withdraw from its nearest NO_3^- ion, if only there is enough electrically negative free space in the surroundings, while may not easily circle along the surface of a NO_3^- ion because of its large size. Thus, at low temperatures, Li^+ is more mobile than Tl^+ in Li^+ rich mixtures where there is little free space large enough for Tl^+ motion. At high temperatures, it is

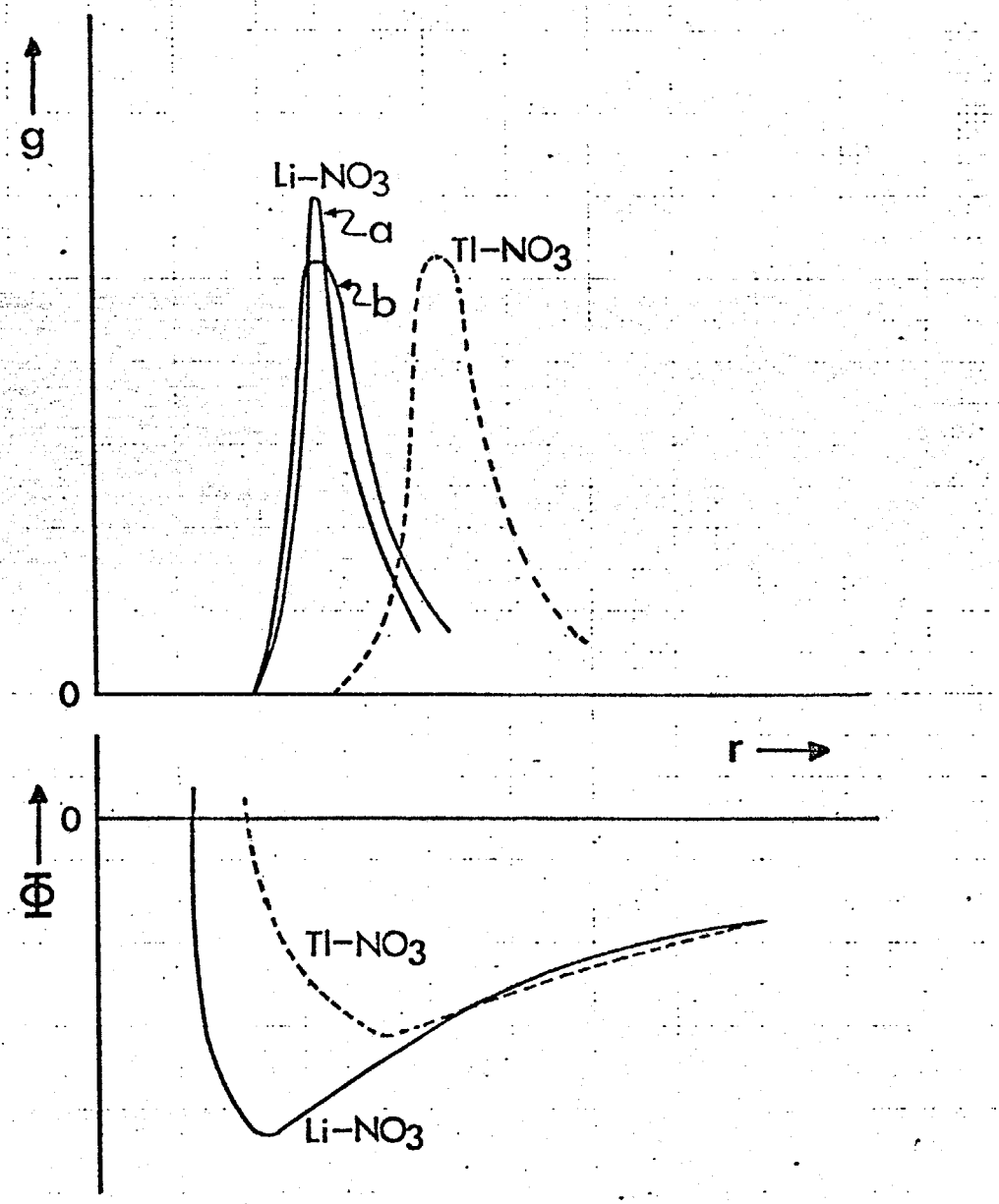

Fig. 6 Schematic representation of the pair distribution function g and of the assumed pair potential between Li^+ and NO_3^- and between Tl^+ and NO_3^-. The curves are sketched in view of the findings with molecular dynamics studies of molten LiCl[19,20], and TlCl[21], the pair potential for the latter being taken from Ref.[33], **a**: low temp., **b**: high temp. For $TlNO_3$, g is much the same at low and high temperatures.

anticipated that Li^+ will be much more mobile than Tl^+, because it is able to move along the surface of the NO_3^- ions and in the Li-NO_3 direction as well. This happens above say 400°C at tracer concentrations of Tl^+, but it cannot be realised experimentally at high $TlNO_3$ concentrations because of thermal decomposition.

As for the isotherms, the Li^+ mobility decreases with increasing concentration of $TlNO_3$, as seen in Figure 3. This may be so partly because the motion of a Li^+ ion around a NO_3^- ion is hindered by the presence of Tl^+ ions, particularly at low temperatures, and partly because the presence of Tl^+ ions will increase the mean distance between nearest neighbouring NO_3^- ions, which is unfavourable for the transfer of the Li^+ ions from one NO_3^- ion to another. On the other hand, in the region very rich in $LiNO_3$, the Tl^+ mobility increases rapidly as the concentration of Tl^+ increases. This may be so because, as the concentration of $TlNO_3$ increases, the volume of the free space increases to a kind of critical volume large enough for a Tl^+ motion. As the concentration increases further, the isotherms slightly decrease, presumably because the volume of the negative free space, which is favourable for Tl^+ motion, decreases due to the presence of more Tl^+ ions. The maximum of the Tl^+ mobility shifts toward higher concentrations of $TlNO_3$ with decreasing temperature. This is accounted for by the assumption that at lower temperatures, the free space being smaller, more $TlNO_3$ is required for enlarging the free space enough for a Tl^+ motion.

Incidentally, the phenomenon that for small concentrations of the larger cation its mobility increases sharply with its concentration has not been found in the systems $NaNO_3$-$TlNO_3$[22,23], $NaNO_3$-$RbNO_3$[24], and $NaNO_3$-$CsNO_3$[25], probably because, the two cations being more equal in

size than in the present system $LiNO_3$-$TlNO_3$, free space for the motion of the larger cation is more readily available.

The anticipation[26] that the diffusion coefficient of Li^+ would always be greater than that of Tl^+ in the mixture is not contradictory to the model presented above. The motion of a Li-NO_3 pair would not contribute to the electrical mobility but to the diffusion coefficient.

Concerning the system $RbNO_3$-$TlNO_3$, a concentration dependence of the relative mobility difference is not detected within the experimental accuracy, as seen in Figure 3. Consequently, the mobilities of both Rb^+ and Tl^+ increase linearly with the concentration of Tl^+ as shown in Figure 5.

A slight but obvious temperature dependence of the relative mobility difference is, however, observed as seen in Figure 3.

For this system, Forcheri and coworkers have previously measured the internal mobilities at 325°C with mole fractions of $TlNO_3$ of about 0.25, 0.5, 0.75 by means of zone electrophoresis[23]. The relative differences in the internal mobilities estimated from the figure they have drawn agree well with the present data (see Figure 3). They have not paid attention, however, to the temperature dependence of this quantity, and thus their presumption that the (internal) "mobilities differ by not more than 6 % for this system" would be too hasty.

In this system, the ionic radii of the two cations are much the same, while the masses are very different. The similar magnitude of the mobilities of the two cations would suggest that the mass would play a minor role compared with the size of the ions. An alternative possibility is that the big difference of the masses would be compensated exactly by the difference of the pair potentials. The former suggestion would be supported by the following facts. Similar mobilities of two cations have also been

found for the system $NaNO_3$-$AgNO_3$[27] in which the radii of the two cations are much the same. In the present experiments, as the free space is enlarged with rising temperature, the relative mobility differences become smaller. Unfortunately, it is impossible on account of the thermal decomposition to see whether the mobilities of Tl^+ and Rb^+ become reversed at still higher temperatures.

In conclusion, in such binary systems as the ones studied here, the volume of the free space in relation to that of the ions would be one of the main factors that affect the mobilities of the ions. When one of the cations is Li^+, the pair potential between Li^+ and the anion with the deep minimum as well as the very small size of Li^+ would have a great influence on the mobility of Li^+.

In the interpretation presented above for the system $LiNO_3$-$TlNO_3$, the pair potential is assumed to be independent of the concentration of the constituent cations, that is to say, the present model does not take into account the assumption in the polarization model[3] that the pair potential between a large cation and an anion be very much affected by a small cation present near the anion. Thus, even if the polarization is ignored or the association model[28-30] is not adopted, the isotherms of the mobilities of two cations in the present binary mixtures could be qualitatively accounted for. Further experiments as well as molecular dynamics studies on such systems as LiCl-CsCl are required to verify the present model.

References

[1] J. Périé and M. Chemla, C.R.Acad.Sci. Paris, 250, 3986 (1960)

[2] J. Périé, M. Chemla, and M. Gignoux, Bull. Soc. Chim. France, 1961, 1249

[3] C.T. Moynihan and R.W. Laity, J. Phys. Chem., 68, 3312 (1964)

[4] O.P. Mehta, F. Lantelme, and M. Chemla, Electrochim. Acta, 14, 505 (1969)

[5] Y. Yamamura and S. Suzuki, J. Nucl. Sci. Technol., 7, 522 (1970)

[6] For nitrates, there are many studies. See e.g. Ref. in A. Lundén, Z. Naturforsch., 25a, 1362 (1970) and J. Richter and E. Amkreutz, Z. Naturforsch., 27a, 280 (1972)

[7] V. Ljubimov and A. Lundén, Z. Naturforsch., 21a, 1592 (1966)

[8] A. Kvist, Z. Naturforsch., 21a, 1221 (1966)

[9] C.T. Moynihan, "Ionic Interactions", Ed. by I. Petrucci, Academic Press, New York 1971, pp. 369

[10] N. Saito, K. Hirano, K. Okuyama, and I. Okada, Z. Naturforsch., 27a, 288 (1972)

[11] A. Cingolani, M.A. Berchiesi, G. Piantoni, and D. Leonesi, Z. Naturforsch., 27a, 159 (1972)

[12] A. Cingolani, G. Berchiesi, and P. Franzosini, Gazz. Chim. Ital., 101, 981 (1971)

[13] A. Klemm, Z. Phys., 123, 10 (1944)

[14] A. Klemm, Z. Naturforsch., 1, 252 (1946)

[15] N.P. Popovskaja, P.I. Protsenko, and A.F. Eliseeva, Russian J. Inorg. Chem., 11, 392 (1966)

[16] S. Brillant, Thesis, Strasbourg (1967)

[17] V. Wagner and S. Forcheri, Z. Naturforsch., 23a, 926 (1968)

[18] L.V. Woodcock and K. Singer, Trans. Faraday Soc., 67, 12 (1971)

[19] Private communication with I. Okada and R. Takagi.

[20] R. Takagi, I. Okada, and K. Kawamura, Bull. Tokyo Inst. Technol., 127, 45 (1975)

[21] Private communication with I. Okada; Report on the 7th EUCHEM Conference in Sweden (1978)

[22] S. Forcheri and V. Wagner, Z. Naturforsch., 22a, 1171 (1967)

[23] S. Forcheri, V. Wagner, and E. Berra, Electrocim. Metallorum, III, 123 (1968)

[24] V.P. Shvedov and I.A. Ivanov, EleKtrokhim., 3, 95 (1967)

[25] V.P. Shvedov and I.A. Ivanov, Elektrokhim., 1, 1479 (1965)

[26] The diffusion coefficient of Tl^+ ion in $LiNO_3$ at very low concentrations of Tl^+ ion is known to be much smaller than the self-diffusion coefficient of Li^+ in $LiNO_3$. See I. Okada and S.E. Gustafsson, Electrochim.A cta, 18, 275 (1973)

[27] F.P. Duke, R.W. Laity, and B. Owens, J. Electrochem. Soc., 104, 299 (1957)

[28] F. Lantelme and M. Chemla, Bull. Soc. Chim. France 1963, 2200

[29] F. Lantelme and M. Chemla, Electrochim. Acta, 10, 663 (1965)

[30] F. Lantelme and M. Chemla, Electrochim. Acta, 11, 1023 (1966)

[31] G.J. Janz, "Molten Salts Handbook", Academic Press, New York 1967

[32] A. Timidei and G.J. Janz, Trans. Faraday Soc., 64, 202 (1968)

[33] J.E. Mayer, J. Chem. Phys., 1, 327 (1933)

CHAPTER 2

High-Dilution Diffusion of K^+, Rb^+, Cs^+, and Tl^+ Ions in Molten (Li-K)NO_3 Sysyem Studied by Wave-Front-Shearing Interferometry.

The high-dilution diffusion coefficients of potassium, rubidium, cesium, and thallous ions in molten lithium nitrate and potassium nitrate mixtures are measured over a wide range of temperatures and concentrations by means of wave-front-shearing interferometry.

A slightly positive deviation from a linear dependence on the concentration is found in the isotherms of the diffusion coefficients of potassium, rubidium, and thallous ions, while no deviation is found in the case of diffusion coefficients of cesium ion. This is qualitatively discussed from the point of view of the ionic radii, the free space formed by the solvent components, and the interaction between the solute ion and the surrounding ions.

1 Introduction

Wave-front-shearing interferometry was first applied to the measurement of diffusion coefficients of molten salts up to 500°C by Gustafsson[1]. In general, when the diffusion coefficients of molten salts are measured, the errors in the measured diffusion coefficients tend to become large because of convection of liquids, the difficulty in setting the well-difined initial and boundary conditions, and so on. The measurement of diffusion coefficients in pure molten salts with wave-front-shearing interferometry was remarkably successful[2-4] with the use of "light ports", the inside of which was properly evacuated (~100 Pa), through the wall of the electric furnace. The light ports enabled the light to travel straight in spite of the temperature gradient between the inside and the outside of the furnace, and made it possible to give reliable data as well as the measurement at room temperature. As the variation of the refractive index in the melt is basically a direct object of the measurement, the temperature distribution in the test part can be controlled within variations less than 0.3°C; if such a temperature disturbance occurs, a fringe is observed in the image of the sample conforming to the following equation (see CHAPTER 4)[5]

$$n_f \approx -\ell (\partial\mu/\partial T) \Delta T/\lambda \quad \text{.....(1)}$$

where n_f is the number of fringes, λ the wavelength of the light (632.8 nm), ℓ the geometric length of the light path through the liquid (20 mm in this research), $(\partial\mu/\partial T)$ the temperature gradient of the refractive index ($\sim 1.5 \cdot 10^{-4} K^{-1}$)[6,7], and ΔT the temperature difference in the system.

Since the refractive index of lithium nitrate differs most from that of potassium nitrate in the group of alkali nitrates[6,7], it

might be of interest to apply this optical method to the measurement of diffusion coefficients in molten (Li-K)NO_3 system. There are some investigations on the tracer diffusion coefficients of Li^+, Na^+, and K^+ in molten (Li-K)NO_3 system with a "diffusion out of a capillary" method by Lantelme and Chemla[8,9]. We have measured the high-dilution diffusion coefficients of K^+, Rb^+, Cs^+, and Tl^+ ions in molten (Li-K)NO_3 system by means of wave-front-shearing interferometry. The influence of ionic radii, the free space, and the interaction between the corresponding ion and the surrounding ions to the diffusion coefficients in molten (Li-K)NO_3 system is qualitatively discussed.

2 Experimental

The principle of wave-front-shearing interferometry and its application to the measurement of diffusion coefficients of molten salts have already been described in detail[1,10].

The optical system of the wave-front-shearing interferometer constructed in our laboratory (see APPENDIX I) was similar to that employed for the measurement of diffusion coefficients of some molten nitrates by Gustafsson et al.[2].

A furnace design is illustrated in Fig. 1. A diffusion cell(A) with a 22 x 3 mm slot was closed tightly from each side by quartz window plates(D) (flatness; less than $\lambda/5$, parallelism; with in 2 seconds of arc) which were pressed against the diffusion cell with aluminum holders and stainless steel screws(F). Leakage of a solvent salt in the slot was prevented. The cell was placed in an electric furnace with a large heat capacity. Evacuated light ports(B) were inserted through the wall of the electric furnace in order to prevent an optical path difference produced by temperature gradients

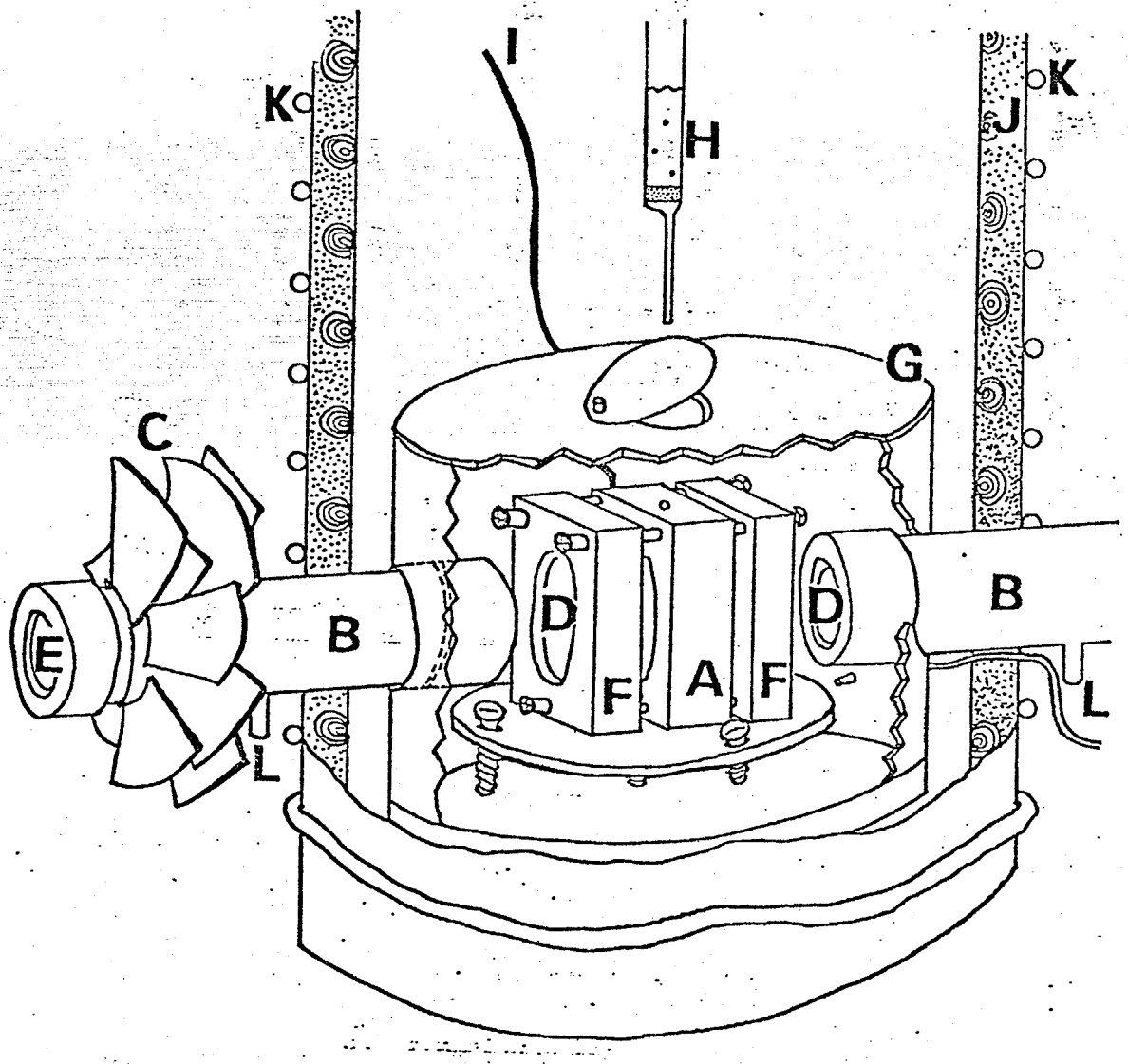

Fig.1 Furnace design

A, diffusion cell; B, light port; C, cooling flanges; D, optical flat (quartz); E, optical flat (BK-7); F, aluminum holder; G, cell container; H, glass tube with a filter; I, thermocouple; J, electric furnace; K, water cooling; L, connection to vacuum pump.

at the wall of the furnace. In order to keep the temperature of the testing materials as constant as possible, the diffusion cell was covered by a small stainless container(G) filled with dried argon. The variation of temperature of the whole diffusion cell during a measurement (20 ~30 min.) was not over 0.5°C. A small amount of the solvent salt(~3g) was melted in a glass tube(H) with a filter and inserted in the slot. After the image of the slot became clear (after ~3 hours), a small solute crystal was dropped into the slot from a position about one meter higher than the top of the diffusion cell. This ensured that the crystal quickly reached the bottom of the slot, resulting in a clearly defined diffusion boundary. The measurement was considered to start when the crystal reached the bottom of the slot. After the image of the shear became clearly detectable, the interferograms were recorded.

How to calculate the diffusion coefficients is described in APPENDIX II.

Crystals of solute were prepared by melting at a temperature about 50°C higher than the melting point of that material in a nitrogen atmosphere and allowing to cool. All chemicals were of analytical reagent grade. The mixtures of lithium nitrate and potassium nitrate solvent salts were dried at 120°C for several hours, once melted at 300°C, and stored in a desiccator. The concentration of the solvent was checked by flame spectrophotometry.

3 Results and Discussion

In the measurement of diffusion coefficients with optical interferometry, the high-dilution diffusion coefficients D are calculated from the refractive index variation caused by the variation of the solute concentration. For this

Table 1 Molar refractivities of molten alkali nitrates at 350°C.

(λ = 632.8 nm)

Salt	Molar weight [9] M / g·mol^{-1}	Density[9] ρ / g·cm^{-3}	Refractive index[8]	Molar refractivity A / cm^3·mol^{-1}
$LiNO_3$	68.95	1.728	1.4547	10.82
$NaNO_3$	85.01	1.875	1.4187	11.44
KNO_3	101.10	1.861	1.4093	13.44
$RbNO_3$	147.49	2.443	1.4165	15.97
$CsNO_3$	194.92	2.894*	1.4409*	17.78

* extrapolated value.

reason, the refractive index difference between the solute and the solvent materials is needed. The refractive indices of alkali nitrates were accurately measured with a modified thermooptic technique by Karawacki[11], and the values of the refractive indices μ and the molar refractivities A calculated from the Lorentz-Lorenz formula (Eq. (2)) at 350°C (λ=632.8 nm) are tabulated in Table 1 together with their molar weight M and the density ρ[12]:

$$A = M/\rho \cdot (\mu^2 - 1)/(\mu^2 + 2) \quad \text{.....(2)}$$

In order to check the influence of the refractive index on the measurement we should know how the refractive index varies with the concentration of the solvent. The concentration dependence of refractive index $(\partial\mu/\partial C)$ can be obtained from the following equation if we know the total amount of substance S diffusing through cross section of the bottom layer, and the wavelength of the light λ[1]:

$$(\partial\mu/\partial C)=k\lambda(\pi Dt)^{1/2}\cdot(S\ell)^{-1}\left\{\exp(-(X_j+b/2)^2/4Dt) - \exp(-(X_j-b/2)^2/4Dt)\right.$$
$$\left. - \exp(-(X_{j+k}+b/2)^2/4Dt) + \exp(-(X_{j+k}-b/2)^2/4Dt)\right\}^{-1} \quad \text{.....(3)}$$

where k is an arbitrary integer equal to the number of the fringes counted from the fringe of a level X_j, and b is the shear produced by the beam splitter of the interferometer. Applying Equation (2) to the mixture, μ is expressed as follows[13];

$$(\mu^2 - 1)/(\mu^2 + 2) = p_1\rho_1A_1/M_1 + (1 - p_1)\rho_mA_m/M_m \quad \text{.....(4)}$$
$$\rho_m = (p_2\rho_2 + p_3\rho_3)/(1 - p_1)$$
$$M_m = (p_2M_2 + p_3M_3)/(1 - p_1)$$

where the subscripts 1, 2, and 3 denote the solute salt and the components of the solvent salts, p the mole fraction ($p_1+p_2+p_3=1$), and A_m the molar refractivity of the solvent mixture[13]. Differentiating the refractive index μ with respect to the concentration of the solute C ($=p_1\rho_1$) in

Equation (4), $(\partial\mu/\partial C)$ is expressed as Equation (5).

$$(\partial\mu/\partial C)=(\partial\mu/\partial x_1)/\rho_1=(3/2)(A_1/M_1-\rho_m A_m/(\rho_1 M_m))(1-p_1\rho_1 A_1/M_1-(1-p_1)\rho_m A_m/M_m)^{-3/2}$$
$$(1+2p_1\rho_1 A_1/M_1+2(1-p_1)\rho_m A_m/M_m)^{-1/2} \quad \cdots\cdots\cdots \quad (5)$$

Neglecting the concentration of the solute, x_1, in Equation (5), the concentration dependence of the refractive index is expressed as

$$(\partial\mu/\partial C)=3(A_1/M_1-\rho_M A_M/\rho_1 M_M)(1-\rho_M A_M/M_M)^{-3/2}(1+2\rho_M A_M/M_M)^{-1/2}/2 \quad \cdots\cdots \quad (6).$$

In Table 2 the calculated values for $(\partial\mu/\partial C)$ of KNO_3, $RbNO_3$, and $CsNO_3$ from Equation (6) at 350°C are shown. The value for $(\partial\mu/\partial C)$ of $TlNO_3$ is calculated from Equation (3) and also tabulated in Table 2. Considering the relationship between the number of the fringes and the concentration of the solute salt with using a similar equation to Equation (1), that is to say,

$$n_f \approx -\ell(\partial\mu/\partial C)\cdot C/\lambda ,$$

the limit value of $(\partial\mu/\partial C)$ is estimated at the magnitude of 10^{-2} cm^3/mol for obtaining the suitable number of fringes in the measurement as long as the length of the cell along the light path is not extended. As can be seen from Table 2, $(\partial\mu/\partial C)$ is very small for the measurement of K^+ in $LiNO_3$25mol%-$KNO_3$75mol% and of Rb^+ in $LiNO_3$51mol%-$KNO_3$49mol%. Since $(\partial\mu/\partial C)$ of $TlNO_3$ was very large compared with that of alkali ions we could obtain much more reliable results in this case. (The refractive index can be calculated to be approximately 1.67 from the results in Table 2.)

The high-dilution diffusion coefficients of K^+ in pure $LiNO_3$ and of Rb^+ and Cs^+ in pure $LiNO_3$ and KNO_3 were also remeasured at some different temperatures in order to assure that there is virtually no systematic difference between the data obtained by the interferometer used by Gustafsson et al.[2] and by ours. The present data are given in Table 3.

The logarithm of the present results in the mixtures of 75, 51, and

Table 2 Concentration dependence of the refractive index $(\partial\mu/\partial C)$ in the system (Li - K)NO_3 at 350°C.

The values of $(\partial\mu/\partial C)$ are given in cm^3/mol, and those in parentheses are given in cm^3/g.

diffusing ion	concentration of $LiNO_3$ (mol %) 100	75	51	25	0
K^+	-2.507 (-0.0248)	-1.233 (-0.0122)	-0.475 (-0.0047)	-0.051 (-0.0005)	———
Rb^+	-2.330 (-0.0158)	-0.929 (-0.0063)	-0.088 (-0.0006)	0.383 (0.0026)	0.442 (0.0030)
Cs^+	-0.936 (-0.0048)	0.604 (0.0031)	1.540 (0.0079)	2.047 (0.0105)	2.105 (0.0108)
Tl^+	11.455 (0.043)	12.521 (0.047)	13.054 (0.049)	13.586 (0.051)	13.586 (0.051)

Table 3 High-dilution diffusion coefficients of K^+ in molten $LiNO_3$ and those of Rb^+ and Cs^+ in molten $LiNO_3$ and KNO_3.

diffusing ion	in $LiNO_3$			in KNO_3		
	T (°C)	$\langle C \rangle$ [a] (mol%)	D x 10^9 [b] ($m^2 s^{-1}$)	T (°C)	$\langle C \rangle$ [a] (mol%)	D x 10^9 [b] ($m^2 s^{-1}$)
K^+	332	0.48	1.85 ± 0.03			
	346	0.52	2.01 ± 0.05			
	349	0.60	1.95 ± 0.06			
	353	0.55	2.00 ± 0.03			
	364	0.63	2.15 ± 0.08			
	370	0.64	2.49 ± 0.08			
Rb^+	332	0.55	1.36 ± 0.06	338	1.77	1.22 ± 0.11
	349	0.78	1.52 ± 0.08	340	1.50	1.22 ± 0.08
	364	0.64	1.68 ± 0.08	348	1.66	1.25 ± 0.08
				348	1.74	1.38 ± 0.04
				349	1.95	1.29 ± 0.07
Cs^+	332	1.81	1.40 ± 0.11	338	0.77	1.15 ± 0.02
	349	1.34	1.50 ± 0.14	348	0.85	1.17 ± 0.03
	364	2.01	1.79 ± 0.11	350	0.73	1.16 ± 0.04
				356	0.89	1.30 ± 0.06
				360	0.93	1.29 ± 0.09

a) This is the concentration at $\sqrt{2Dt}$, i.e. the inflexion point of the concentration curve, t being set as the earliest time when the interferograms are read for the calculation of the diffusion coefficients.

b) The sign ± represents the standard deviation of errors.

25 mol % of $LiNO_3$ component, which are tabulated in Table 4, is plotted against the reciprocal of the absolute temperature in Figs. (2), (3), and (4), respectively. The results for the tracer diffusion of Li^+, Na^+, and K^+ ions by Lantelme and Chemla with a "diffusion out of a capillary" method[8] are also shown in the figure by dashed lines. Since the concentration of the solute is small, the high-dilution diffusion coefficients in the present work may be safely regarded as the thermodynamic mutual diffusion coefficient[14] and identical to the tracer diffusion coefficient. The present results are in fair agreement with those by Lantelme and Chemla. As can be seen from Figs. (2), (3), and (4), D_K is larger than D_{Rb}, D_{Tl}, and D_{Cs}. D_{Rb} and D_{Tl} are larger than D_{Cs}. D_{Tl} seems to be lower than D_{Rb} at relatively low temperatures. This has been clearly found in the region rich in $LiNO_3$[3], in which the free space would be small and the average distance between Rb^+ or Tl^+ ion and the nearest neighbouring NO_3^- ion is rather short. In view of the fact that in the solid state the well of the pair potential between Tl^+ ion and Cl^- ion[15] is somewhat deeper at the minimum than that between Rb^+ ion and Cl^- ion[16] (as shown in Figure 5), although these are quite the same at larger distance (>0.46 nm), Tl^+ ion is expected to be more attracted to NO_3^- ion than Rb^+ ion when the distance between Tl^+ or Rb^+ ion and NO_3^- ion is short. This may be the reason why D_{Tl} is lower than D_{Rb} at lower temperatures. At higher temperatures, D_{Tl} is nearly the same as D_{Rb}. D_{Tl} and D_{Rb} were also found equal in the case of the diffusion in pure $NaNO_3$, KNO_3, and $RbNO_3$ over a wide range of temperatures[4], and in $(Rb-Tl)NO_3$ system at 320°C[17]. This may be explained by the assumption that under these conditions the pair potential for Rb^+-NO_3^- and Tl^+-NO_3^- would be quite the same and that the ionic radii of Rb^+ ion and Tl^+ ion be nearly the same. An Arrhenius type

Table 4 High-dilution diffusion coefficients of K^+, Rb^+, Cs^+, and Tl^+ in the molten (Li-K)NO_3 system.

K^+		Rb^+		Cs^+		Tl^+	
Temp. (°C)	D x10^9 (m^2s^{-1})	Temp. (°C)	D x10^9 (m^2s^{-1})	Temp. (°C)	D x10^9 (m^2s^{-1})	Temp. (°C)	D x10^9 (m^2s^{-1})
			$LiNO_3$ 75mol% - KNO_3 25mol%				
261	1.32 ± 0.05	275	1.21 ± 0.09	297	0.84 ± 0.01	276	1.02 ± 0.04
300	1.65 ± 0.08	296	1.42 ± 0.13	305	1.10 ± 0.07	293	1.24 ± 0.03
300	1.67 ± 0.13	308	1.51 ± 0.07	341	1.21 ± 0.05	294	1.29 ± 0.03
312	1.76 ± 0.08	336	1.65 ± 0.16	345	1.20 ± 0.05	323	1.49 ± 0.02
337	2.09 ± 0.10	337	1.67 ± 0.04	350	1.44 ± 0.01	333	1.61 ± 0.01
352	2.14 ± 0.17	351	1.94 ± 0.05	376	1.54 ± 0.07	356	1.76 ± 0.08
376	2.67 ± 0.15	377	2.31 ± 0.11	380	1.78 ± 0.08	372	2.11 ± 0.01
388	2.73 ± 0.10					376	2.35 ± 0.02
						391	2.48 ± 0.04
						395	2.57 ± 0.04
						397	2.30 ± 0.08
			$LiNO_3$ 51mol% - KNO_3 49mol%				
260	0.98 ± 0.01	271	1.23 ± 0.08	259	0.70 ± 0.02	264	0.85 ± 0.04
280	1.13 ± 0.01	284	1.26 ± 0.10	265	0.70 ± 0.01	294	1.13 ± 0.02
282	1.30 ± 0.05	295	1.41 ± 0.12	290	0.94 ± 0.01	318	1.32 ± 0.04
284	1.26 ± 0.03	324	1.67 ± 0.05	293	0.98 ± 0.02	339	1.53 ± 0.08
305	1.67 ± 0.08	341	1.81 ± 0.07	315	1.01 ± 0.01	347	1.49 ± 0.01
308	1.55 ± 0.03	359	1.93 ± 0.05	317	1.11 ± 0.02	363	1.78 ± 0.04
325	2.03 ± 0.09	378	2.04 ± 0.09	358	1.34 ± 0.02	365	1.84 ± 0.12
338	2.18 ± 0.11			361	1.37 ± 0.03	370	1.82 ± 0.06
357	2.36 ± 0.18					382	1.88 ± 0.05
363	2.64 ± 0.11						
382	2.97 ± 0.12						
387	2.71 ± 0.11						
			$LiNO_3$ 25mol% - KNO_3 75mol%				
268	1.13 ± 0.09	261	0.94 ± 0.07	272	0.65 ± 0.03	267	0.88 ± 0.02
284	1.51 ± 0.16	284	1.07 ± 0.09	286	0.64 ± 0.01	323	1.34 ± 0.02
310	1.62 ± 0.12	306	1.15 ± 0.10	303	0.82 ± 0.02	336	1.45 ± 0.01
342	1.85 ± 0.13	346	1.41 ± 0.08	341	1.13 ± 0.02	338	1.46 ± 0.01
345	1.73 ± 0.10	359	1.69 ± 0.13	350	1.12 ± 0.02	358	1.67 ± 0.03
398	2.42 ± 0.13	394	2.29 ± 0.14	350	1.25 ± 0.04	368	1.69 ± 0.01
				369	1.29 ± 0.02	372	1.82 ± 0.02
				387	1.33 ± 0.08	384	1.94 ± 0.03
				395	1.45 ± 0.02		

The sign ± represents the standard deviation of errors.

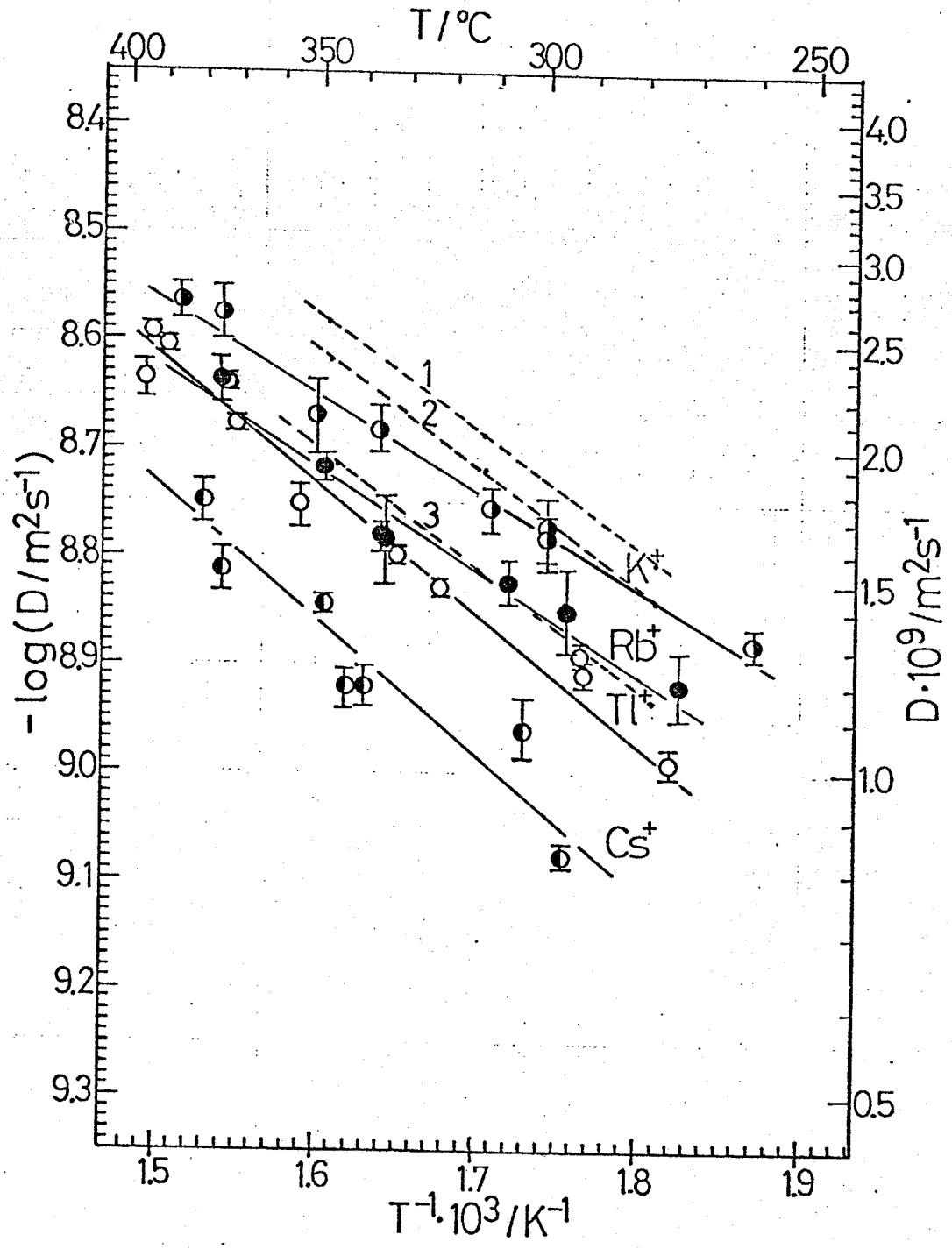

Fig. 2 High-dilution diffusion coefficients of alkali ions and Tl^+ ion in the molten $LiNO_3$ 75mol%-KNO_3 25mol% mixture. ⊕ : K^+, ⊕ : Rb^+, ⊕ : Cs^+, ⊕ : Tl^+; the dashed line: tracer diffusion coefficients[8]. 1 - Li^+, 2 - Na^+, 3 - K^+.

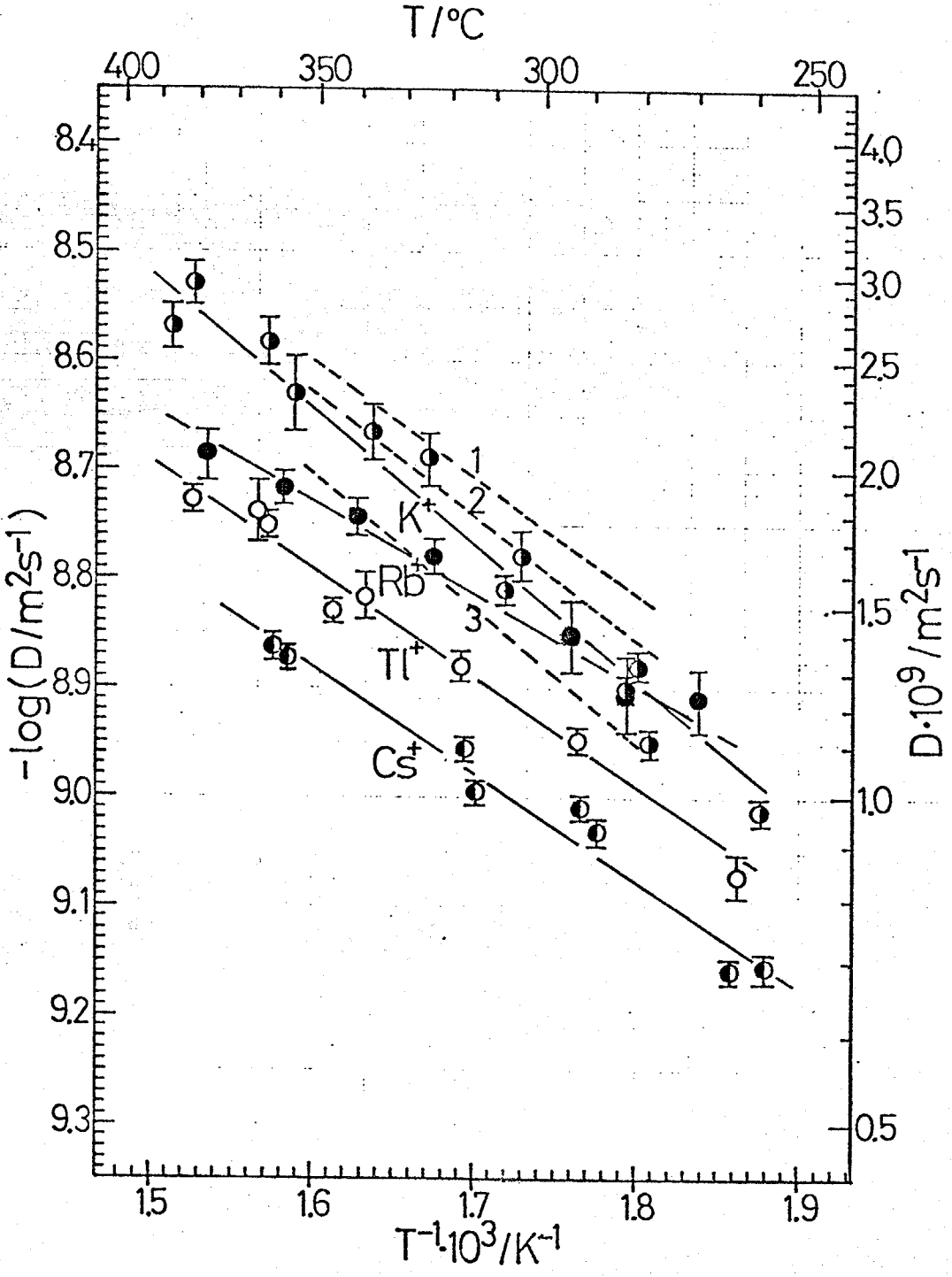

Fig. 3 High-dilution diffusion coefficients of alkali ions and Tl^+ ion in the molten $LiNO_3$ 51mol%-KNO_3 49mol% mixture. ⊕ : K^+, ● : Rb^+, ⊕ : Cs^+, ○ : Tl^+; the dashed line: tracer diffusion coefficients[8]. 1 - Li^+, 2 - Na^+, 3 - K^+.

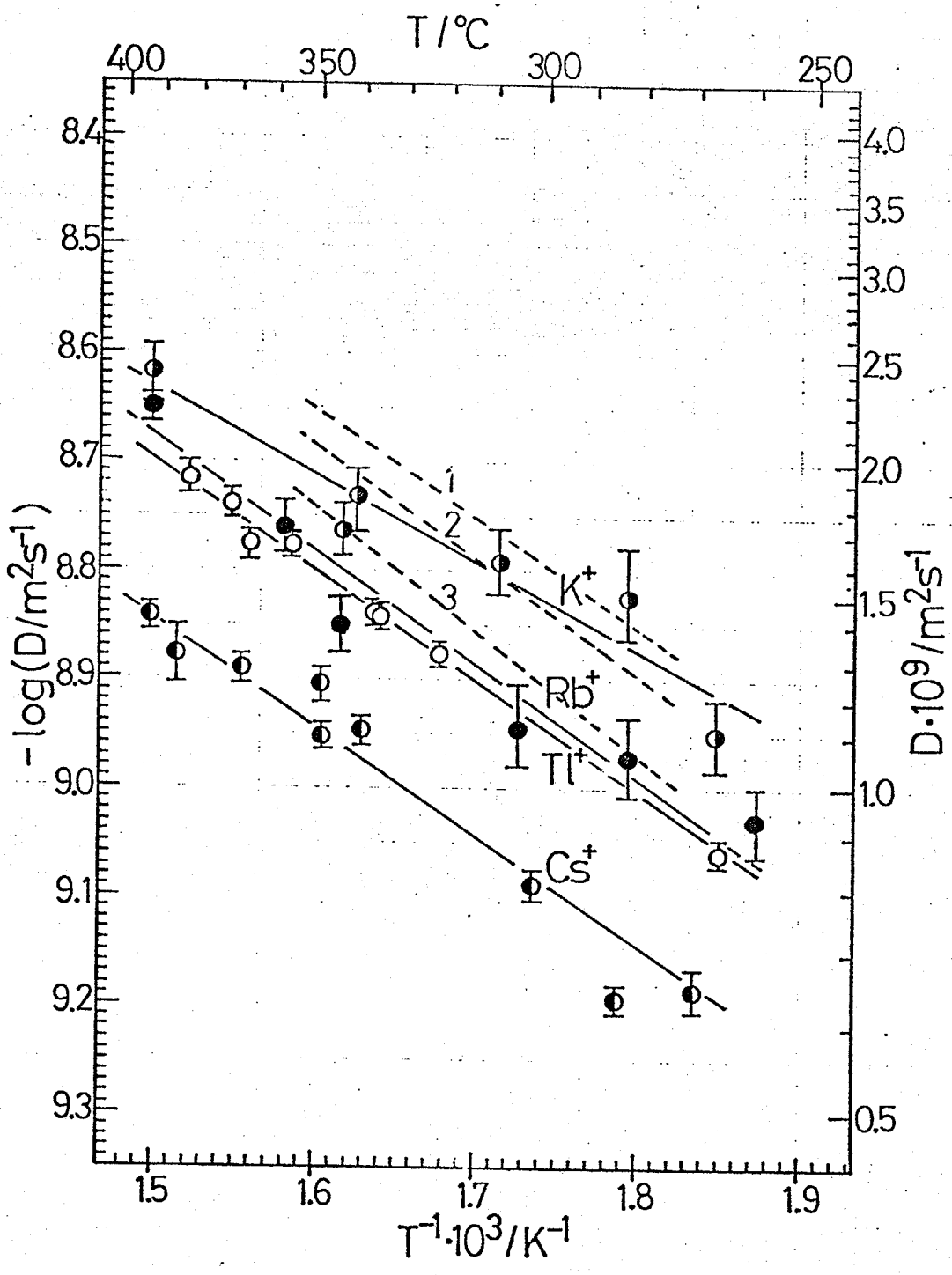

Fig. 4 High-dilution diffusion coefficients of alkali ions and Tl^+ ion in the molten $LiNO_3$25mol%-KNO_3mol% mixture. ⊕: K^+, ●: Rb^+, ⊖: Cs^+, ○: Tl^+; the dashed line: tracer diffusion coefficients[8]. 1 - Li^+, 2 - Na^+, 3 - K^+.

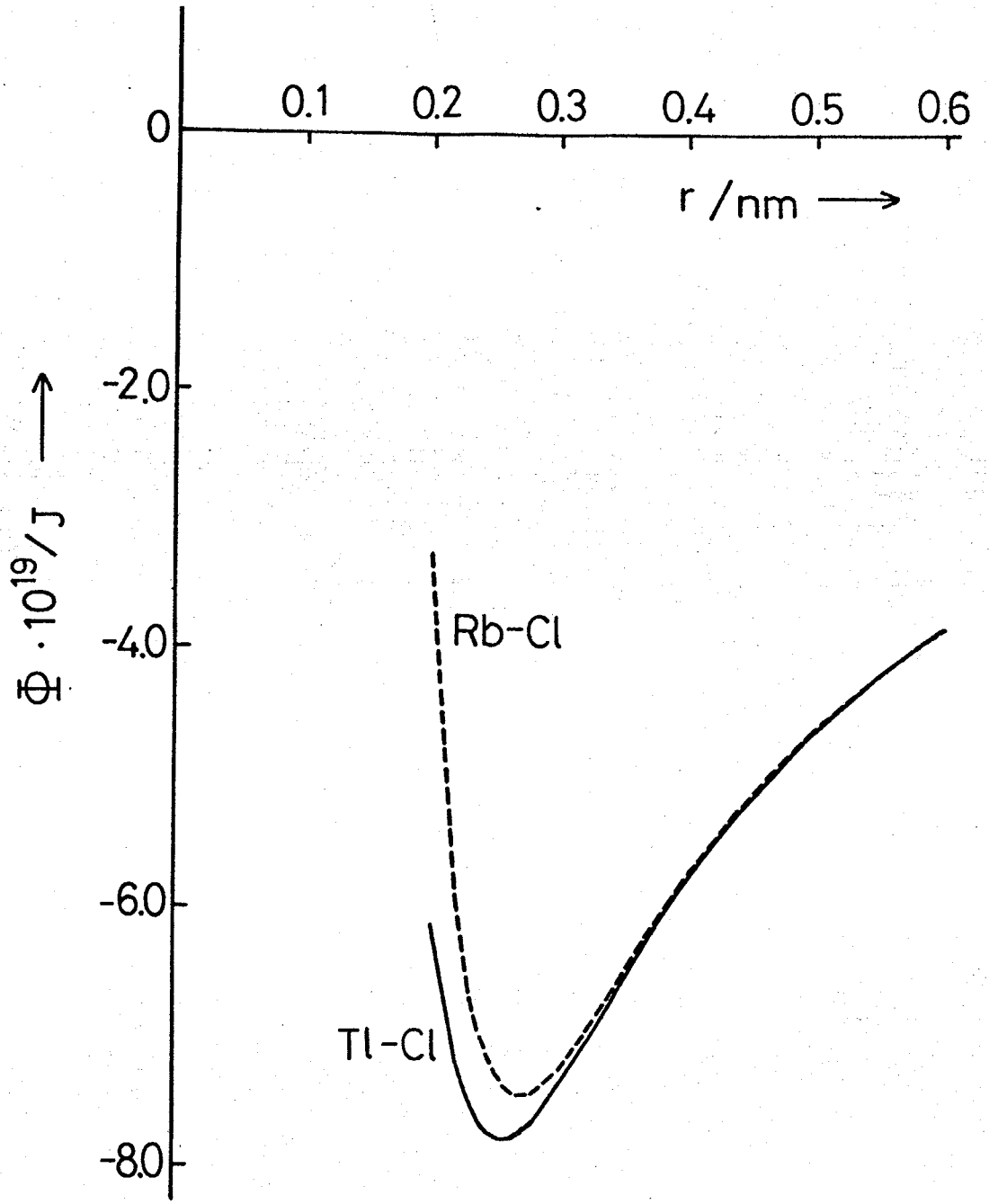

Fig. 5 Schematic representation of the pair potential between Rb^+ and Cl^- and between Tl^+ and Cl^-.

equation $D = D_\infty \exp(-E/RT)$ is assumed for D, and D_∞ and E are calculated with a non-linear least squares method. The results are tabulated in Table 5. In Table 5, D_∞ and E of D_{Tl} in pure $LiNO_3$ and KNO_3 are taken from Refs. [3] and [4], and those of D_K in KNO_3 are from Ref. [18]. Those of D_{Rb} and D_{Cs} in pure $LiNO_3$ and KNO_3 and of D_K in pure $LiNO_3$ were recalculated based on the data by Gustafsson et al.[2] and ours.

The high values of D_{Rb} in $LiNO_3$51mol%-$KNO_3$49mol% compared with D_{Tl} might be caused by the high amount of the solute concentration (5~8 mol%), which is inevitable if a suitable number of fringes has to be obtained, since $(\partial\mu/\partial C)$ of $RbNO_3$ is small in $LiNO_3$51mol%-$KNO_3$49mol%.

The isotherms of D_K, D_{Rb}, D_{Cs}, and D_{Tl} are shown in Fig. 6 at 350°C. The results for D_{Li}, D_{Na}, and D_K by Lantelme et al. are also shown in the figure. Although the present results of D_K are about 10% higher than those by Lantelme and Chemla, the tendency of the concentration dependence of them was almost similar in these region. As can be seen from Fig.6, the diffusion coeficients of monovalent cations in (Li-K)NO_3 system at 350°C lie in the following order;

$$D_{Li} > D_{Na} > D_K > D_{Rb} \gtrsim D_{Tl} > D_{Cs}$$

The concentration dependence of D_K, D_{Tl}, and D_{Rb} deviates positively from the "ideality". Meanwhile, D_{Li}, D_{Na}, and D_{Cs} are almost linearly dependent on the concentration of the solvent. In order to interpret the concentration dependence of D of those monovalent cations, two effects are taken into account. One is the effect by the solvent ions surrounding the diffusing ion. This makes the motion of the diffusing ion more mobile with increasing $LiNO_3$ concentration because the diffusive motion of the solvent ions becomes more active[19]. The other one is the effect of the free space formed by the solvent ions, which acts on the diffusing ion itself

Table 5 Parameters of Arrhenius type equation $D_\infty \times \exp(-E/RT)$. Arrhenius coefficients $E \cdot 10^{-4}$ are given in J/K·mol and pre-exponential constants $D_\infty \cdot 10^{7}$ in parentheses are given in m^2/s.

diffusing ion	concentration of $LiNO_3$ (mol %) 100	75	51	25	0
K^+	2.26 ± 0.25 (1.67)	1.80 ± 0.10 (0.70)	2.36 ± 0.18 (2.11)	1.52 ± 0.20 (0.38)	2.30 (1.32)
Rb^+	2.05 ± 0.11 (0.85)	1.87 ± 0.19 (0.69)	1.46 ± 0.08 (0.31)	2.01 ± 0.25 (0.78)	1.97 ± 0.13 (0.65)
Cs^+	2.07 ± 0.15 (0.86)	2.29 ± 0.40 (1.12)	1.77 ± 0.13 (0.40)	2.00 ± 0.18 (0.54)	2.18 ± 0.15 (0.73)
Tl^+	2.84 ± 0.14 (3.95)	2.34 ± 0.17 (1.66)	1.97 ± 0.13 (0.72)	2.00 ± 0.08 (0.70)	1.88 ± 0.14 (0.54)

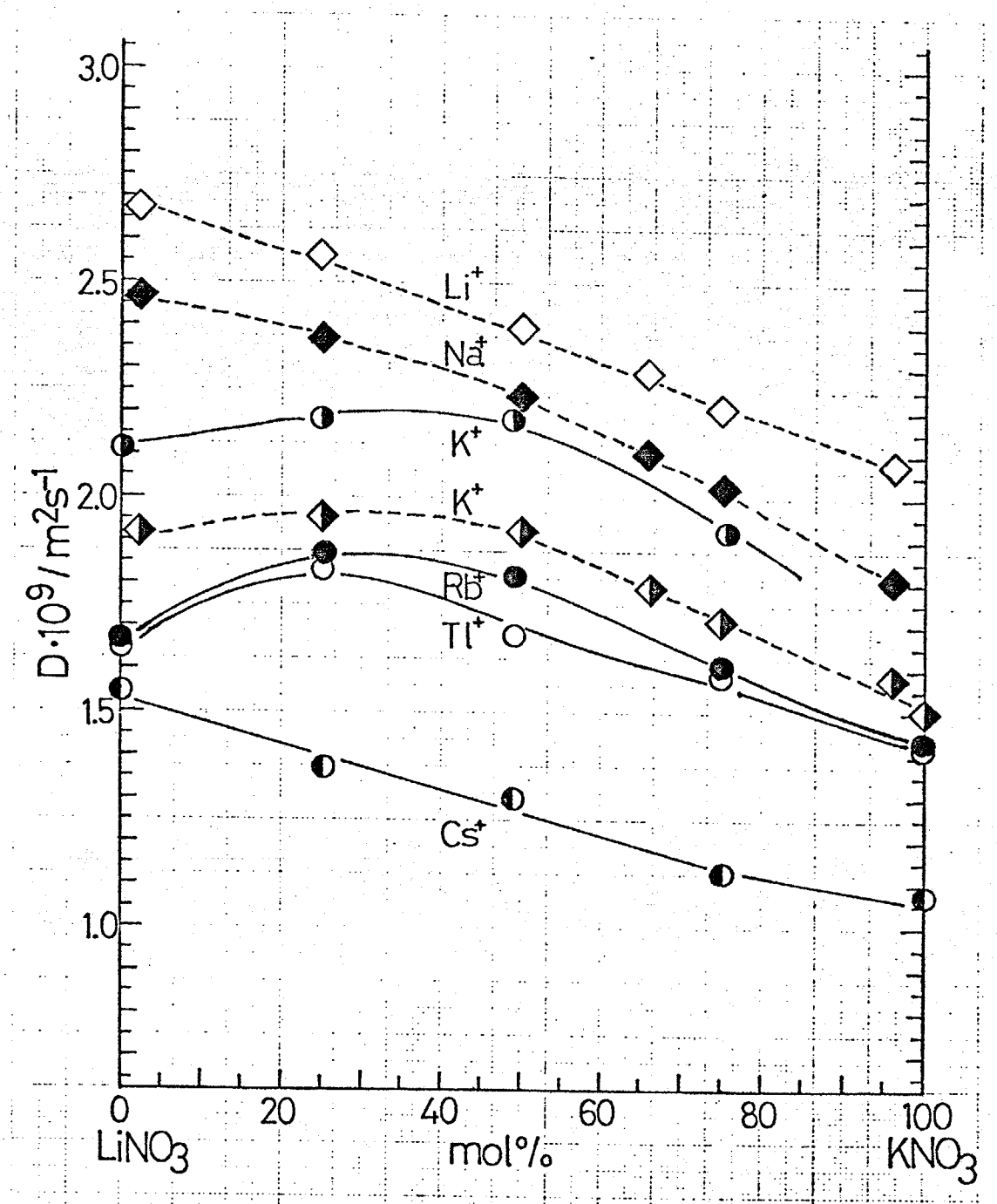

Fig. 6 Isotherms of the diffusion coefficients of alkali ions and Tl^+ ion in the molten (Li-K)NO_3 system at 350 °C.

◑ : K^+, ● : Rb^+, ○ : Tl^+, ◐ : Cs^+, ———— Present work

◇ : Li^+, ◆ : Na^+, ◑ : K^+, ---------- Lantelme and Chemla[8].

to become less mobile with increasing $LiNO_3$ concentration. The molar volume of molten (Li-K)NO_3 system is linearly dependent on the concentration[20]. Therefore, the free space of this system is supposed to be proportional to the change of the molar volume and become small with increasing $LiNO_3$ concentration. Since the sizes of Li^+ ion and Na^+ ion are small compared with the free space available in $LiNO_3$ and KNO_3 mixtures, it is expected that the effect of the free space would not influence the motion of Li^+ and Na^+ in these mixtures so much. Therefore, D_{Li} and D_{Na} would become larger with $LiNO_3$ concentration due to the effect of the solvent ions. To the motion of the diffusing ion, which is somewhat larger than the solvent ions (cations in this case) such as K^+, Rb^+, and Tl^+ions, the effect of the free space might pronouncedly contribute in a $LiNO_3$ rich region because the motion of the larger ion than Li^+ ion is strongly hindered in the high concentration of $LiNO_3$. In data for the internal mobility of Tl^+ or Rb^+ ion in the system of (Li-Tl)NO_3 (see CHAPTER 1)[21] or (Li-Rb)NO_3[22], respectively, the effect of the free space can also be seen at high $LiNO_3$ concentrations, where the mobility decreases drastically. Thus, it is expected that D_K, D_{Rb}, and D_{Tl} first increase with adding $LiNO_3$ to KNO_3, and in the region rich in $LiNO_3$ they decrease mainly due to the influence of the free space. For Cs^+ ion, the free space formed by the mixture of $LiNO_3$ and KNO_3 seems to be small compared with the size of Cs^+ ion. Therefore, the effect of the free space would not play an important role as it does for K^+, Rb^+, and Tl^+ ions in the region rich in $LiNO_3$, and D_{Cs} would increase almost linearly with increasing $LiNO_3$ concentration.

Thus, the diffusion coefficients of alkali ions and Tl^+ ion in the mixture of $LiNO_3$-KNO_3 can be qualitatively interpreted with the simple assumption that the size of the free space compared with that of diffusing

ions and the pair potential between cation and anion would be the main factors which rule a diffusion process as well as an electromigration process (discussed in CHAPTER 1)[21,22].

A positive deviation of the diffusion coefficients from "ideality" has been found also in the measurement of D_{Ag} in $(Li-K)NO_3$ system at 350°C with chronopotentiometry[23] and in the measurement of D_{Na} and D_{Tl} in $(Na-Tl)NO_3$ system at 316°C by Forcheri and Wagner[24], although this is in contract with the large negative deviation of D_{Na} and D_{Tl} found by Zuca and Constantinescu[17]. The latter observation can not be explained with the present model. Diffusion coefficients of Rb^+ and Cs^+ ions have been measured in $(Li-Na)NO_3$, $(Li-K)NO_3$, $(Li-Rb)NO_3$, and $(Li-Cs)NO_3$ systems with a paper strip method (see CHAPTER 3)[25]; the results can also be explained with the present model.

References

[1] S. E. Gustafsson, L.-E. Wallin, and T. E. G. Arvidsson, Z. Naturforsch., 23a, 1261 (1968)

[2] T. E. G. Arvidsson, S.-Å. Afsenius, and S. E. Gustafsson, J. Chem. Phys., 53, 2621 (1970)

[3] I. Okada and S. E. Gustafsson, Electrochim. Acta, 18, 275 (1973)

[4] I. Okada and S. E. Gustafsson, Z. Naturforsch., 33a, 447 (1978)

[5] O. Odawara, I. Okada, and K. Kawamura, J. Chem. Eng. Data, 22, 222 (1977)

[6] S. E. Gustafsson, and E. Karawacki, Appl. Opt., 14, 1105 (1975)

[7] E. Karawacki, and S. E. Gustafsson, Z. Naturforsch., 31a, 956 (1976)

[8] F. Lantelme, and M. Chemla, C. R. Acad. Sc. Paris, 258, 1484 (1964)

[9] F. Lantelme, and M. Chemla, Electrochim. Acta, 11, 1023 (1966)

[10] O. Bryngdahl, Ark. Fys., 21, 289 (1962)

[11] E. Karawacki, Thesis, Chalmers University of Technology, Sweden (1977)

[12] G. J. Janz, "Molten Salts Handbook", Academic Press, New York, N. Y. p 42 (1967)

[13] M. Born and E. Wolf, "Principles of Optics", Pergamon Press, Oxford p 89 - 90 (1964)

[14] R. W. Laity, J. Phys. Chem., 63, 80 (1959)

[15] J. E. Mayer, J. Chem. Phys., 1, 327 (1933)

[16] J. E. Mayer, J. Chem. Phys., 1, 270 (1933)

[17] S. Zuca, and M. Constantinescu, Z. Naturforsch., 32a, 1435 (1977)

[18] A. S. Dworkin, R. B. Escue, and E. R. Van Artsdalen, J. Phys. Chem., 64, 872 (1960)

[19] According to the molecular dynamics simulation in (Li-Rb)Cl equimolar mixture and in the pure salts, the separating velocity between an Rb^+

ion and a Cl^- ion in the mixture is faster than that in the pure RbCl.

[20] I. G. Murgulescu, and S. Zuca, Electrochim. Acta, 11, 1383 (1966)

[21] K. Kawamura, I. Okada, and O. Odawara, Z. Naturforsch., 30a, 69 (1975)

[22] I. Okada, R. Takagi, and K. Kawamura, to be published.

[23] K. Kawamura, Denki Kagaku, 38, 12 (1970)

[24] S. Forcheri, and V. Wagner, Z. Naturforsch., 22a, 1171 (1967)

[25] O. Odawara, J. C. T. Kwak, and J. A. A. Ketelaar, to be published.

CHAPTER 3

Diffusion Coefficients of Rb^+ and Cs^+ Ions in the Binary Molten Alkali Nitrate Systems at 350 °C.

The tracer diffusion coefficients of ^{86}Rb and ^{137}Cs ions have been measured by a paper strip method in the molten $(Li\text{-}Na)NO_3$, $(Li\text{-}K)NO_3$, $(Li\text{-}Rb)NO_3$, and $(Li\text{-}Cs)NO_3$ systems at 350 °C. The isotherm of the diffusion coefficents is found to be almost linearly dependent on the solvent concentrations except that of ^{86}Rb ion in the molten $(Li\text{-}K)NO_3$. The concentration dependence of the obtained diffusion coefficients is discussed from standpoints of the free space formed by the solvent system and the ionic interaction between the diffusing ion and the surrounding ions. The Stokes-Einstein relation between viscosity and diffusion coefficient is discussed.

1 Introduction

Although a relatively large number of papers dealing with the diffusion coefficient D in binary molten nitrate systems have been published in recent years, only a little progress has been made towards explaining the diffusion coefficient isotherms. In Table 1, all the diffusion experiments reported since 1965 in the literature for the binary molten nitrate systems[1-19] are listed, including the type of the method employed and the substances investigated. In order to explain the observed characteristics of the diffusion coefficient isotherms, the anion polarization model[20,21] or the association model[3] has been adopted by several authors with the assumption that the ionic radius, the polarizability, and the mass of the diffusing ion are the main factors to determine the rate of diffusion. However, considering the fact that D_{Rb} and D_{Tl} in the pure nitrates[19,22] and in the nitrate mixtures[6,18] are almost the same in spite of the large difference in their masses and polarizabilities, it is supposed that the size of the diffusing ion is more significant for the explanation of the diffusion process than the mass or the polarizability.

In the present work, the tracer diffusion coefficients of ^{86}Rb and ^{137}Cs ions in the molten (Li-Na)NO_3, (Li-K)NO_3, (Li-Rb)NO_3, and (Li-Cs)NO_3 systems at 350 °C have been measured by means of a paper strip method. The obtained values of D_{Rb} and D_{Cs} are qualitatively explained in terms of the size difference of the diffusing ion from the free space formed by the solvent system and the interaction between the diffusing ion and the surrounding ions.

Table 1. Experiments performed to determine the diffusion coefficients in the binary molten nitrate systems since 1965.

Author and (year)[Ref.]	type of method	solute ion	solvent
Sjoblom(1965)[1]	porous frit	Ag^+	$(Ag-K)NO_3$
Lantelme(1965)[2]	diff. out of capillary	Na^+, K^+	$(Na-K)NO_3$
Lantelme & Chemla(1966)[3]	diff. out of capillary	Li^+,Na^+,K^+,NO_3^-	$(Li-K)NO_3$
Honig & Ketelaar(1966)[4]	paper strip	Na^+, K^+	$(Na-K)NO_3$
Forcheri & Wagner(1967)[5]	zone diffusion	Na^+, Tl^+	$(Na-Tl)NO_3$
Forcheri & Wagner(1968)[6]	zone diffusion	Na^+,Tl^+,Rb^+	$(Na-Rb)NO_3$,$(Na-Tl)NO_3$
Ketelaar & Kwak(1969)[7]	paper strip	Na^+, Cs^+	$(Na-Cs)NO_3$
Bowcott & Plunkett(1969)[8]	linear diff. cell of variable path length	Ag^+	$(Na-K)NO_3$
Sternberg & Herdlicka(1969)[9]	chronopotentiometry	Ag^+	$(Li-K)NO_3$
Kawamura(1970)[10]	chronopotentiometry	Ag^+	$(Li-K)NO_3$
Andreasson, Behn & Sjoblom(1970)[11]	gravimetric porous frit	interdiff.	$(Na-Ag)NO_3$,$(Na-Rb)NO_3$
Mazzocchin & Schiavon(1972)[12]	chronopotentiometry	Ag^+,Cl^-,Br^-,I^-	$(Li-K)NO_3$, $(Ca-K)NO_3$
Zuca & Constantinescu (1973)[13]	diff. into capillary	Ag^+,Na^+,K^+	$(Ag-Na)NO_3$,$(Ag-K)NO_3$
Richter(1973)[14]	diaphragm cell	interdiff.	$(Na-Ag)NO_3$,$(Li-Ag)NO_3$
Zuca & Constantinescu (1974)[15]	diff. into capillary	Ag^+,Li^+,Na^+, K^+,Rb^+,Cs^+	(Ag- Li,Na,K,Rb,Cs)NO_3
Kawamura(1974)[16]	chronopotentiometry	Ag^+	$(Li-Cs)NO_3$,$(K-Cs)NO_3$
Emons, Brautigam, & Winger(1976)[17]	diff. into capillary	Na^+	$(Na-Rb)NO_3$
Zuca & Constantinescu (1977)[18]	diff. into capillary	Na^+,Tl^+,Rb^+	$(Na-Tl)NO_3$,$(Tl-Rb)NO_3$
Okada & Gustafsson (1978)[19]	optical interferometry	Tl^+	$(Na-Tl)NO_3$

The paper strip method used in the present work is an application of a paper electrophoresis mehtod, which was originally developed by Arnikar[23] and improved by Honig[24] and Kwak[25] for the measurement of ionic mobilities of molten salts and for also the measurement of diffusion coefficients. The measurement with the paper strip method is rather simpler than that with other methods[26-31]. Since several series of experiment can be performed at the same time with the same experimental atmosphere, it is expected that this method is very useful to investigate the diffusion coefficient isotherms.

2 Experimental

The principle of a paper strip method and its application to the measurement of diffusion coefficients in molten salts have already been described in detail elsewhere[24,25].

A furnace design is shown in Fig. 1. A strip of glass fibre paper(A) (120 x 5 x 0.2 mm) impregnated with the solvent salt was placed on a supporting Pyrex glass plate(B), which was placed horizontally on an aluminum tray in an electric furnace. The experiment was initiated by dropping a small crystal of the tracer salt (1 mg) on the center of the strip through a stainless tube(D). The tracers used in the present work were ^{86}Rb ($T_{1/2}$= 19 days) and ^{137}Cs ($T_{1/2}$= 33 years) purchased from The Radiochemical Center Ltd. in England, which were prepared as a nitrate type (about 50 μCi/g). After 18~20 hours diffusion, the paper strip was quickly removed from the furnace and allowed to cool for solidifying the impregnated salts.

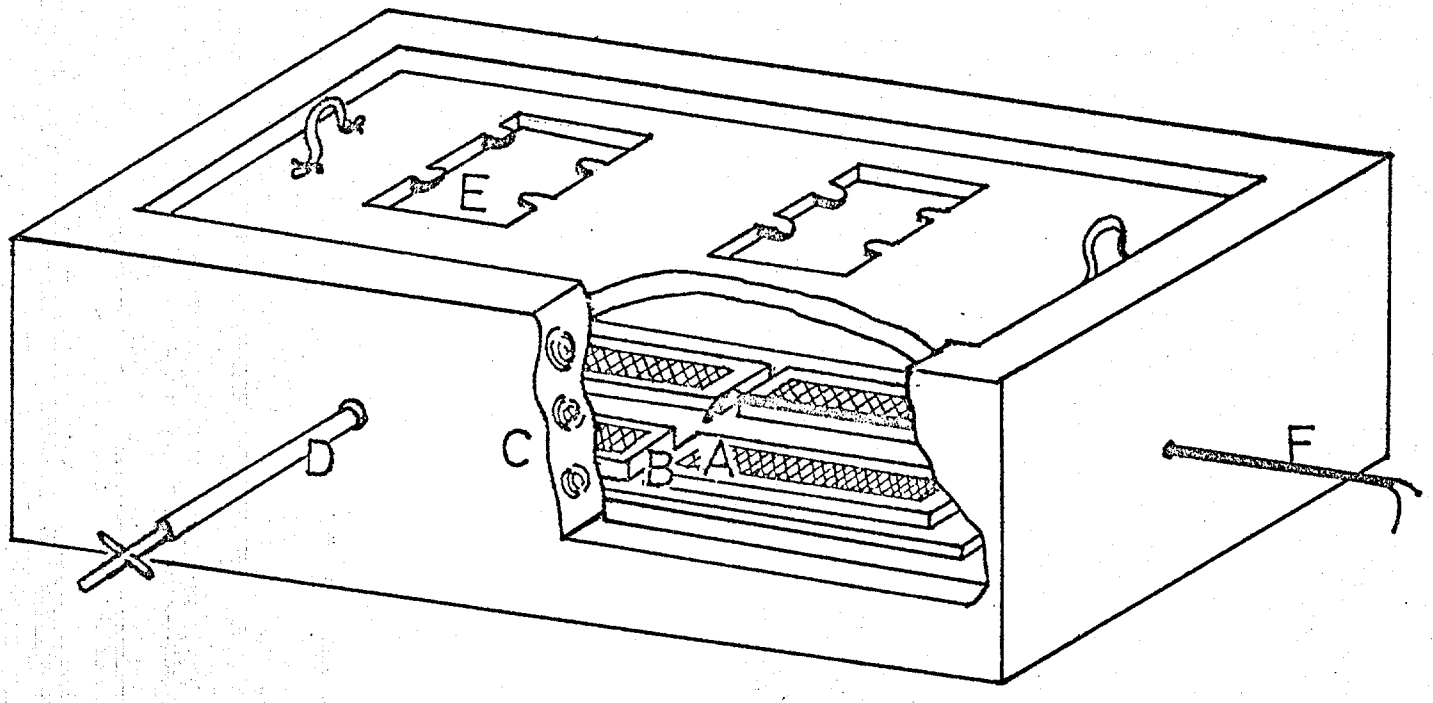

Fig.1 Furnace design.
A: paper strip, B: glass plate (Pyrex),
C: electric furnace, D: stainless tube,
E: glass window, F: thermocouple,

The distribution of the radioactivity in the paper strip was measured at 2 mm or 4 mm intervals by means of a GM counter, and D was calculated from the following equation with the obtained tracer distribution curve;

$$C(x,t) = S \exp(-x^2/4Dt)/2\sqrt{\pi Dt} \quad \ldots\ldots\ldots (1)$$

where C is the concentration of the solute (≡ the radioactivity) at the distance x, S the total amount of the solute, and t the diffusion time. The value of D was determined from the gradient of ln C against x^2.

All chemicals were of analytical reagent grade and fully dried before use without further purification. The mixtures were prepared by directly weighing each component.

3 Results and Discussion

In Table 2, D_{Cs} in pure $LiNO_3$, $NaNO_3$, and KNO_3 are given with the experimental conditions. The mean concentration shown in Table 2 is the concentration of the solute at the inflexion point of Eq. (1), $\sqrt{2Dt_f}$, where t_f is the duration of diffusion. In Fig. 2, 3, and 4 the logarithm of the present results is plotted against the reciprocal of the absolute temperature with the data previously measured with a paper strip method [24,32]. There are no available data for D_{Cs} in these solvent by other methods except those by optical interferometry[33], which are also plotted in the figures for comparison. Since D by optical interferometry is regarded as the thermodynamic mutual diffusion coefficient[34] because of the quite low concentration of the solute (<1 mol % in most cases), D obtained by the present method (i.e., tracer diffusion coefficient) may be identical with that by optical interferometry. The reproducibility

Table 2 Conditions and the results of D_{Cs} in the molten $LiNO_3$, $NaNO_3$, and KNO_3.

Temp.(°C)	Diffusion duration(s)	Weight of solvent(gcm^{-1})	Mean concentration(mol %)	D_{Cs} $x10^9(m^2s^{-1})$
		$LiNO_3$		
280	62100	0.0343	0.26	1.21 ± 0.09
280	62100	0.0328	0.27	1.14 ± 0.06
339	65220	0.0325	0.23	1.60 ± 0.03
339	65220	0.0314	0.24	1.55 ± 0.06
347	65200	0.0304	0.25	1.57 ± 0.03
350	72400	0.0278	0.25	1.67 ± 0.05
350	63360	0.0393	0.18	1.72 ± 0.02
350	63360	0.0373	0.20	1.66 ± 0.06
350	58980	0.0306	0.25	1.68 ± 0.08
379	61020	0.0307	0.22	1.99 ± 0.07
379	61020	0.0350	0.19	2.09 ± 0.10
		$NaNO_3$		
311	68400	0.0374	0.25	1.47 ± 0.08
346	64800	0.0324	0.27	1.78 ± 0.05
346	64800	0.0367	0.24	1.78 ± 0.08
373	55020	0.0351	0.24	2.22 ± 0.01
399	63300	0.0329	0.22	2.62 ± 0.06
400	57600	0.0378	0.21	2.42 ± 0.11
408	64980	0.0420	0.18	2.40 ± 0.18
427	54000	0.0285	0.27	2.72 ± 0.12
427	54000	0.0339	0.22	2.89 ± 0.13
		KNO_3		
339	65220	0.0283	0.42	1.33 ± 0.06
339	65220	0.0305	0.38	1.40 ± 0.08
346	70200	0.0339	0.33	1.45 ± 0.01
346	70200	0.0311	0.35	1.50 ± 0.02
346	70200	0.0339	0.32	1.54 ± 0.02
350	63360	0.0329	0.35	1.44 ± 0.04
350	63600	0.0297	0.39	1.48 ± 0.04
350	63600	0.0300	0.39	1.44 ± 0.03
350	70200	0.0303	0.36	1.45 ± 0.06
350	70200	0.0347	0.32	1.44 ± 0.02
350	67200	0.0327	0.35	1.44 ± 0.01
376	64740	0.0381	0.27	1.85 ± 0.01
376	59520	0.0389	0.27	1.83 ± 0.01
376	59520	0.0405	0.25	1.96 ± 0.12
380	62400	0.0298	0.36	1.73 ± 0.02
380	62400	0.0303	0.33	1.93 ± 0.02
427	52500	0.0393	0.25	2.39 ± 0.15
427	52500	0.0369	0.28	2.28 ± 0.02

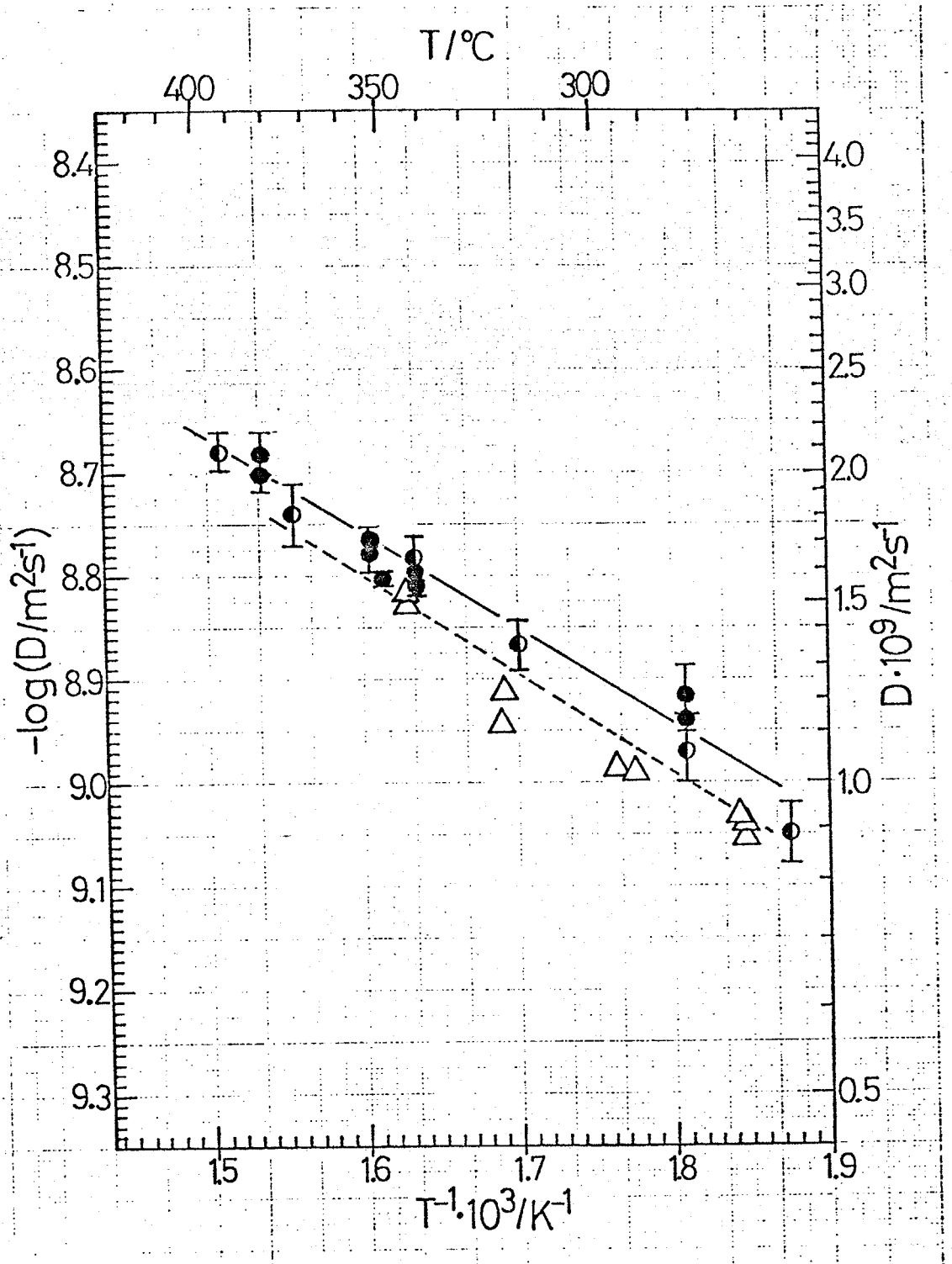

Fig. 2 Diffusion coefficients of Cs^+ ion in the molten $LiNO_3$. ● : Present work, ⊖ : Ref. [32](a paper strip method), △ : Ref. [33](optical interferometry).

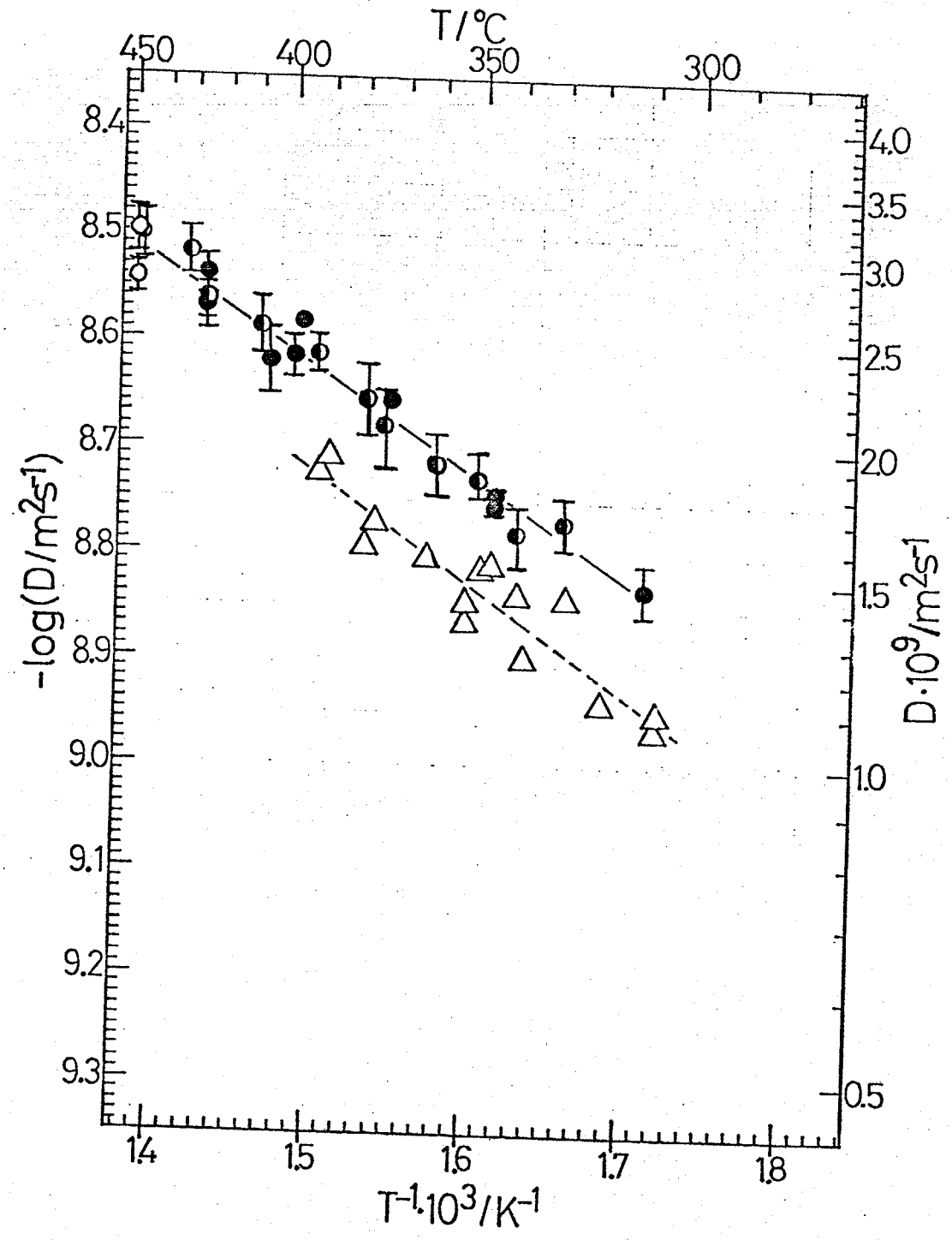

Fig. 3 Diffusion coefficients of Cs^+ ion in the molten $NaNO_3$. ● : Present work, ○ : Ref. [24](a paper strip method), ◐ : Ref. [32](a paper strip method), △ : Ref. [33](optical interferometry)

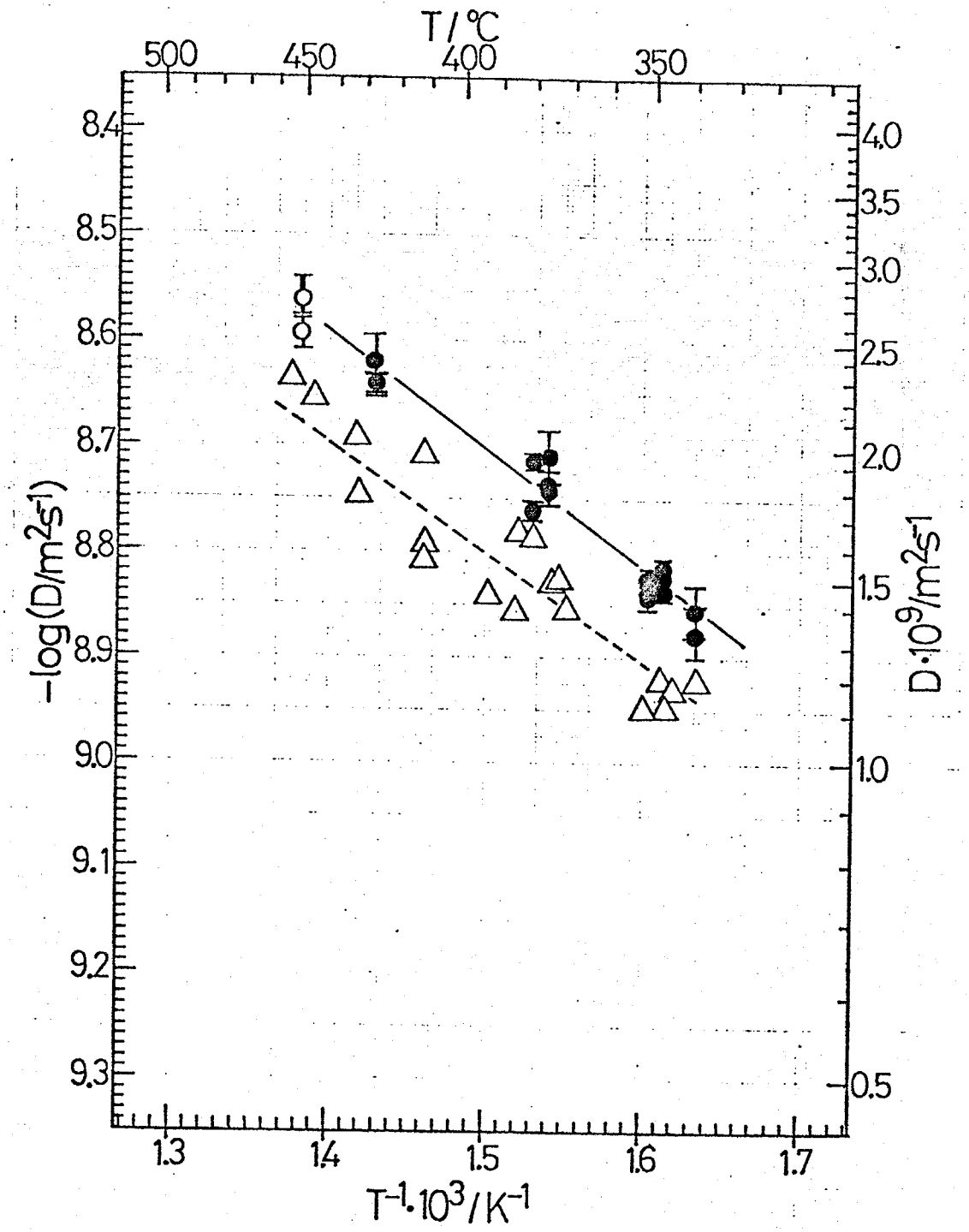

Fig. 4 Diffusion coefficients of Cs^+ ion in the molten KNO_3. ● : Present work, ○ : Ref. [24](a paper strip method), △: Ref. [33](optical interferometry).

of the present method is reasonably good as long as the experimental conditions are properly controlled; the amount of the solvent salt impregnated into the glass fibre paper and the radioactivity of the solute should be carefully chosen inorder to prevent the unwanted influence such as eddy flow, surface diffusion, statistical counting error, etc. In the present work, the amount of the solvent is about 0.03 g/cm which occupies about 95 % of the impregnated paper strip, and the radioactivity of the tracer salt is about 50 μCi/g (1000 cpm/mg with the GM counter used in this work).

Considering the large difference of the experimental conditions between the measurement by the paper strip method and that by optical interferometry as shown in Table 3, The results in the present work are in fair agreement with those by optical interferometry.

D_{Rb} and D_{Cs} in the molten (Li-Na)NO_3, (Li-K)NO_3, (Li-Rb)NO_3, and (Li-Cs)NO_3 systems at 350 °C are tabulated in Table 4. The results of D_{Rb} and D_{Cs} are also shown in Figs. 5 and 6, respectively. As can be seen from the figures, D_{Rb} and D_{Cs} slightly decrease in (Li-Na)NO_3 system and almost monotonously increase in (Li-K)NO_3, (Li-Rb)NO_3, and (Li-Cs)NO_3 systems with increasing $LiNO_3$ concentration except that D_{Rb} in (Li-K)NO_3 system shows a positive deviation from a linear dependence on the concentration. The positive deviation of D_{Rb}, D_{Tl}, and D_K in molten (Li-K)NO_3 system has been also found in the previous work with optical interferometry (see CHAPTER 2)[35], where the positive deviation was explained with the assumption that the size of the diffusing ion compared with that of the free space formed by the solvent and the interaction between the diffusing ion and the surrounding ions play predominant role in the diffusion process;

Table 3 Comparison of the experimental conditions between a paper strip method and optical interferometry.

	Paper strip method	Optical interferometry
direct object for determine D	tracer	refractive index difference
The value of D is determined from	the tracer distribution curve at the end of the experiment.	the fringe pattern caused by the concentration difference at every time checked.
duration of a experiment	18～20 hours	～0.5 hours
concentration of solute	～0.3 mol % at the end of a experiment	～1 mol %
Temp. control	$<\pm$ 1 °C	$<\pm$0.5 °C
error included in the statistical treatment	～$\pm$5 %	～$\pm$5 %
direction of diffusion	horizontal	vertical (from the bottom)
experimental technique	easy	a little difficult

Table 4 Tracer diffusion coefficients of Rb^+ and Cs^+ ions in the molten (Li-Alk, Alk=Na,K,Rb,and Cs)NO_3 systems at 350°C.

$D_{Rb} \times 10^9$ ($m^2 s^{-1}$)

	$LiNO_3$ mol %				
Alk-NO_3	0	25	50	75	100
$NaNO_3$	1.90 ± 0.06	1.88 ± 0.05	1.90 ± 0.05	1.87 ± 0.05	1.77 ± 0.02
KNO_3	1.56 ± 0.02	1.60 ± 0.05	1.81 ± 0.04	1.86 ± 0.04	1.77 ± 0.02
$RbNO_3$	1.22 ± 0.03	1.30 ± 0.03	1.45 ± 0.05	1.67 ± 0.05	1.77 ± 0.02
$CsNO_3$	————	1.27 ± 0.04	1.36 ± 0.05	1.52 ± 0.05	1.77 ± 0.02

$D_{Cs} \times 10^9$ ($m^2 s^{-1}$)

	$LiNO_3$ mol %				
Alk-NO_3	0	25	50	75	100
$NaNO_3$	1.81 ± 0.05	1.80 ± 0.03	1.74 ± 0.07	1.73 ± 0.05	1.69 ± 0.03
KNO_3	1.45 ± 0.02	1.47 ± 0.04	1.62 ± 0.03	1.67 ± 0.06	1.69 ± 0.03
$RbNO_3$	1.18 ± 0.04	1.31 ± 0.05	1.45 ± 0.04	1.58 ± 0.03	1.69 ± 0.03
$CsNO_3$	————	1.21 ± 0.06	1.34 ± 0.05	1.52 ± 0.03	1.69 ± 0.03

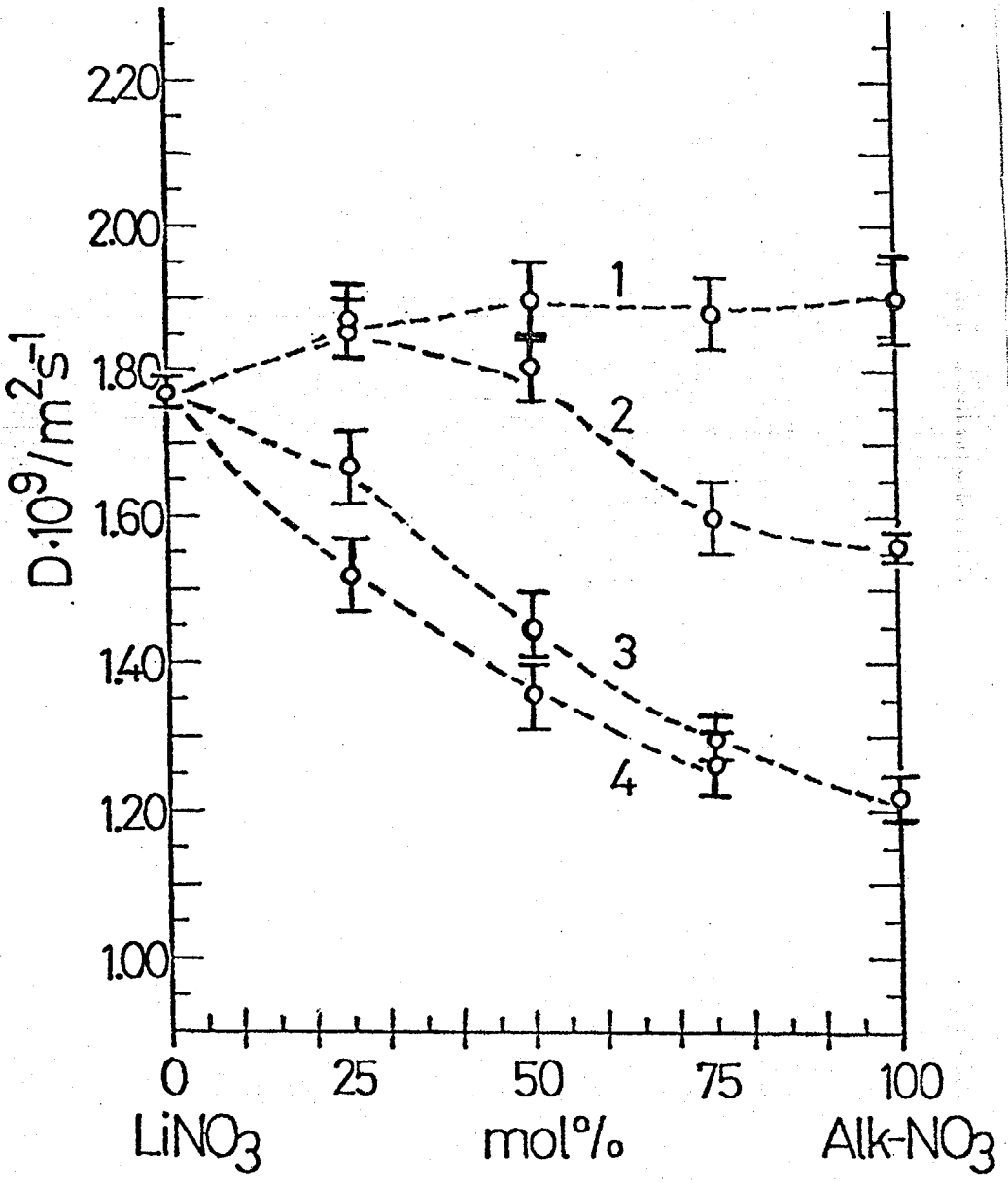

Fig. 5 Isotherms of D_{Rb} in the molten (Li-Alk, Alk= Na,K,Rb,and Cs)NO_3 systems at 350°C.
1 : (Li-Na)NO_3, 2 : (Li-K)NO_3, 3 : (Li-Rb)NO_3, 4 : (Li-Cs)NO_3.

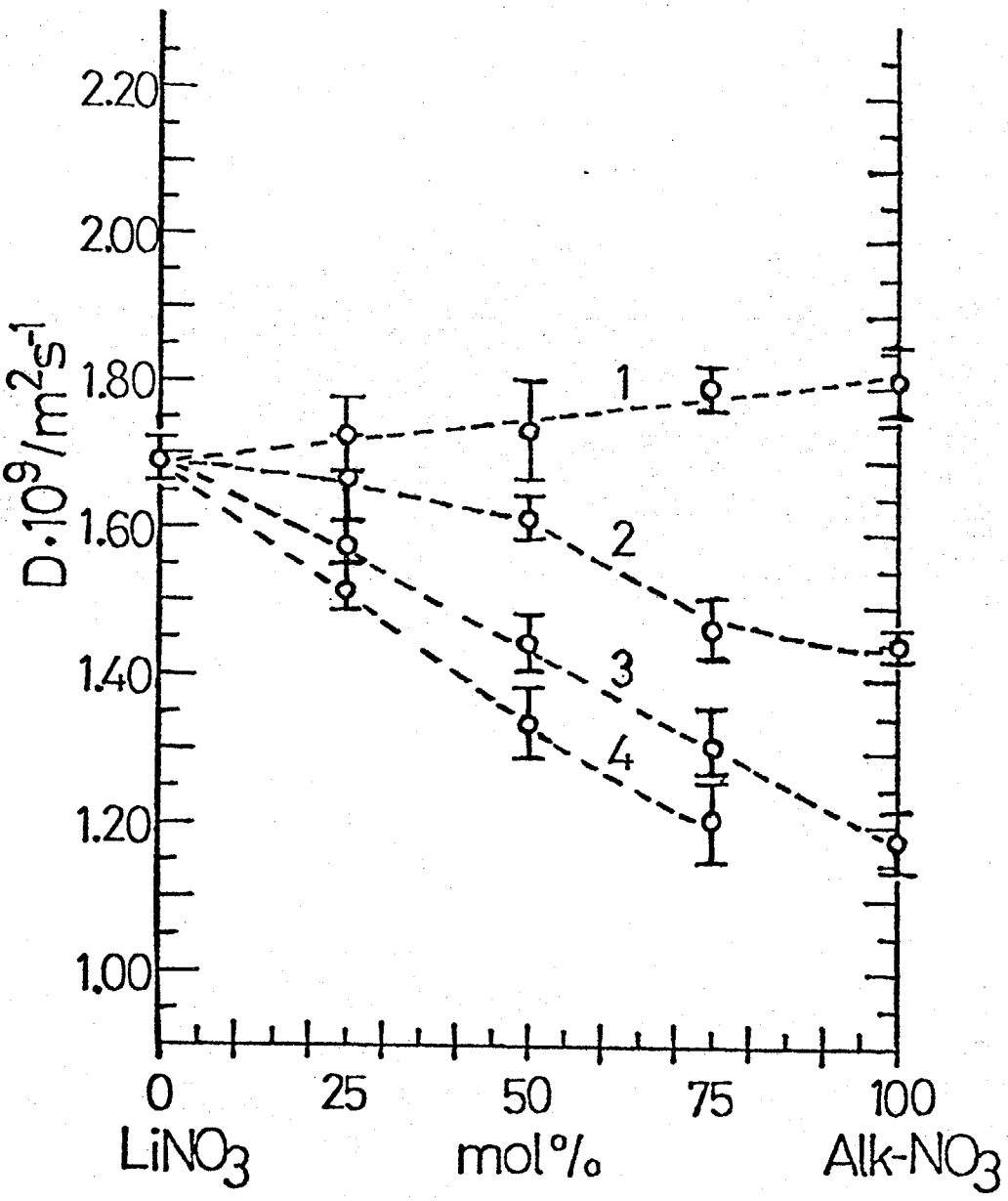

Fig. 6 Isotherms of D_{Cs} in the molten (Li-Alk, Alk= Na,K,Rb,and Cs)NO_3 systems at 350°C.
1 : (Li-Na)NO_3, 2 : (Li-K)NO_3, 3 : (Li-Rb)NO_3, 4 : (Li-Cs)NO_3.

since the solvent ions of the system become more mobile with increasing $LiNO_3$ concentration*, D in the region rich in KNO_3 increases with $LiNO_3$ concentration, and with further increasing $LiNO_3$ D of Rb^+, Tl^+, and K^+ ions decreases because the size of the free space becomes small compared with that of Rb^+, Tl^+, and K^+ ions. Considering the size of Cs^+ ion is rather larger than that of free space formed by (Li-K)NO_3 mixtures, a linear increase of D_{Cs} with increasing $LiNO_3$ concentration was explained.

In the molten (Li-Rb)NO_3 and (Li-Cs)NO_3 systems no positive deviation of D_{Rb} or D_{Cs} is found like that of D_{Rb} in the molten (Li-K)NO_3 system within experimental error. Provided that the effect of the interaction between the diffusing ion and the surrounding ions acts on D much larger in the molten (Li-Rb)NO_3 or (Li-Cs)NO_3 system than in the molten (Li-K)NO_3 system, the monotonous increases of D_{Rb} and D_{Cs} are clearly explained with the assumption that the latter effect becomes more predominant than the effect of the free space formed by the solvent system even in the region rich in $LiNO_3$ where the diffusing ion would be incommodious to move. According to the data for the ultrasonic velocity in pure $LiNO_3$, $NaNO_3$, and KNO_3[37-39], the sound velocities in $LiNO_3$ and KNO_3 are almost the

---

* According to the molecular dynamics simulation study in (Li-Rb)Cl equimolar mixture[36], the separating velocity between an Rb^+ ion and a Cl^- ion in the mixture is faster than that in the pure RbCl, and the self-diffusion coefficients of Rb^+ and Cl^- ions in the mixture are larger than those in the pure RbCl. These results will explain that the motion of the solvent becomes more mobile with increasing $LiNO_3$ concentration.

same and somewhat lower than that in $NaNO_3$ (see CHAPTER 5). Besides, from the data for the hypersonic velocity in pure alkali nitrates[40] the sound velocities in $RbNO_3$ and $CsNO_3$ are considered to be rather low compared with that in $LiNO_3$. Therefore, combinig the above aspects and the kinetic velocity of the ions themselves, it is expected that the effect of the interaction by adding $LiNO_3$ to $RbNO_3$ or $CsNO_3$ will be quite large for the motion of the system, and would increase more steeply in the region rich in $LiNO_3$ with increasing $LiNO_3$ concentration, which causes D_{Rb} and D_{Cs} increasing monotonously with the concentration of $LiNO_3$. The decrease of D_{Rb} and D_{Cs} with increasing $LiNO_3$ concentration in the molten (Li-Na)NO_3 system would be also explained by considering the effect of the solvent motion described above. In the molten (Li-Na)NO_3 system the size of the free space must be rather small for the movement of Rb^+ or Cs^+ ion.

Thus, the diffusion coefficient isotherms of relatively large ions in size such as Rb^+ and Cs^+ in the binary molten $LiNO_3$- other nitrate systems can be interpreted by introducing the simple model that the interaction between the diffusing ion and the surrounding ions and the size difference of the diffusing ion from the free space formed by the solvent mainly rule the diffusion process.

It would be thus worthwhile to examine the validity of the Stokes-Einstein equation that relates diffusion coefficients with the radius of the diffusing ion and also the viscosoty of the solvent. According to the equation the diffusion coefficients are expressed as

$$D = k_B T/n\pi r\eta \quad \ldots\ldots\ldots\ldots\ldots\ldots \quad (2)$$

where k_B is the Boltzmann constant, r the ionic radius of the diffusing ion, and η the viscosity of the solvent system. Here, n is the "shape"

parameter, and the values of n tabulated in Table 5 are calculated from Eq. (2) with the present results, the data for the ionic radius of the diffusing ion[41], and the interpolated values of the viscosity in the solvent systems at 350°C[42]. As can be seen from Table 5, the values of n are somewhat small in the region rich in $LiNO_3$ and become large with increasing the size of the component constituting the system with $LiNO_3$. Comparing the viscosity and diffusion coefficient isotherms in the corresponding systems, it is considered that the movement of the Li-NO_3 direction would be also important in viscous flow and that be hindered in the region rich in $LiNO_3$ because of the relatively small free space for its movement. Therefore, the term of the viscosity which directly plays a role of the opposing force in the Stokes-Einstein relation might be less than the value obtained experimentally, and the "shape" parameter n would be meaningfully constant. Although it is a little difficult to make clear the validity of the Stokes-Einstein equation in the binary mixtures with the present results, it is considered that the Stokes-Einstein equation will be useful for the explicit relation between the viscosity and the diffusion coefficient, for both processes must be explained by adopting the present model which takes into account only the size of the diffusing ion, that of the free space formed by the solvent, and the interaction between the corresponding ion and the surrounding ions, and which may be a similar spirit to that in the Stokes-Einstein equation.

Table 5 "Shape" parameters n of the Stokes-Einstein equation.

$LiNO_3$ mol %	$(Li-Na)NO_3$		$(Li-K)NO_3$		$(Li-Rb)NO_3$		$(Li-Cs)NO_3$	
	n_{Rb}	n_{Cs}	n_{Rb}	n_{Cs}	n_{Rb}	n_{Cs}	n_{Rb}	n_{Cs}
100	3.38	3.10	3.38	3.10	3.38	3.10	3.38	3.10
75	3.60	3.40	3.75	3.66	4.10	3.80	4.68	4.10
50	3.85	3.68	4.19	4.10	4.94	4.33	5.55	4.93
25	4.08	3.73	4.68	4.46	5.17	4.49	5.52	5.07
0	4.04	3.71	4.36	4.11	4.75	4.49	——	——

References

[1] C.-A. Sjöblom, Z. Naturforsch., 20a, 1572 (1965)

[2] F. Lantelme, Thesis, Paris (1965)

[3] F. Lantelme and M. Chemla, Electrochim. Acta, 11, 1023 (1966)

[4] E.P. Honig and J.A.A. Ketelaar, Trans. Faraday Soc., 62, 190 (1966)

[5] S. Forcheri and V. Wagner, Z. Naturforsch., 22a, 1171 (1967)

[6] S. Forcheri, V. Wagner, and E. Berra, Electrochim. Metallorum, III, 123 (1968)

[7] J.A.A. Ketelaar and J.C.Th. Kwak, Trans. Faraday Soc., 65, 139 (1969)

[8] J.E.L. Bowcott and B.A. Plunkett, Electrochim. Acta, 14, 363 (1969)

[9] S. Sternberg and C. Herdlicka, Rev. Roum. Chim., 14, 991 (1969)

[10] K. Kawamura, Denki Kagaku, 38, 12 (1970)

[11] D. Andreasson, A. Behn, and C.-A. Sjöblom, Z. Naturforsch., 25a, 700 (1970)

[12] G.-A. Mazzocchin and G. Schiavon, J. Electroanal. Chem., 39, 367 (1972)

[13] S. Zuca and M. Constantinescu, Z. Naturforsch., 28a, 51 (1973)

[14] J. Richter, J. Chem. Eng. Data, 18, 400 (1973)

[15] S. Zuca and M. Constantinescu, Z. Naturforsch., 29a, 497 (1974)

[16] K. Kawamura, Trans. JIM, 15, 413 (1974)

[17] H.H. Emons, G. Bräeutigam, and A. Winzer, Z. Chem., 16, 164 (1976)

[18] S. Zuca and M. Constantinescu, Z. Naturforsch., 32a, 1435 (1977)

[19] I. Okada and S.E. Gustafsson, Z. Naturforsch., 33a, 447 (1978)

[20] C.A. Moynihan and R.W. Laity, J. Phys. Chem., 68, 3312 (1964)

[21] J. Lumsden, Disc. Faraday Soc., 32, 138 (1961)

[22] I. Okada and S.E. Gustafsson, Electrochim. Acta, 18, 275 (1973)

[23] H.J. Arnikar, Thesis, Paris (1959)

[24] E.P. Honig, Thesis, Amsterdam (1964)

[25] J.C.Th. Kwak, Thesis, Amsterdam (1967)

[26] C.A. Angell and J.O'M. Bockris, J. Sci. Inst., 35, 458 (1958)

[27] J.S. Anderson and K. Saddington, J. Chem. Soc., S2, 381 (1949)

[28] S. Djordjevic and G.J. Hills, Trans. Faraday Soc., 56, 269 (1960)

[29] S.E. Gustafsson, L.-E. Wallin, and T.E.G. Arvidsson, Z. Naturforsch., 23a, 1261 (1968)

[30] M.W. Ozelton and R.A. Swallin, Phil. Mag., 153, 441 (1968)

[31] J. Petit and N.H. Nachtrieb, J. Chem. Phys., 24, 1056 (1956)

[32] J.C.Th. Kwak and J.A.A. Ketelaar, J. Phys. Chem., 73, 94 (1969)

[33] T.E.G. Arvidsson, S.-Å. Afsenius, and S.E. Gustafsson, J. Chem. Phys., 53, 2621 (1970)

[34] R.W. Laity, J. Phys. Chem., 63, 80 (1959)

[35] O. Odawara, I. Okada, and K. Kawamura, to be published.

[36] I. Okada, Private Communication, Report on the 7th EUCHEM Conference on Molten Salts, Sweden(1978)

[37] R.W. Higgs and T.A. Litovitz, J. Acoust. Soc. Amer., 32, 1108 (1960)

[38] J.O'M. Bockris and N.E. Richards, Proc. Roy. Soc. London, A241, 44 (1957)

[39] P. Cerisier, G. Finiels, and Y. Doucet, J. Chim. Phys., 6, 836 (1974)

[40] H.E.G. Knappe and L.M. Torell, J. Chem. Phys., 62, 4111 (1975)

[41] R.D. Schannon, Acta Cryst., A32, 751 (1976)

[42] I.G. Murgulescu and S. Zuca, Electrochim. Acta, 11, 1383 (1966)

PART II

CONDUCTION OF HEAT IN MOLTEN SALTS.

CHAPTER 4

Measurement of the Thermal Diffusivity of HTS (a Mixture of Molten $NaNO_3$-KNO_3-$NaNO_2$; 7-44-49 mol%) by Optical Interferometry.

The thermal diffusivity of HTS (Heat Transfer Salt; $NaNO_3$-KNO_3-$NaNO_2$; 7-44-49 mol%) is measured over a wide range of temperatures by means of wave-front-shearing interferometry. The thermal conductivity K is calculated from this result and the existing data on the density and the specific heat and found to be expressed by $K = 0.519 - 4.7 \times 10^{-5}(T - 142)$, (160 - 420°C). The temperature dependence of K in the present study is smaller than that in previous studies ($\sim -5 \times 10^{-4}$ W $m^{-1}deg^{-2}$). In order to check the reliability of the present method at high temperatures the thermal diffusivity of molten $NaNO_3$ is also measured; molten $NaNO_3$ is one of the salts whose data on the thermal diffusivity and the relating properties are widely available.

1 Introduction

Thermal conductivity of liquids is one of the most difficult ones of all thermophysical properties to be determined experimentally. The difficulties are primarily due to the unreliability of temperature measurements, the inadequancy of thermal insulation, and the simultaneous transfer of heat by mechanism other than conduction. In addition to conduction, radiation also may be present with transparent substances, and the experimental technique must be capable of identifying and separating these two mechanisms. In the case of the fluids, convection may also be present. Then only a limited number of experimental techniques are available for the determination of the thermal conductivity of the fluids.

Thermal conductivity can be measured by steady-state, quasi-steady-state, or transient-state heat flow methods. Experimental determinations of thermal conductivity using the steady-state methods depend on the attainment of suitable boundary conditions that will allow the Laplace equation to be solved for the temperature distribution. Thermal conductivity is then calculated from the Fourier heat-transfer equation. The transient method requires the solution of the diffusion equation with suitable initial and boundary conditions for the thermal diffusivity: the density and the specific heat must be known to calculate the conductivity. The quasi-steady-state methods are based on the solution of the diffusion equation for the unique initial and boundary conditions that the thermal conductivity can be directly determined.

In Table 1, we have listed all thermal conductivity experiments reported since 1960 in the literature for molten salts, including the substances studied and the type of apparatus used.

Table 1 Experiments performed to determine the thermal conductivity of molten salts.

Author	type of apparatus	year	substances studied
Turnbull[1]	Hot-wire	1961	$NaHSO_4$, $KHSO_4$, KNO_3, KCNS, NH_4HSO_4, $AgNO_3$, $ZnCl_2$, HTS.
McLaughlin[17]	Hot-wire	1964	$NaNO_3$, (Pb)(liquid metal).
Bloom et al.[2]	Concentric cylinder	1965	$NaNO_3$, KNO_3, $AgNO_3$, $NaNO_2$, (Na-K)NO_3, (Ag-K)NO_3, (Ag-Na)NO_3.
White & Davis[3]	Concentric cylinder	1967	$LiNO_3$, $NaNO_3$, KNO_3, $RbNO_3$, $CsNO_3$.
Gustafsson et al.[4]	Optical interferometry	1967	$LiNO_3$, $NaNO_3$, KNO_3, $RbNO_3$, $CsNO_3$.
Cornwell & Dyson[5]	Hot-wire	1969	$ZnCl_2$, AgCl-AgI eutectic.
McDonald & Davis[6]	Concentric cylinder	1970	$LiNO_3$, $NaNO_3$, KNO_3, $RbNO_3$, $CsNO_3$, (Li-Cs)NO_3, (Na-K)NO_3, (Na-Cs)NO_3, (K-Rb)NO_3, (Rb-Cs)NO_3.
Schriempf[7]*	Laser-flash	1972	(Hg)(liquid metal).
Cooke[8]	Variable-gap	1973	HTS, (Hg)(liquid metal).
Kato et al.[9]*	Stepwise heating	1975	$NaNO_2$, $NaNO_3$.

* Data for the thermal diffusivity.

In this work we used a method similar to the optical method used by Gustafsson[10]. This technique is similar to the transient hot wire technique [1,5] except in two respects: (1) a thin foil is substituted for the fine wire to provide a plane heat source; with the hot wire method the electrical conduction of such fluids as molten salts would lead to a large power leakage and subsequent inaccurate results, and (2) the temperature is measured with a wave-front-shearing interferometer, which means that this temperature measuring technique is extremely sensitive, and the heat flux from the foil can be greatly reduced, and the temperature increase in the liquid becomes very small (say, 0.2°C). This small temperature increase is very favourable, in the first place because no temperature correction of the measured properties is needed, and in the second place because the start of the convective motion in the liquid is greatly delayed.

The heat transfer material HTS is useful since it is stable over a relatively wide range of temperature (200 - 600°C) and its heat transfer coefficient is large[11]. Reliable thermal data for this material are therefore indispensable for practical purposes. In the present study the thermal diffusivity of HTS is measured over a wide range of temperatures and the thermal conductivity is calculated from the existing data on the density and the specific heat. In order to check this method with a interferometer set up in our laboratory, the thermal diffusivities of distilled water and molten $NaNO_3$ were first measured; data on the thermal diffusivity of distilled water and molten $NaNO_3$ measured with various methods by various investigators are available.

2 Experimental

The optical system of the wave-front-shearing interferometer used in present work is the same as that employed for the measurement of the high-dilution diffusion coefficients described in CHAPTER 2. A 15 mW He-Ne gas laser was used as a light source. The cell was a stainless steel cylinder with an internal diameter of 90 mm and a height of 150 mm. Two slits of 20 mm in width and 10 mm in height, through which the light was to pass, were made at both sides of the cell wall. Two quartz windows, each with a diameter of 35 mm and a thickness of 10 mm, were attached tightly to the wall of the cell by aluminum holders to cover the slits from the outside and to keep a liquid inside the cell. The flatness of the windows was less than $\lambda/5$ and the parallelism of both surfaces was less than 2 seconds of arc. In experiments at elevated temperatures thecell was placed inside an electric furnace with a large heat capacity and a salt was melted in the cell. Then, an apparatus (see Figure 1) supporting a heat source was inserted into the liquid in the cell, and placed in such a way that the plane of heat source should be in parallel to the direction of the light. The heat source was made of a silver foil whose approximate dimension was 85 mm in length, 20 mm in width, and 0.006 mm in thickness. Both the upper and lower ends of the foil were rolled round small silver rods, which were in turn connected to the copper support by screws. Two Pyrex-glass cylinders were pressed to the foil, the position of these being adjusted with stainless steel wires so that the foil was parallel to the copper support. The copper support had been electroplated with a thick layer ($\sim$20 μm) of silver in order to be free from corrosion. The upper silver plate was strained upward

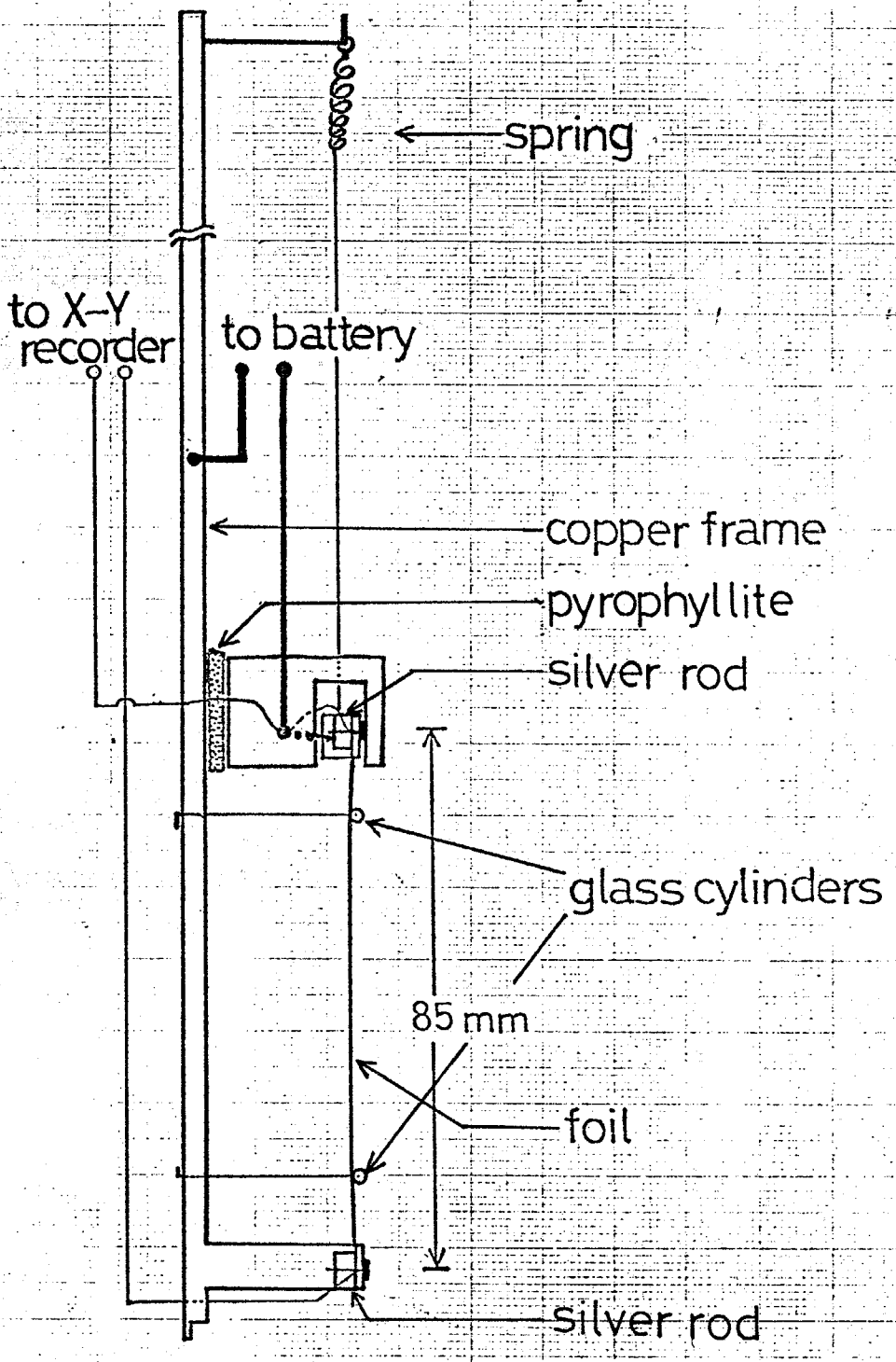

Fig.1 Arrangement for the support of the foil.

by a force of a spring. An alkaline storage battery 2.4 V with a very small internal resistance was used as a power supply for the heating foil. The switch which started the supply of elctric current to the foil was synchronized with the shutter for the first exposure of the film. Interferograms were taken at intervals of 0.5 sec. over the period of about 15 seconds. The electric current and the voltage drop across the foil were recorded with an X-Y recorder.

First, distilled water was used as a testing material. Then, thermal diffusivities of molten $NaNO_3$ and HTS were measured.

HTS was prepared by weighing accurately and mixing the three salts ($NaNO_3$, KNO_3, $NaNO_2$), which had been fully dried. The ratio of the constituent cations, Na^+, and K^+ was checked by flame spectrophotometry and that of NO_2^- by iodometric titration.

The volume of the liquids needed for an experiment of the measurement of thermal diffusivity was about 700 ml.

3 Results

In the interferograms, a pair of dark fringes successively appeared at both sides of the foil images and spread outward with the elapse of time. If we designate the distances between a pair of fringes as X_1, X_2, X_3, ... in ascending order of magnitude, it follows theoretically that $(X_i/\sqrt{D_T t})$ should be constant before the onset of convection[10](see Appendix III) and that

$$\mathrm{erfc}(X_1/4\sqrt{D_T t}) - \mathrm{erfc}(X_2/4\sqrt{D_T t}) = \mathrm{erfc}(X_2/4\sqrt{D_T t}) - \mathrm{erfc}(X_3/4\sqrt{D_T t}) = \ldots \quad \ldots\ldots\ldots\ldots (1)$$

where $\mathrm{erfc}(s) = (2/\sqrt{\pi})\int_s^\infty \exp(-\xi^2)d\xi = 1 - \mathrm{erf}(s)$. Thus, from successive interferograms, D_T can be calculated on the basis of at least three consecutive pairs of fringes using Equation (1). For a typical experiment of HTS, X_i^2 is plotted against t in Fig. 2. As seen from Fig. 2, X_i^2 varies linearly with t until the convection occurs.

With a least squares fit for the linear part of the line, X_i^2/t was calculated and the value of D_T was determined.

The thermal diffusivity of distilled water determined in the present work is compared with the recommended value in Table 2. This indicates that the present method is reliable at least at room temperature.

Since the refractive index of liquids μ can be determined independently by means of wave-front-shearing interferometry[13,14], the thermal conductivity is calculated from the temperature dependence of the refractive index $(\partial\mu/\partial T)$

$$K = bQd(\partial\mu/\partial T)\left\{\mathrm{erfc}(X_2/4\sqrt{D_T t}) - \mathrm{erfc}(X_1/4\sqrt{D_T t})\right\}/\lambda \quad \ldots\ldots (2)$$

Alternatively, K can be calculated from the density and the specific heat by

$$K = D_T \cdot C_p \cdot \rho \quad \ldots\ldots (3)$$

For molten $NaNO_3$, the thermal diffusivity and the thermal conductivity calculated by Equation (2) [14] and (3) [15] are tabulated in Table 3. The thermal conductivity is compared with those previously determined in Fig. 3.

The thermal diffusivity of HTS is given in Table 4. Since $(\partial\mu/\partial T)$ has not been determined for HTS, the thermal conductivity is calculated from the thermal diffusivity with the aid of Equation (3)[16]. This is tabulated in Table 4 and compared those so far determined in Fig. 4.

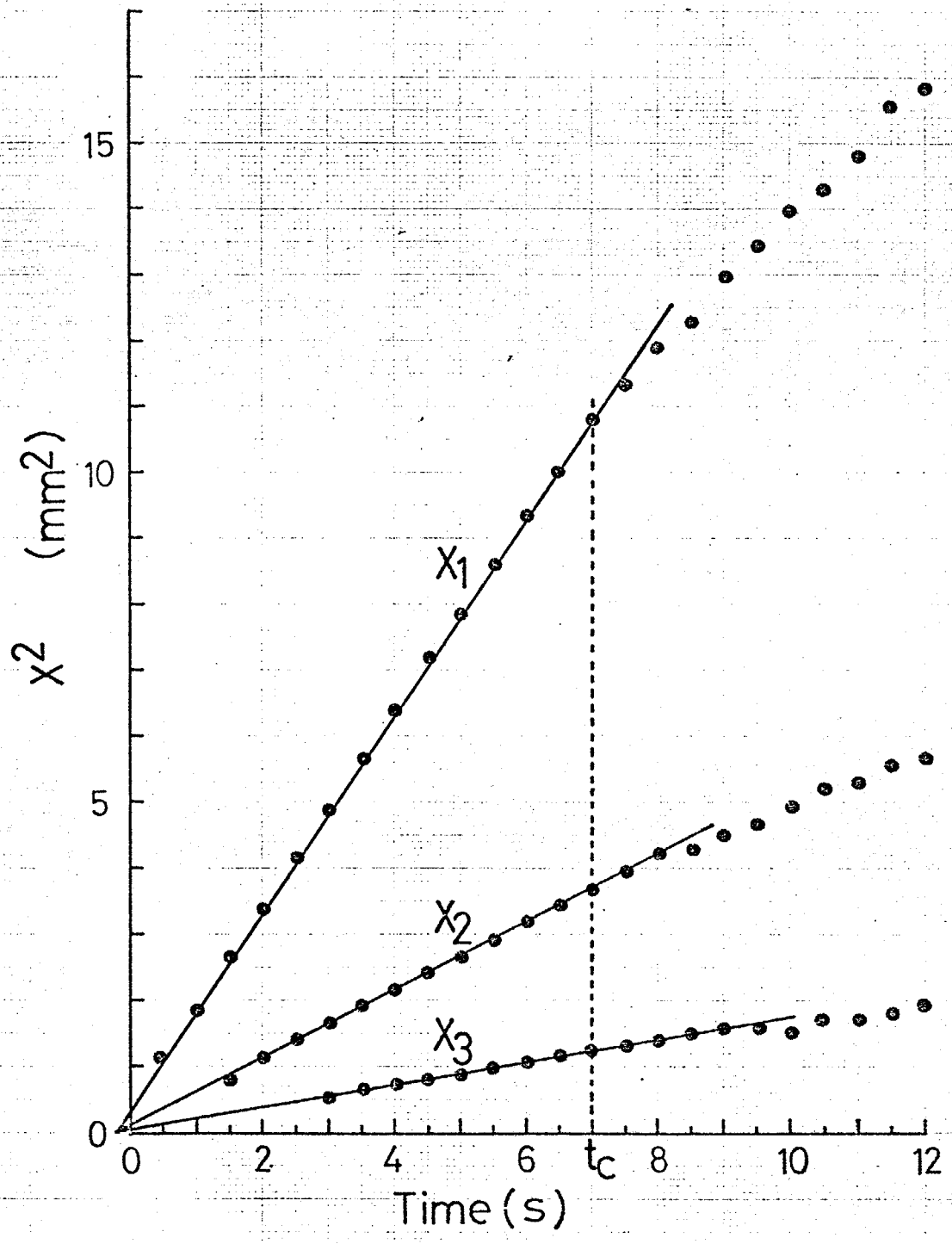

Fig.2 Plots of X^2 as a function of time for a typical experiment in HTS (168°C).

Table 2 Experimental results obtained from measurement on distilled water.

Temperature (^{o}C)	Thermal diffusivity x 10^{7} ($m^{2}s^{-1}$)	Onset of convection (s) exptl.	calcd.	Recommended values[a] x 10^{7} ($m^{2}s^{-1}$)
18.0	1.409	12	13	1.41_{2}
18.0	1.407	12	14	
18.5	1.411	15	15	1.41_{4}
18.5	1.417	16	17	
22.5	1.432	12	14	1.43_{5}
23.3	1.442	14	15	
23.3	1.447	14	16	1.44_{0}
23.3	1.444	15	16	
27.2	1.469	15	16	1.46_{4}
27.2	1.479	15	17	

[a]Literature values taken from TPRC Data. [12]

Table 3 Experimental data for molten $NaNO_3$.

Temperature (^{o}C)	Power Qd ($W\ m^{-1}$)	Thermal diffusivity x 10^{7} ($m^{2}s^{-1}$)	Thermal conductivity ($W\ m^{-1}deg^{-1}$)	
			from Eq. A[a]	from Eq. B[b]
308	36.59	1.65	0.568	0.567
310	38.31	1.69	0.588	0.580
343	36.38	1.70	0.552	0.576
351	36.51	1.70	0.565	0.575
371	24.70	1.70	0.567	0.570
380	38.07	1.69	0.572	0.565
390	29.77	1.67	0.562	0.555
417	40.94	1.68	0.580	0.553
418	43.53	1.68	0.582	0.553

[a]Calculated with $(\partial\mu/\partial T) = -1.4232 \times 10^{-4}$ [14].

[b]Calculated with $C_p = 0.429$ cal $g^{-1}deg^{-1}$ and $\rho = 2.32 - 7.15\times10^{-4}(T+273)$ g cm^{-3} [15].

$$K = bQd(\partial\mu/\partial T)[\mathrm{erfc}(X_2/4\sqrt{D_T t}) - \mathrm{erfc}(X_1/4\sqrt{D_T t})]/\lambda \quad \ldots\ldots\ldots(A)$$

$$K = D_T \cdot C_p \cdot \rho \quad \ldots\ldots\ldots(B)$$

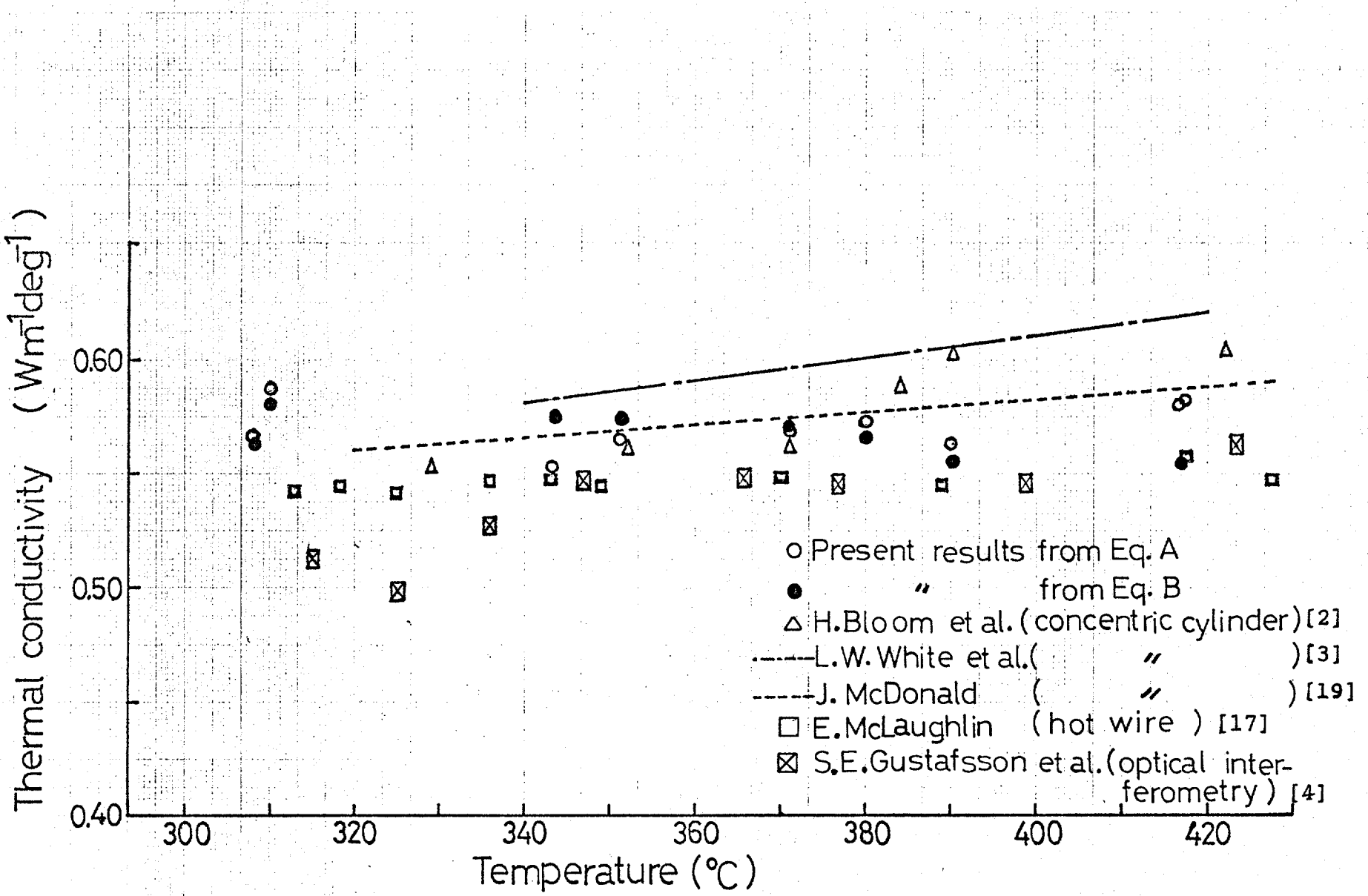

Fig.3 Thermal conductivity of molten $NaNO_3$.

Table 4 Experimental data for HTS.

Temperature (^{o}C)	Thermal diffusivity x 10^{7} ($m^{2}s^{-1}$)	Thermal conductivity[a] ($W\ m^{-1}deg^{-1}$)
167	1.69	0.517
168	1.68	0.514
208	1.69	0.509
208	1.73	0.521
212	1.71	0.514
231	1.67	0.499
232	1.72	0.514
257	1.73	0.512
263	1.76	0.519
286	1.80	0.526
293	1.82	0.531
294	1.72	0.501
302	1.77	0.514
304	1.76	0.511
305	1.80	0.523
324	1.76	0.507
336	1.84	0.528
360	1.75	0.497
391	1.84	0.516
403	1.75	0.488
419	1.81	0.502

[a]alculated with C_p=0.373 cal $g^{-1}deg^{-1}$ and ρ=1.98-7.29x10^{-4}(T-142) g cm^{-3}.[16]

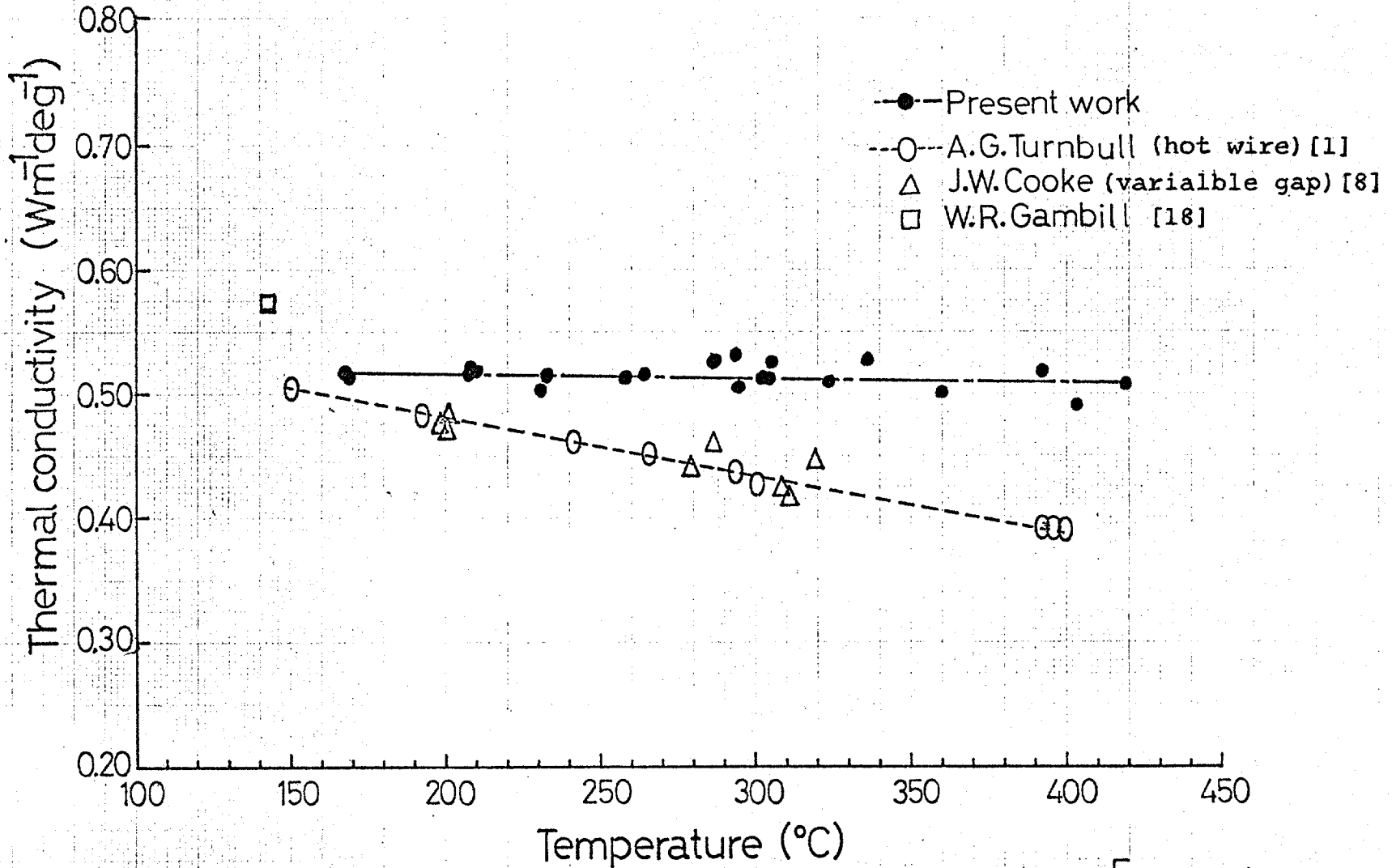

Fig.4 Thermal conductivity of HTS. $[K = 0.519 - 4.7 \times 10^{-5}(T - 142)]$

4 Discussion

Since the thermal diffusivity of distilled water measured in the present study is consistent with the recommended value within experimental error, the optical system of this interferometer is considered reliable.

A rise in the temperature at the heating foil during experiments is estimated roughly from the number of pairs of fringes m, using Equation (4):

$$\Delta T = \Delta\mu / (\partial\mu/\partial T) = \Delta R / \ell\,(\partial\mu/\partial T) \simeq -m\lambda / \ell\,(\partial\mu/\partial T) \quad \ldots\ldots (4)$$

For example, in the case of molten $NaNO_3$, substituting $m = 4$, $\lambda = 632.8$ nm, $\ell = 90$ mm, and $(\partial\mu/\partial T) = -1.4 \times 10^{-4}$ into Equation (4) yields $\Delta T \simeq 0.2$°C; thus, the rise in temperature is very small as compared with that of other methods, such as a concentric cylinder method and a hot wire method.

The time of onset of convective motion t_c is expressed by

$$t_c = \sqrt{R_a \eta C_p / \pi g \alpha Q} \quad \ldots\ldots\ldots\ldots\ldots (5)$$

When convection starts to take place, a plot of X_i^2 versus t deviates from a straight line. From the analysis of a plot of X_i^2 versus t in the experiments of distilled water, the value of R_a is estimated for this apparatus from Equation ((5) to be about 900. With this value and Q (~ 0.3 W cm^{-2}), t_c at 350°C for $NaNO_3$ is calculated to be about 10.5 sec., which is about 2 seconds longer than the experimental finding. At about 400°C, the calculated t_c is even longer than the experimentally determined value (4.5 sec.).

As the temperature of the bulk liquid rises, the linear part of a plot X_i^2 against t becomes shorter and therefore the value $X_i/\sqrt{t}$ calculated from the linear part is expected to become less reliable.

In the case of $NaNO_3$, however, this is not a serious problem at least at 400°C, where the standard deviations of the slopes of the linear parts

are less than 0.5 % in the least squares fits.

In connection with experiments using the hot wire method, White[3] pointed out the possibility of electric current leaking through the testing liquid. This phenomena should be negligible in the present case, since the fringes are parallel to the heating foil before the onset of convection, and the calculated diffusivity or conductivity is not high in comparison with those measured by others, as seen from Fig. 3. Figure 3 indicates that the thermal conductivities calculated from our thermal diffusivity data by Equations (2) and (3) are in good agreement in the case of molten $NaNO_3$. Thus, for the calculation of thermal conductivity from thermal diffusivity, it is more convenient and probably more reliable to employ the relation of Equation (3) than of Equation (2), since C_p and can be measured accurately to at least three significant digits, whereas the measurement of $(\partial\mu/\partial T)$ is rather troublesome.

A method of directly measuring the thermal diffusivity of molten salts has been proposed by Kato et al.[9], and our results on the thermal diffusivity of $NaNO_3$ are in good agreement with theirs, although the precision of their results is not so good as that of the results reported in this paper.

As seen from Fig. 3, the thermal conductivity determined for molten $NaNO_3$ in the present experiment is consistent with those determined by others; however, in the present experiment and in the hot wire experiment by McLaughlin[17] it is almost independent of temperature, while in other experiments it increases slightly with temperature.

In the case of experiments using mixtures such as HTS, the present method has the advantage that a check on the uniformity of interferograms before charging the foil with electric current can confirm complete mixing

of the salts. Table 4 shows that in the present study the thermal diffusivity of HTS increases slightly with temperature. Applying the least squares method to the values for the thermal conductivity calculated from Equation (3) combined with Equation (1), we have found that the thermal conductivity is expressed as a function of temperature by

$$K = 0.519 - 4.7 \times 10^{-5} (T - 142).$$

This equation shows that the thermal conductivity of HTS is practically independent of temperature, which is in contrast with the findings by Turnbull[1] and Cooke[8], that the thermal conductivity decreases with increasing temperature, the temperature coefficient being about -5×10^{-4} $W\ m^{-1} deg^{-2}$.

According to Bloom[2] and McDonald[19], the temperature dependence of the thermal conductivity of a molten mixture $NaNO_3$-KNO_3 is much the same as that of the single salts. The thermal conductivity of $NaNO_2$ has been reported by Bloom[2] to increase slightly with increasing temperature. Therefore, it would seem reasonable that the thermal conductivity of HTS is almost independent of temperature, as the present obsevation shows.

Glossary

K = thermal conductivity, W $m^{-1} deg^{-1}$

D_T = thermal diffusivity, $m^2 s^{-1}$

T = temperature, °C

X = distance between a pair of fringes

t = time, s

b = shear produced by the beam splitter of the interferometer

Q = heat liberated at the foil, W m^{-2}

d = half width of the heating foil

λ = wave length of the light, nm

μ = refractive index

C_p = specific heat, W $g^{-1} deg^{-1}$

ϱ = density, g m^{-3}

R_a = Rayleigh number

η = viscosity

g = acceleration of gravity

α = thermal expansivity

ΔR = optical path difference

ℓ = geometric length of the light path through the liquid

References

[1] A.G. Turnbull, Aust. J. Appl. Sci., 12, 30, 324 (1961)

[2] H. Bloom, A.A. Doroszkowski, and S.B. Tricklebank, Aust. J. Chem., 18, 1171 (1965)

[3] L.R. White and H.Ted Davis, J. Chem. Phys., 47, 5433 (1967)

[4] S.E. Gustafsson, N.-O. Halling, and R.A.E. Kjellander, Z. Naturforsch., 23a, 44, 682 (1968)

[5] K. Cornwall and R.W. Dyson, Brit. J. Appl. Phys., ser.2, No. 2, 305 (1969)

[6] J. McDonald and H.Ted Davis, J. Phys. Chem., 74, 725 (1970)

[7] J.T. Schriempf, Rev. Sci. Instr., 43, 781 (1972)

[8] J.W. Cooke, ORNL-4831 (1973)

[9] Y. Kato, K. Kobayashi, N. Araki, and K. Furukawa, J. Phys. E, 8, 461 (1975)

[10] S.E. Gustafsson, Z. Naturforsch., 22a, 1005 (1967)

[11] V.W. Uhl and H.P. Voznick, Chem. Eng. Progr., 59, 33 (1963)

[12] Y.S. Touloukian, "Thermophysical Properties of Matter"(TPRC Data Series) Vol. 10, IFI/Plenum Data Corp., New York (1971)

[13] L.W. Wendelov, S.E. Gustafsson, N.-O. Halling, and R.A.E. Kjellander, Z. Naturforsch., 22a, 1363 (1967)

[14] S.E. Gustafsson and E. Karawacki, Appl. Optics, 14, 1105 (1975)

[15] G.J. Janz, "Molten Salts Handbook", Academic Press, pp42, pp200 (1967)

[16] W.E. Kirst, W.M. Nagle, and J.B. Castner, Trans. Am. Inst. Chem. Eng., 36, 371 (1940)

[17] E. McLaughlin, Chem. Rev., 64, 389 (1964)

[18] W.R. Gambill, Chem. Eng., 66, 129 (1959)

[19] J. McDonald, Ph. D. Thesis, University of Minnesota (1969)

CHAPTER 5

Thermal Conductivity of Molten Salts Evaluated by the Velocity of Sound.

Thermal conductivity of molten alkali nitrates and HTS is examined by adopting some theories of conduction of heat in liquids which relate the thermal conductivity with the velocity of sound and the mean vibrational frequency. The data for the velocity of sound in molten $LiNO_3$, $NaNO_3$, KNO_3, and HTS are previously obtained in our laboratory by means of an ultrasonic pulse echo method, which are available in the present work.

1 Introduction

As previously described in CHAPTER 4, it is very difficult to measure the thermal conductivity of molten salts accurately and the errors in the obtained results always tend to be large compared with those included in the corresponding measurement at room temperature. In recent years, considerable effort has been expended in the experimental determination of the thermal conductivity of molten salts. There are, however, few available data for the thermal conductivity of molten salts except for molten nitrates. In CHAPTER 4, wave-front-shearing interferometry is recommended as one of the useful methods for determining the thermal conductivity of transparent liquids, which offers rather reliable results with its high sensitivity for the difference of temperature in the system. Although it was confirmed that this optical method is useful for the measurement in molten nitrates up to 500 °C, it is still difficult to apply this method to the measurement at further higher temperature and measure the thermal conductivity of molten halides, with which the mechanism of the conduction of heat in ionic melts must be interpreted rather clearly.

Since a number of equations, almost empirical equations, have been proposed to determine the thermal conductivity of liquids, it is of interest to apply some of them to the investigation on molten salts and confirm the validity of the equations. Because of the lack of data, we are forced to investigate with the data for molten nitrates which have been studied comparatively at large and the data of which are available.

In the present work some approaches to the mechanism of conduction of heat in molten salts are performed with several theoretical equations

relating the thermal conductivity with the velocity of sound or the mean vibrational frequency. The values of sound velocity in $LiNO_3$, $NaNO_3$, KNO_3, $NaNO_2$, and HTS were previously measured in our laboratory.

2 Measurement of the sound velocity

In our laboratory, an ultrasonic pulse echo method was applied to the measurement of the sound velocity in molten nitrates. The principle of this method is described in detail elsewhere[1,2].

The advantage of this method is that only one quartz rod is in need as a conductor of sound wave, which allows the sample at constant temperature ($\pm$ 1°C). The value of the sound velocity is determined by dividing the propagating distance of the sound wave in the sample ($\sim$10 mm) by the time interval between two adjacent echos ($\sim$5 μs). The measurement was performed in molten $LiNO_3$, $NaNO_3$, KNO_3, $NaNO_2$, and HTS. The results are tabulated in Table 1 as a function of temperature with the data in the literature[3,4]. There exist no data for the sound velocity in molte $RbNO_3$ and $CsNO_3$ except hypersonic velocity studied by Brillouin spectroscopy[5], the results of which are also shown in Table 1 for comparison. Since the hypersonic velocities in $RbNO_3$ and $CsNO_3$ measured in Ref. [5] may be taken as the velocities at infinite frequency, the sound velocities in $RbNO_3$ and $CsNO_3$ are rather small compared with those in $LiNO_3$, $NaNO_3$, and KNO_3.

The results in pure $LiNO_3$, $NaNO_3$, and KNO_3 measured in our laboratory are in good agreement with other results within experimental error.

Table 1 Results of the sound velocities in the molten alkali nitrates and HTS.

	U_s (m s^{-1}) ultrasonic velocity			Hypersonic velocity
	Present work	Bockris & Richards[3]	Higgs & Litovitz[4]	Knappe & Torell[5]
$LiNO_3$	1800-0.794(T-254)	1853-1.259(T-254)	1799-0.84(T-254)	1805-0.94(T-254)
$NaNO_3$	1789-0.968(T-310)	1807-1.150(T-310)	1817-1.16(T-310)	1825-1.10(T-310)
KNO_3	1756-1.187(T-337)	1755-1.194(T-337)	1767-1.12(T-337)	1853-1.45(T-337)
$RbNO_3$	———	———	———	1569-1.10(T-316)
$CsNO_3$	———	———	———	1260-0.93(T-414)
$NaNO_2$	1906-1.47(T-271)	———	———	———
HTS	2040-1.323(T-142)	———	———	———

T is in °C.

The discrepancy between the ultrasonic and hypersonic velocities in KNO_3 may be caused by the measurement of the hypersonic velocity close to the infinite frequency of KNO_3. The additivity of the sound velocity in HTS is confirmed.

3 Theory and Discussion

In general, the vibrational ("collide") and translational ("diffusion") contributions are considered as the main factors to determine the rate of conduction of heat in molten salts. However, the latter contribution must be small, cosidering high value of the thermal diffusivity ($\sim 10^{-7}$ $m^2 s^{-1}$) compared with those of the self-diffusion coefficient ($\sim 10^{-9}$ $m^2 s^{-1}$), and it might be also evidenced from the Lorenz number L_N which is constant for solid and liquid metals because electron drift is responsible for both thermal and electrical conduction:

$$L_N = K / \sigma T_K \quad \text{..... (1)}$$

where K is the thermal conductivity, σ the electric conductivity, and T_K the absolute temperature. The calculated Lorenz number for molten alkali nitrates at the melting point are shown in Table 2, where σ is taken from Ref. [6] and K is the mean value of the present result (CHAPTER 4) and Refs. [7-12]. The experimental results of thermal conductivity of molten pure alkali nitrates are tabulated in Table 3. For comparison, the self-diffusion coefficients [13] are also shown in Table 2. Since the translational ion motion is the carrier for electrical conduction, it must be a minor carrier for thermal conduction in molten salts.

Table 2 Lorenz's number of molten alkali nitrates at the melting point.

	T_m (°C)	σ [6] $\times 10^{-2}$ ($ohm^{-1}m^{-1}$)	K ($Wm^{-1}deg^{-1}$)	D [13] $\times 10^{9}$ (m^2s^{-1})	ratio of Lorenz's number $(K/\sigma T_m)/(3(k_B/e)^2/2)^* \times 10^3$
$LiNO_3$	254	0.804	0.610	1.31	1.29
$NaNO_3$	310	0.984	0.548	1.77	0.86
KNO_3	337	0.630	0.465	1.38	1.08
$RbNO_3$	316	0.431	0.364	1.06	1.29
$CsNO_3$	414	0.540	0.327	1.89	0.79

* $(K/\sigma T_m)$ is constant for metals, = $3\ (k_B/e)^2/2$.

Table 3 Thermal conductivities of molten alkali nitrates.

($W\ m^{-1}\ deg^{-1}$)

	Reference
$LiNO_3$	
$0.638 - 0.1 \times 10^{-4}(T - 254)$	[7]
$0.610 + 2.1 \times 10^{-4}(T - 254)$	[8]
$0.583 + 6.1 \times 10^{-4}(T - 254)$	[9]
$NaNO_3$	
$0.513 + 4.4 \times 10^{-4}(T - 310)$	[7]
$0.559 + 2.7 \times 10^{-4}(T - 310)$	[8]
$0.567 + 4.8 \times 10^{-4}(T - 310)$	[9]
$0.541 + 6.4 \times 10^{-4}(T - 310)$	[10]
$0.568 + 4.2 \times 10^{-5}(T - 310)$	present work
$0.542 + 7.8 \times 10^{-5}(T - 310)$	[12]
KNO_3	
$0.482 + 0.9 \times 10^{-4}(T - 337)$	[7]
$0.460 + 3.6 \times 10^{-4}(T - 337)$	[8]
$0.431 + 5.0 \times 10^{-4}(T - 337)$	[9]
$0.455 + 8.0 \times 10^{-4}(T - 337)$	[10]
$0.495 + 6.0 \times 10^{-4}(T - 337)$	[11]
$RbNO_3$	
$0.361 - 1.1 \times 10^{-4}(T - 316)$	[7]
$0.352 + 2.8 \times 10^{-4}(T - 316)$	[8]
$0.379 + 3.7 \times 10^{-4}(T - 316)$	[9]
$CsNO_3$	
$0.337 + 1.0 \times 10^{-4}(T - 414)$	[7]
$0.308 + 0.8 \times 10^{-4}(T - 414)$	[8]
$0.337 + 0.1 \times 10^{-4}(T - 414)$	[9]

T is in °C.

Therefore, considering the vibrational contribution is predominant for determining the thermal conductivity of these molten nitrates, we can apply some theories proposed for predicting the thermal conductivity of liquids in relation to the sound velocity or the mean vibrational frequency to evaluate the thermal conductivity in molten salts.

One such equation was developed in 1923 by P. W. Bridgeman[14], who assumed that the liquid ions were arranged in a cubical lattice at a distance **d** apart, vibrating around centers,

$$d = (V_M / N n)^{1/3}$$

where V_M is the molar volume, N the Avogadro number, and n the number of discrete ions of the dissociated molten salt. The total energy of a particle is taken as $3k_BT$ and assumed to be propagated with the velocity of sound U_s in the liquid. Thus, Bridgeman obtained the equation

$$K = 3 k_B U_s / d^2 \quad ..... (2)$$

Kardos in 1934 [15] modified the Bridgeman equation to avoid specifying the amount of the particle energy. He considered an energy drop between adjacent particle surfaces and substituted the distance L between the surfaces of adjacent particles, instead of the distance **d** of their centers. He arrived by a reasoning similar to that of Bridgeman at the following relation;

$$K = L U_s \rho C_p \quad ..... (3)$$

Considering the relationship between the thermal conductivity and the thermal diffusivity D_T ($K = D_T \rho C_p$), LU_s should be equal to D_T when Eq. (3) is used. The difficulty in using the above equation lies in the finding of suitable values for the variables included, especially the distance L.

Besides, in 1938 an improved equation of the Bridgeman equation has been proposed by Kinkaid and Eyring[16], who applied the kinetic theory of gases directly and introduced the Eucken factor to account for internal degrees of freedom, so that the constant 3 in Eq. (2) is replaced by $2.79/\gamma^{1/2}$, where γ is the ratio of specific heat;

$$K = 2.79 / \gamma^{1/2} \cdot k_B \cdot U_s / d^2 \quad \ldots\ldots\ldots\ldots (4)$$

With the mean vibrational frequency ν, a different approach to determine the thermal conductivity has been proposed by several authors;

$$K = 2\nu C_V / d \quad \ldots\ldots\ldots\ldots\ldots\ldots\ldots (5)$$

where C_V is the specific heat at constant volume ($= C_p/\gamma$) taken here as $3k_B$ assuming six vibrational degrees of freedom.

As an estimation of the mean vibrational frequency the Lindemann model [17] may be valid because of no requiry of unknown parameters for these nitrates, which is based on the assumption that the ions behave as harmonic oscillators;

$$\nu = (\pi L)^{-1} (2k_B T_m/m)^{1/2} \quad \ldots\ldots\ldots (6)$$

where T_m is the melting point and m is the weight of the ion. Combining Eqs. (5) and (6), K is expressed as follows:

$$K = 6 k_B (\pi L d)^{-1} (2k_B T_m/m)^{1/2} \quad \ldots\ldots\ldots (7)$$

Adopting the available values of Debye frequency of AgBr, AgCl, CaF_2, KBr, KCl, and NaCl, Turnbull[11] derived a similar equation as Eq. (7) for molten salts as

$$K = 5.29 \times 10^{-22} (T_m / m \cdot d^4)^{1/2} \quad \ldots\ldots (8)$$

where m is the weight of the molecule divided by the number of the descrete ions. Using the effective value m of the cation and anion ($= (m_a \cdot m_c)^{1/2}$), Gustafsson et al.[7] expressed as follows;

$$K = 6\, k_B\, (\pi L d)^{-1}\, (2k_B T_m / (m_a \cdot m_c)^{1/2})^{1/2} \quad \ldots (9)$$

It is also possible to get a proper approximation of the frequency and derive an improved equation similar to Eqs. (8) and (9) from Eq. (5), if we could know the optimum pair potential of these molten nitrates.

The results calculated from Eqs. (2), (3), (4), (8), and (9) in for molten alkali nitrates and HTS at their melting point are shown in Table 4. The interionic distance L used here is obtained by subtracting the distance of the third peak of the radial distribution function in the X-ray diffraction data[18] corresponding to the distance between cation-NO_3 ion from the interionic distance between the centers of adjacent ions d. For the ionic radius between Li-NO_3, we selected 0.222 nm as the closest value although it is in contrast with the experimentally obtained value from the X-ray diffraction (0.27 nm). The value of L for HTS was estimated from the assumption $U_s L = D_T$, where U_s and D_T are measured in the present work. The interionic distance d of HTS was determined with the same treatment in the case of pure nitrates, i.e., $d = (V_M/Nn)^{1/3}$.

Comparing the calculated thermal conductivity with the experimental results in Table 3, we find that the results from Eqs. (4) and (8) are in good agreement with the experimentally obtained ones. Equation (8) was derived by equating to the Debye frequency, while Eq. (4) is based on the comparison of the velocity of sound in liquids with the kinetic theory velocity of the ions. Since the errors included in the measured sound velocity in molten salts are expected to be smaller than those in the thermal conductivity, it is very meaningful that it would be possible to estimate the thermal conductivity from the sound velocity.

As an application of the estimation by these equations, the thermal

Table 4 Thermal conductivities of alkali nitrates and HTS estimated by several models.

	ρ [20] $\times10^{-3}$ (kgm^{-3})	V_M $\times10^{6}$ (m^3)	r_a+r_b [18] $\times10^{10}$ (m)	d $\times10^{10}$ (m)	L $\times10^{10}$ (m)	Thermal conductivity (Wm^{-1}deg^{-1}) Eq.(2)	Eq.(3)	Eq.(4)	Eq.(8)	Eq.(9)
$LiNO_3$	1.785	38.62	2.22	3.18	0.96	0.742	0.507	0.658	0.647	0.561
$NaNO_3$	1.909	44.53	2.65	3.33	0.68	0.652	0.422	0.565	0.558	0.580
KNO_3	1.875	53.92	3.00	3.55	0.55	0.560	0.254	0.475	0.461	0.603
$RbNO_3$	2.502	58.94	3.05	3.66	0.61	0.470	———	———	0.353	0.427
$CsNO_3$	2.810	69.36	3.25	3.86	0.61	0.348	———	———	0.298	0.396
HTS	1.98*	42.55	———	3.29	0.82	0.785	0.518	0.651	0.485	0.404

* $\rho = 1.98\times10^{-3} - 7.29\times10^{-7}(T-142)$ (kgm^{-3}) [21]

conductivity of HTS is also calculated and tabulated in Table 4. The agreement between the calculated value by Eq. (4) and the experimental one is not very good, while Eq. (8) seems to relate them in good correspondence. Since the melting point of HTS is very low (142°C) compared with that of each component and then it is considered that the space of each component may be very small at such a temperature, the approach from the solid state might show better approximation than that from the gas state. This might be the reason why Eq. (4) does not fit to HTS at its melting point.

As can be seen in Table 3, the temperature dependence of the thermal conductivity in molten alkali nitrates is not clearly detected to be positive or negative, although it is clear that the magnitude of it is much less than that of viscosity or diffusion coefficient.

According to the equations described above, the thermal conductivity of molten salts might decrease with increasing temperature because the velocity of sound decreases with increasing temperature. However, considering the increase of the translational contribution to the thermal conductivity ($2DC_V/d^3$)[19] with increasing temperature, it is also considered that the thermal conductivity increases with increasing temperature.

Therefore, in conclusion, although the temperature dependence of the thermal conductivity of molten salts is still in question, the thermal conductivity may be evaluated reasonably by relating it with the sound velocity and the mean vibrational frequency at least at the melting point. A similar equation to that derived by Turnbull with using the Debye frequency would give an excellent approximation to the experimentally obtained thermal conductivity of molten salts.

In order to estimate the thermal conductivity of molten salts from the expressions derived by using equilibrium statistical mechanics[22-26], we have examined the average time correlation of fluctuations of energy flux in the equilibrium system by means of molecular dynamics simulation. Since the work of Woodcock and Singer[27], a number of investigations have been performed to calculate the transport properties of molten salts by molecular dynamics simulation and those for self-diffusion coefficient are reasonably successful(reviewed in Ref.[28]). However, our trial for calculating the thermal conductivity of molten NaCl with the pair potential proposed by Michielsen et al.[29] did not succeed, for the fluctuation of the correlation function at each time step was unexpectedly large and any decay of it could not be detected. Although it may be caused by the poor averaging of the correlation functions, further improvement in this type calculation for thermal conductivity seems to be hopeless because it will expend much longer calculation time to get some reasonable figure.

References

[1] M. Mikami, Master Thesis, Tokyo Institute of Technology (1978)

[2] M. Mikami, O. Odawara, and K. Kawamura, to be published.

[3] J.O'M. Bockris and N.E. Richards, Proc. Roy. Soc. London, A241, 44 (1957)

[4] R.W. Higgs and T.A. Litovitz, J. Acoust. Soc. Amer., 32, 1108 (1960)

[5] H.E.G. Knappe and L.M. Torell, J. Chem. Phys., 62, 4111 (1975)

[6] F.M. Jaeger and B. Kapma, Z. Anorg. Chem., 113, 27 (1920)

[7] S.E. Gustafsson, N.-O. Halling, and R.A.E. Kjellander, Z. Naturforsch., 23a, 682 (1968)

[8] J. McDonald and H.Ted Davis, J. Phys. Chem., 74, 725 (1970)

[9] L.R. White and H.Ted Davis, J. Chem. Phys., 47, 5433 (1967)

[10] H. Bloom, A.A. Doroszkowski, and S.B. Tricklebank, Aust. J. Chem., 18, 1171 (1965)

[11] A.G. Turnbull, Aust. J. Appl. Sci., 12, 324 (1961)

[12] E. McLaughlin, Chem. Rev., 64, 389 (1964)

[13] S. Dworkin, R.B. Escue, and E.R. Van Artsdalen, J. Phys. Chem., 64, 872 (1960); and for D_{Rb}, S. Zuca and M. Constantinescu, Z. Naturforsch., 29a, 497 (1974)

[14] P.W. Bridgeman, Amer. Acad. Arts Sci., 49, 141 (1923)

[15] A. Kardos, Forsch. Gebiete Ingenieurw., 5, 14 (1934)

[16] J.F. Kincaid and H. Eyring, J. Chem. Phys., 6, 620 (1938)

[17] F.A. Lindemann, Phys. Z., 11, 609 (1910)

[18] H. Ohno and K. Furukawa, J. Chem. Soc. Faraday Trans. I, 74, 297 (1978)

[19] J.K. Horrocks and E. McLaughlin, Trans. Faraday Soc., 56, 206 (1960)

[20] G.J. Janz, "Molten Salts Handbook", Academic Press (1967)

[21] W.E. Kirst, W.M. Nagle, and J.B. Castner, Trans. Amer. Inst. Chem. Eng., 36, 371 (1940)

[22] A. Einstein, Ann. Physik, 17, 549 (1905)

[23] R. Kubo, J. Phys. Soc. Japan, 12, 570 (1957)

[24] M. S. Green, J. Chem. Phys., 20, 1281 (1952); 22, 398 (1954)

[25] H. Mori, J. Phys. Soc. Japan, 11, 1029 (1956)

[26] E. Helfand, Phys. Rev., 119, 1 (1960)

[27] L.V. Woodcock and K. Singer, Trans. Faraday Soc., 67, 12 (1971)

[28] K. Kawamura and I. Okada, At. Energy Rev., 16, 209 (1978)

[29] J. Michielsen, P. Woerlee, F. v.d. Graaf, and J.A.A. Ketelaar, J. Chem. Soc. Faraday Trans. II, 71, 1730 (1975)

APPENDIX I

Optical Arrangement of a Wave-Front-Shearing Interferometer

The schematic outline of the optical arrangement of a wave-front-shearing interferometer used in this work is illustrated in Fig. I. The light source (1) was a He-Ne gas laser (λ= 632.8 nm)-CR-80 made by RCA. The coherent rays from it were polarized by a polarizer (2) so that the vibration plane of the passed rays was horizontal, and then collimated with a Tropel-280 laser collimater (3). The slit of the cell (7) was illuminated by the rays which passed through a light port (5). The slit was covered with quartz window plates (6) pressed from the both sides with screws. A pair of lenses (9) and (10), the focal lengths of which were 100 and 10 cm, respectively, produced a miniature inverse image of the slit on the polariscope (11). The Savart plate was employed as the polariscope.

The double-refracting principle of the Savart plate is shown in Fig. II. The Savart plate consists of two identical uniaxial plates, cut at 45° and crossed. In the first plate the incident ray are sheared in two, namely, the ordinary ray o and the extraordinary ray e. Because the second plate is oriented at 90° with respect to the first, the ordinary ray o in the first plate becomes the extraordinary ray e in the second and vice versa. Accordingly, the rays are split in two by the Savart plate. The two rays are polarized at right angles with each other, are of equal intensity, and are in the same phase. They are displaced by a distance b, where b is

$$b = \sqrt{2}\, \ell\, (\mu_e^2 - \mu_o^2) \,/\, (\mu_e^2 + \mu_o^2) \quad .$$

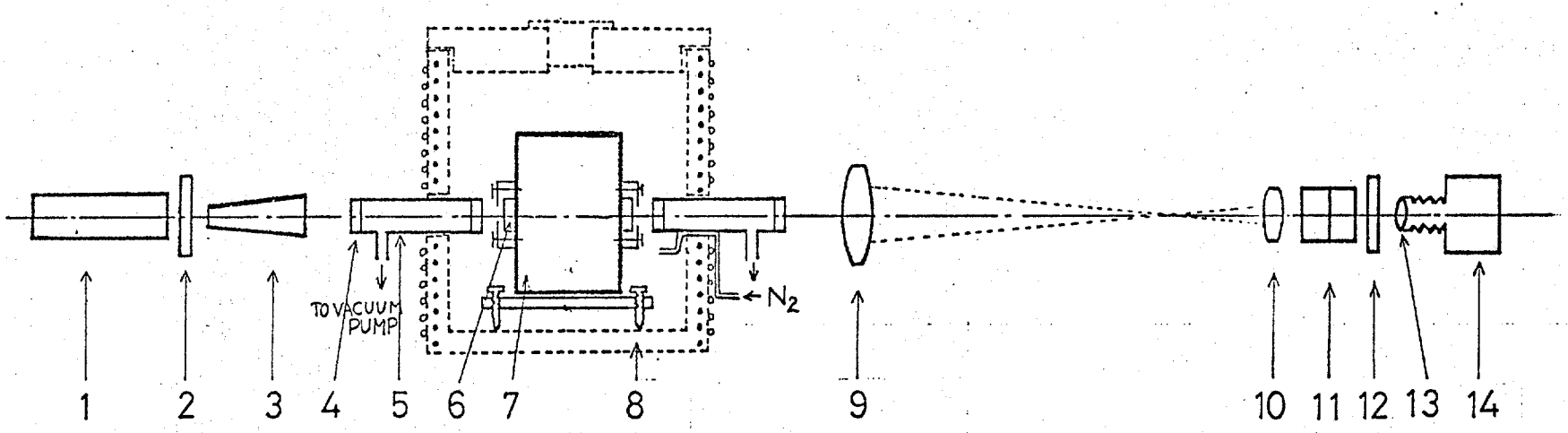

Fig. I Scheme of the optical arrangement of Interferometer

1. He-Ne gas laser
2. Polarizer
3. Collimator
4. Glass plate
5. Light port
6. Quartz plate
7. Cell
8. Electric furnace
9. Lens (f = 100 cm)
10. Lens (f = 10 cm)
11. Savart plate
12. Analyzer
13. Objective lens
14. Camera

Here, μ_o and μ_e denote the refractive indices for the ordinary and extraordinary rays, respectively, and ℓ is the thickness of each half part of the Savart plate.

Since the analyzer (12) was placed perpendicularly to the polarizer, the light was extinguished when the optical difference was integral multiples of the wave length; dark fringes were obtained on the film (14).

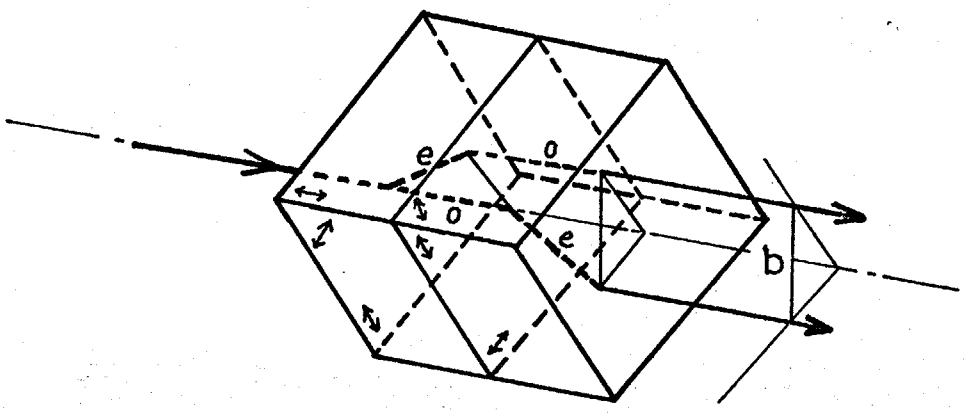

Fig.II Savart plate
o: ordinary ray
e: extraordinary ray

APPENDIX II

Calculation of High-Dilution Diffusion Coefficients with Wave-Front-Shearing Interferometry.

In the measurement of high-dilution diffusion coefficients a bottom layer diffusion technique was used, and the diffusion coefficient was calculated as follows.

The optical path of a ray traversing the cell at an arbitrary level x is calculated as follows by integrating the refractive index u over the length L of the cell in the direction z of the optical axis;

$$R(x,t) = \int_0^L \mu \, dz \qquad \cdots\cdots\cdots \text{(I)}$$

u is related with the concentration of the solute as

$$\mu = \mu_0 + C(\partial\mu/\partial C) \qquad \cdots\cdots\cdots \text{(II)}$$

where μ_0 is the refractive index of the solvent.

In the case of bottom layer diffusion, the concentration at distance x from the bottom at time t can be expressed by using the simple plane source solution of Fick's second law. It follows

$$C(x,t) = M \cdot \exp(-x^2 / 4Dt) \Big/ \sqrt{\pi Dt}, \qquad \cdots\cdots\cdots \text{(III)}$$

where M is the total amount of the solute divided by the cross section of the bottom layer, and D is the high-dilution diffusion coefficient. Substituting Eqs. (II) and (III) into Eq. ((I), we get

$$R(x,t) = \mu_0 L + ML \frac{(\partial\mu/\partial C)}{Dt} \exp(-x^2/4Dt) \qquad \cdots\cdots\cdots \text{(IV)}$$

The optical path difference ΔR is expressed from Eq. (IV) by

$$\begin{aligned} R &= R(x+b/2) - R(x-b/2) \\ &= (\partial\mu/\partial C) \frac{M \cdot L}{Dt} \left[\exp\left(-\frac{(x+b/2)^2}{4Dt}\right) - \exp\left(-\frac{(x-b/2)^2}{4Dt}\right) \right], \quad \text{..(V)} \end{aligned}$$

where b is the shear of the wave-fronts in the cell plane. From the fact that ΔR has the same value for a pair of fringes at the places

x_i and x_j, it follows

$$4Dt\,[\ln \sinh(bx_i/4Dt) - \ln \sinh(x_j/4Dt)] - (x_i^2 - x_j^2) = 0 \quad \ldots \text{(VI)}$$

If the shear b is small and the early interferogram can be disregarded when the gradient is comparatively high, it follows that

$$dR/dx = \Delta R/b \quad \ldots\ldots\ldots\ldots\ldots\ldots \text{(VII)}$$

From Eqs. (IV) and (VII), we get

$$D = (x_i^2 - x_j^2)/4t \cdot \ln(x_i/x_j) \quad \ldots\ldots\ldots \text{(VIII)}$$

In this experiment, we determined high-dilution diffusion coefficients by measuring the fringe length and calculating with Eq. (VI) by iteration technique.

APPENDIX III

Calculation of Thermal Properties with Wave-Front-Shearing Interferometry

In the measurement of thermal properties we used a thin foil instead of a "hot wire" as a heat source which was heated by a constant electrical power. Accordingly, we must solve the differential equation of conduction of heat (I) in three dimentions under the condition of a continuous plane source.

$$\partial T/\partial t = D_T(\partial^2 T/\partial x^2 + \partial^2 T/\partial y^2 + \partial^2 T/\partial z^2) \quad \cdots\cdots\cdots \text{(I)}$$

$$D_T = K/C_p\rho \quad \cdots\cdots\cdots\cdots\cdots\cdots\cdots\cdots \text{(II)}$$

If we assume that the y- and z- axes in a system of orthogonal coordinates define the plane which contains the foil (as shown in Fig. 3) and a constant heat per unit area per unit time Q is liberated at a point (x', y', z', t'), we get the solution for a continuous plane source by integrating throughout the region $-h \leqq z \leqq h$, $-d \leqq y \leqq d$, and the time t' the equation derived by Eq. (1) under the condition of an instantaneous point source.*

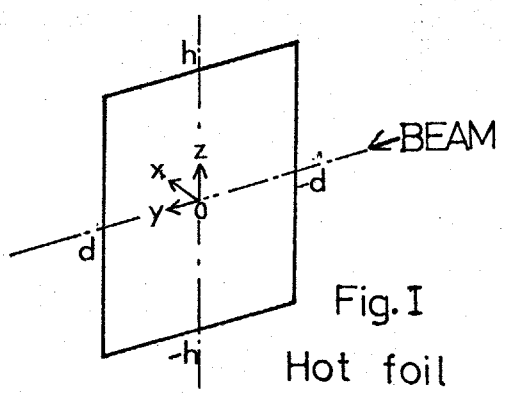

Fig. I Hot foil

$$T(x,y,z,t) - T(0) = \frac{Q}{8\pi K\sqrt{\pi D_T}} \int_0^t dt' \cdot \frac{\exp(-x^2/4D_T(t-t'))}{(t-t')^{3/2}} \int_{-d}^{d} dy' \cdot \exp\left\{\frac{-(y-y')^2}{4D_T(t-t')}\right\} \int_{-h}^{h} dz' \cdot \exp\left\{\frac{-(z-z')^2}{4D_T(t-t')}\right\}$$

$$\cdots\cdots\cdots\cdots \text{(III)}$$

---

* H.S. Carslaw and J.C. Jaeger, "Conduction of Heat", Univ. Press, Oxford p 256 (1959)

$$= \frac{Q}{8K\sqrt{\pi}} \int_0^{2\sqrt{D_T t}} d\beta \exp(-x^2/\beta^2) \left\{ \mathrm{erf}\left(\frac{y+d}{\beta}\right) - \mathrm{erf}\left(\frac{y-d}{\beta}\right) \right\} \left\{ \mathrm{erf}\left(\frac{z+d}{\beta}\right) - \mathrm{erf}\left(\frac{z-d}{\beta}\right) \right\} \quad \text{.....(IV)}$$

where $\mathrm{erf}(s) = \frac{2}{\sqrt{\pi}} \int_0^s dk \exp(-k^2) = 1 - \mathrm{erfc}(s)$,

and $\beta = 2\sqrt{D_T (t - t')}$.

At the x-y plane in the middle of the foil (z=0), Eq. (IV) becomes,

$$T(x,y,z,t) - T(0) = \frac{Q}{2K\sqrt{\pi}} \mathrm{erf}\left(\frac{h}{2\sqrt{D_T \theta}}\right) \int_0^{2\sqrt{D_T t}} d\beta \exp\left(-\frac{x^2}{\beta^2}\right) \left\{ \mathrm{erf}\left(\frac{y+d}{\beta}\right) - \mathrm{erf}\left(\frac{y-d}{\beta}\right) \right\} \quad \text{..... (V)}$$

As h is about 40 mm, θ is about 20 s, and D_T is about 0.15 $mm^2 s^{-1}$ in this work, $\mathrm{erf}(h/2\sqrt{D_T \theta})$ is equal to unity. Consequently, the temperature distribution we need is described as follows:

$$T(x,y,t) - T(0) = \frac{Q}{2K\sqrt{\pi}} \int_0^{2\sqrt{D_T t}} d\beta \exp(-x^2/\beta^2) \left[\mathrm{erf}\left(\frac{y+d}{\beta}\right) - \mathrm{erf}\left(\frac{y-d}{\beta}\right) \right] . \quad \text{..... (VI)}$$

As shown in Fig. II(c)-(d), the optical path difference is directly connected with the observed fringe pattern. The refractive index in a solution is described with temperature as follows:

$$\mu - \mu_0 = (\partial\mu / \partial T) \cdot (T - T_0) \quad \text{..... (VII)}$$

where μ_0 is the refractive index of the liquid at the temperature T_0. $(\partial\mu/\partial T)$ can be considered constant over the limited temperature range of an experiment. The optical path R in the solution whose width is 2r is shown as follows;

$$R = \int_{-r}^{r} \mu \, dy \quad \text{..... (VIII)}$$

From (VI), (VII), and (VIII), we get

$$R(x,t) = \frac{Q}{4K\sqrt{\pi}} (\partial\mu/\partial T) \int_{-r}^{r} dy \int_0^{2\sqrt{D_T t}} d\beta \exp(-x^2/\beta^2) \left\{ \mathrm{erf}\left(\frac{y+d}{\beta}\right) - \mathrm{erf}\left(\frac{y-d}{\beta}\right) \right\} \quad \text{..... (IX)}$$

Rearranging Eq. (IX) by using the first mean value theorem, we get

$$R(x,t) = \frac{Qd}{K\sqrt{\pi}}(\partial\mu/\partial T)[1+G(t)]\int_0^{2\sqrt{D_T t}} d\beta \exp(-x^2/\beta^2) \quad \ldots\ldots\ldots\ldots \text{(X)}$$

$$G(t) = \frac{\tau}{2d\sqrt{\pi}}\left[\exp\left(-\left(\frac{r+d}{\tau}\right)^2\right) - \exp\left(-\left(\frac{r-d}{\tau}\right)^2\right) + \sqrt{\pi}\left(\frac{r-d}{\tau}\right)\mathrm{erfc}\left(\frac{r+d}{\tau}\right) - \sqrt{\pi}\left(\frac{r+d}{\tau}\right)\mathrm{erfc}\left(\frac{r+d}{\tau}\right)\right]$$
$$\ldots\ldots\ldots\ldots \text{(XI)}$$

where $\tau = 2\sqrt{D_T\theta}$ and $0 < \theta < t$.

In Eq. (XI), if $\left(\frac{r-d}{\tau}\right)$ is relatively large value, Eq. (XI) can be shown as

$$\left|G(t)\right| < \frac{\tau}{d\sqrt{\pi}}\left(\frac{r-d}{\tau}\right)^2 \cdot \exp\left(-\left(\frac{r-d}{\tau}\right)^2\right),$$

when making an approximation with an equation $\mathrm{erf}(s) = \frac{1}{\sqrt{\pi}}\exp(-s^2)\left(\frac{1}{s} - \frac{1}{2s^3}\right)$ by using an asymptotic expansion of the error function for large values of s. In this work we used r=45 mm, d=15 mm, and (r-d)=30 mm. Consequently, G(t) can be neglected in Eq. (X), and the optical path is shown as follows:

$$R(x,t) = \frac{2dQ}{K}(\partial\mu/\partial T)\left[(D_T t/\pi)^{1/2}\exp(-x^2/4D_T t) - (x/2)\mathrm{erfc}(x/2\sqrt{D_T t})\right], \ldots \text{(XII)}$$

and

$$dR/dx = -\frac{Q\cdot d}{K}(\partial\mu/\partial T)\ \mathrm{erfc}(x/2\sqrt{D_T t}) \quad \ldots\ldots\ldots\ldots \text{(XIII)}$$

In the present interferometry, the optical path difference ΔR can be described as R(x+b/2) - R(x-b/2). Thus, at the place where Eq. (XIV) holds the dark fringes can be observed (see Fig. II);

$$\Delta R = R(x+b/2) - R(x-b/2) = n\lambda \ (n=0,1,2,\ldots\ldots) \quad \ldots \text{(XIV)}$$

Expanding the respective terms of ΔR, that is R(x+b/2) and R(x-b/2), in series, we get

$$\Delta R = b(dR/dx) + (b^3/4\cdot 3!)(d^3R/dx^3) + \ldots\ldots . \quad \ldots\ldots\ldots \text{(XV)}$$

In this relation the terms other than the first differential on the right hand are negligible, since b is a small value. Thus, since Eq. (XV) can be described as ;

$$\Delta R = b\cdot(dR/dx), \quad \ldots\ldots\ldots\ldots\ldots\ldots\ldots\ldots \text{(XVI)}$$

we get

$$\Delta R = - \frac{bQd}{K} \partial\mu/\partial T) \operatorname{erfc}(x/2\sqrt{D_T t}). \quad \ldots\ldots\ldots \text{(XVII)}$$

When deriving the thermal diffusivity, we use the fact that for one particular fringe ΔR is always constant as shown in Fig. II(c), that is,

$$(\Delta R)_{X_i} = \text{const.} \quad \ldots\ldots\ldots\ldots\ldots \text{(XVIII)}$$

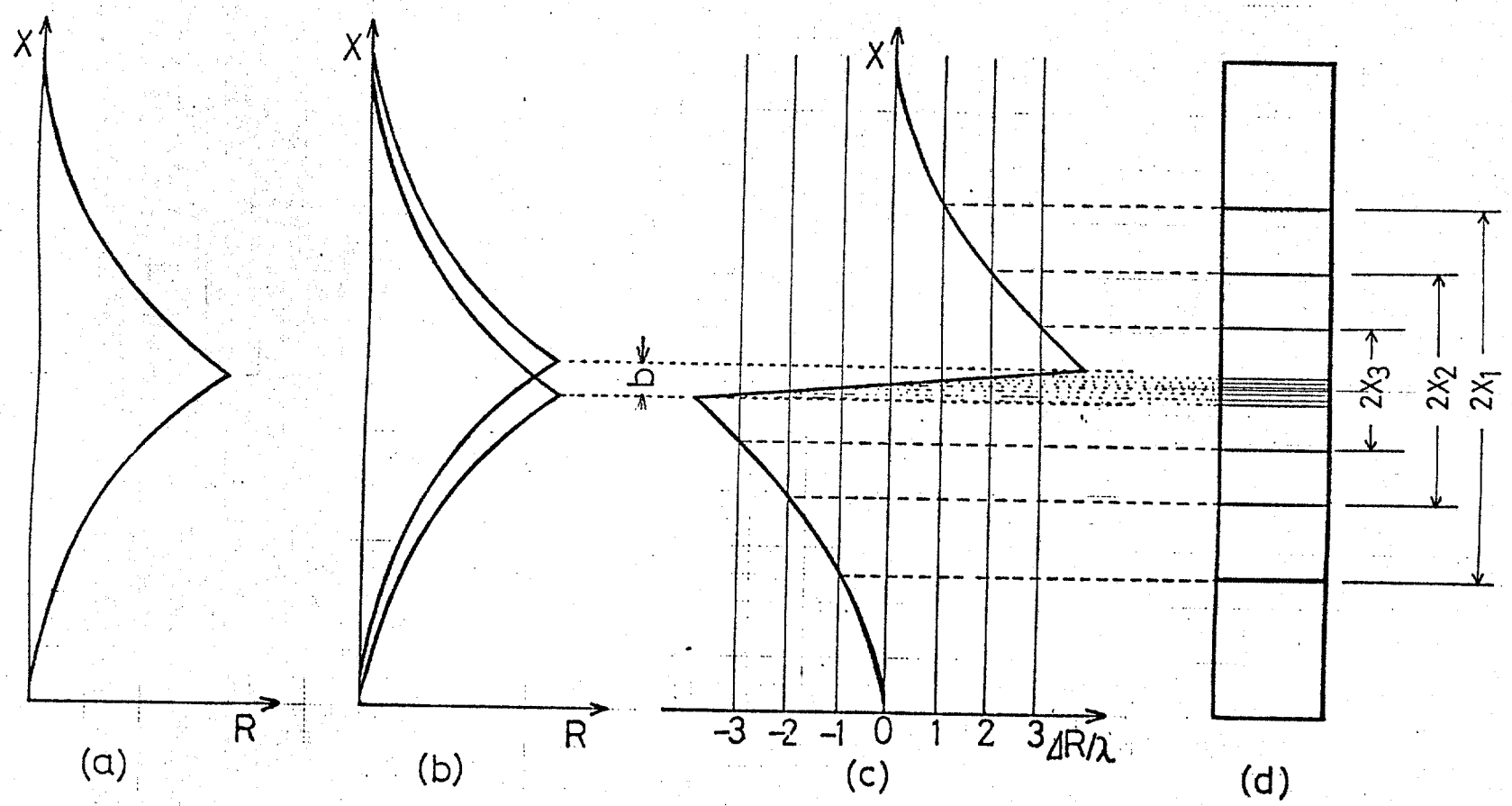

Fig.11 Principle of Wave-front-shearing Interferometry

ACKNOWLEDGEMENTS

The work presented in this thesis has been carried out at Prof. K. Kawamura's laboratory in the Research Laboratory for Nuclear Reactors, Tokyo Institute of Technology, and at the laboratory of Electrochemistry in University of Amsterdam, The Netherlands.

When I started in studying transport properties in molten salts at Prof. Kawamura's laboratory in 1974, the members of the laboratory were only 6 (staffs 3, students 3). Now, the laboratory consists of 12 members, and I am deepened in the impression that "桃李不言下自成蹊 A laboratory of virtue will naturally attract admirers.)."

First, I would like to thank Professor K. Kawamura for his continuing interest and valuable discussions during the course of the present work.

My thanks are due in particular to Professor I. Okada for his never-failing encouragement and continuing guidance.

I am also grateful to Professor J. A. A. Ketelaar for his hospitality and his valuable advise during my study at the University of Amsterdam.

Furthermore, I would like to thank a beard gentleman, Professor J. C.T. Kwak, very much for his useful comments and suggestions to my work during his stay at the University of Amsterdam and also after he returned in Dalhousie University, Canada.

I am grateful to the other members of Prof. Kawamura's laboratory and the staffs at the laboratory of Electrochemistry in the University of Amsterdam: het prettige contact met de medewerkers van de Laboratoria voor Electrochemie der Universiteit van Amsterdam heb ik zeer op prijs gesteld.

Lastly, I would like to thank all those people who have made my stay in The Netherlands so memorable. The financial support of The Netherlands Government Fellowship during my stay in Holland is gratefully acknowledged.